
# Energy Efficient Safe SHip OPERAtion

# SHOPERA

**Collaborative Project**

FP7-SST-2013-RTD-1

**Grant Agreement Number 605221**

List of participants:

| Participant Number | Participant organisation name | Type | Country | Contact Person |
|---|---|---|---|---|
| 1 (Coordinator) | National Technical University of Athens (NTUA) | UNIV | Greece | Apostolos Papanikolaou |
| 2 | Germanischer Lloyd SE (GL) | CLASS | Germany | Vladimir Shigunov |
| 3 | Det Norske Veritas AS (DNV) | CLASS | Norway | Elzbieta Bitner-Gregersen |
| 4 | Lloyds Register EMEA (LR) | CLASS | UK | Reddy Devalapalli |
| 5 | Norsk Marinteknisk Forskningsinstitutt AS (MRTK) | RES | Norway | Florian Sprenger |
| 6 | Instituto Superior Tecnico (IST) | UNIV | Portugal | Carlos Guedes Soares |
| 7 | Universitaet Duisburg-Essen (UDE) | UNIV | Germany | Ould El Moctar |
| 8 | RINA Services SPA (RINA) | CLASS | Italy | Alessandro Giulio Grasso |
| 9 | Flensburger Schiffbau Gesellschaft mbH & Co KG (FSG) | YARD | Germany | Rolf Nagel |
| 10 | Uljanik Brodogradiliste DD (ULJ) | YARD | Croatia | Igor Lalovic |
| 11 | Teknologian Tutkimuskeskus (VTT) | RES | Finland | Martio Jussi |
| 12 | Eigen Vermogen Flanders Hydraulics (EVFH) | RES | Belgium | Katrien Eloot |
| 13 | Canal de Experiencias Hidrodinamicas de el Pardo (CEHIPAR) | RES | Spain | Adolfo Maron |
| 14 | University of Strathclyde (SU) | UNIV | UK | Atilla Incecik |
| 15 | Danmarks Tekniske Universitet (DTU) | UNIV | Denmark | Harry Bingham |
| 16 | Technische Universität Berlin (TUB) | UNIV | Germany | Andres Cura Hochbaum |
| 17 | Technische Universiteit Delft (DUT) | UNIV | Netherlands | Klaas Visser |
| 18 | Naval Architecture Progress (NAP) | DES | Greece | Vassilios Zagkas |
| 19 | Danaos Shipping Company Ltd. (DAN) | OPER | Cyprus | Takis Varelas |
| 20 | FOINIKAS Shipping Company (FNK) | OPER | Greece | Maria Emmanouilidou |
| 21 | Calmac Ferries Ltd. (CAL) | OPER | UK | Louis De Wolff |

# Contents

# 1. Introduction to project SHOPERA – Objectives

The introduction of the Energy Efficiency Design Index (EEDI) was a major step towards improving energy efficiency and reducing greenhouse gas (GHG) emissions of shipping. It has also raised concerns that some ship designers might choose to lower the installed power to achieve EEDI requirements instead of introducing innovative propulsion concepts. This can lead to insufficient propulsion and steering abilities of ships to maintain manoeuvrability under adverse weather conditions, thus to a serious ship safety problem. Work carried out by IACS highlighted this issue and led to the development of first draft guidelines for consideration by IMO in 2011, IMO MEPC 62/5/19 and MEPC 62/INF.21, which resulted later in 2012 Interim Guidelines, see IMO MEPC 64/4/13, MEPC 64/INF.7, updated in 2013 in Res. MEPC.232 (65). Even though the 2013 Interim Guidelines prevent irrational reduction of installed power, their sufficiency was disputed, especially concerning the definition of the minimum power lines, adversity of the weather conditions to be considered in the assessment and removal of comprehensive assessment. Several research initiatives in various European countries and Japan, aiming at updating these guidelines (see, e.g. IMO submissions MSC 93/21/5 and MSC 93/INF.13 by Greece, MEPC 67/INF.22 by Japan, MEPC 67/4/16 by Denmark, Japan and the Republic of Korea, and MEPC 67/INF.14 by Germany, Norway and the United Kingdom) were started and are expected to lead to the rationalization of the interim guidelines, may be at MEPC 70 in October 2016.

To address the above challenges by in-depth research, the EU funded project SHOPERA (Energy Efficient Safe SHip OPERAtion) (2013-2016) was launched in October 2013. SHOPERA is developing suitable numerical methods and software tools and is conducting systematic case studies, which will enable the development of improved guidelines and their submission for consideration to IMO. A strong European RTD consortium was formed, representing the whole spectrum of the European maritime industry, including classification societies, universities, research organisations and model basins, ship designers, shipyards and ship operators. The project's objectives are:

- Develop criteria and corresponding environmental conditions for the assessment of the sufficiency of propulsion and steering systems of ships for manoeuvrability in adverse conditions, including open sea, coastal waters and restricted areas.
- Develop and adapt existing high fidelity hydrodynamic simulation software tools for the efficient analysis of the seakeeping and manoeuvring performance of ships in complex environmental and adverse weather conditions.
- Perform seakeeping and manoeuvring model tests in seaway by using a series of prototypes of different ship types to provide the required basis for the validation of employed software tools.
- Develop simplified assessment procedures, to the extent feasible, which should enable a quick assessment of the safety margins of ship designs with respect to the minimum propulsion and steering requirements for manoeuvrability in adverse weather conditions.
- Integrate validated methods and software tools for manoeuvrability assessment of ships in adverse weather conditions into a ship design software platform and combine it with a multi-objective optimization procedure, targeting sufficient propulsion and steering requirements for safe ship operation in adverse weather conditions while keeping the right balance between ship economy, efficiency and safety.
- Conduct investigations of the impact of the proposed requirements on the propulsion and steering abilities of ships for manoeuvrability in adverse conditions on the design and operational characteristics of various ship types by design teams comprising designers, shipyards, shipowners, classification societies, research institutes and universities. The impact on EEDI was also investigated by implementation of the developed holistic optimisation procedure in a series of case studies.

# 2. Project's outcome

## 2.1. Environmental conditions and requirements for different ships

### 2.1.1. Met-ocean description

#### 2.1.1.1. Wave Height

The existing 2013 Interim Guidelines do not consider manoeuvring criteria for the open sea. SHOPERA has introduced the weather-vaning criterion for the open sea, which requires corresponding standard environmental conditions. A straightforward choice of the North Atlantic scatter table, IACS (2001), is not suitable to define the weather conditions to be used with the weather-vaning criterion. Benchmarking of the existing fleet with respect to the weather-vaning criterion appears as the most rational way to define the standard wave height: the standard wave heights should be defined in such a way that the majority of the existing vessels fulfils the related requirements, taking into account that the present safety level with respect to manoeuvrability-related accidents in heavy weather is satisfactory.

For increasing storm in coastal waters, the 2013 Interim Guidelines use two criteria, course keeping and advance speed. The corresponding standard wave heights were defined by benchmarking of tankers, bulk carriers and container ships. SHOPERA aimed at validation of the proposed weather conditions with respect to the measurements. In Figure 1, wave data are compared for three coastal locations studied in SHOPERA, the access channel to the port of Antwerp (measurement data available from Flemish Banks Monitoring Network, 2016, and cover the period from 1984 to 2004), Scottish waters (hindcast data generated by the UK Met Office for the period from 2000 to 2008) and the port of Leixões (wave hindcast data simulated by IST for the period from 2000 to 2012). The 40 nautical mile long access channel to the port of Antwerp is dredged in a rather protected sand banks area, whereas both the Scottish coastal waters and the port of Leixões are not as protected. Correspondingly, the former area indicates milder wave heights than the latter two. Noting different duration of observations for the three considered areas (which leads to different observed minimum probabilities), and that these probabilities are too high to define design values, the measurements can be compared for the same probability of occurrence (e.g. $10^{-4}$); this leads to the maximum significant wave heights for the access channel to the port of Antwerp, Scottish waters and the port of Leixões of about 4.5 m, 5.5 m and 6.0 m, respectively.

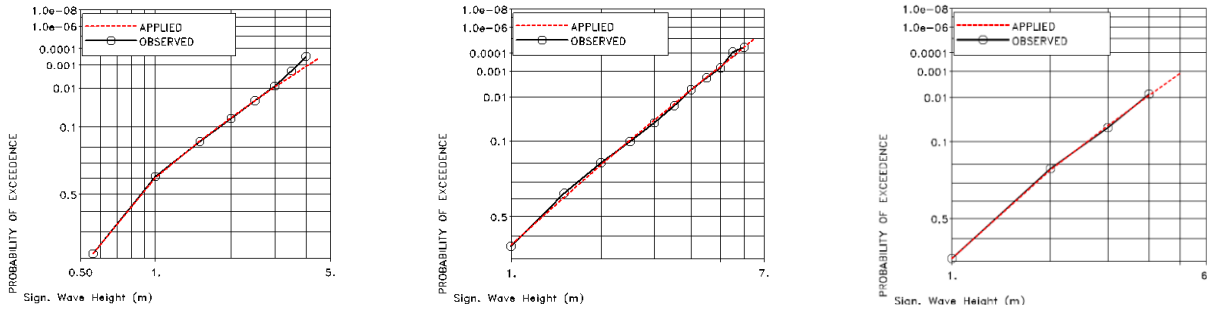


Figure 1. Empirical and fitted marginal distributions of significant wave height for access channel to port of Antwerp (left), Scottish waters (middle) and the port of Leixões (right)

Noting that these measurements refer to fixed observation locations, whereas ship masters do not remain on the same position near the coast in a growing storm, but either search for shelter or leave to the open sea, SHOPERA has used also several other sources to estimate rationally the required standard wave heights. Statistics of the weather conditions during manoeuvring-related accidents in adverse weather conditions, shows remarkably mild environmental conditions during accidents (mean wind speed of about 10 m/s and mean significant wave height about 1.5 m), which agrees with the earlier statistics from the HARDER project, indicating significant wave height below 2.0 m in 80% of collisions and absence of collisions at significant wave heights greater than 4.0 m. The study by IACS, *EE-WG 1/4 (2010)*, also identifies rather mild standard wave heights for weather-vaning (wind speed up to 21 m/s and significant

wave height up to 5.4 m) and advance speed (wind force up to Bft 8 at 6.0 knots advance speed) requirements.

On the other hand, *maximum* significant wave heights and wind speeds during manoeuvrability-related accidents achieve, according to SHOPERA statistics, in rare cases 7.0 m and 20 m/s, respectively. Detailed accident reports indicate wind force up to Bft 10 (in excess of 23 m/s) and significant wave heights above 6.0 m during few accidents in coastal areas. However, the well-documented case *ATSB (2008)*, where the significant wave height exceeded 6.0 m, clearly indicates unacceptably long waiting of the vessel at anchor in an increasing storm as the reason of the accident. Similar conclusions follow from the interviews of ship masters, Figure 2: 50% of the ship masters prefer to leave coastal areas before wind increases to Bft 8 and significant wave height achieves 5.0 m. Therefore, benchmarking of the existing fleet with respect to the new criteria appears as the most rational way to define the standard wave height. In SHOPERA, dedicated case studies were undertaken concerning all ship types considered in the EEDI regulations; results are presented in the Chapter Case Studies.

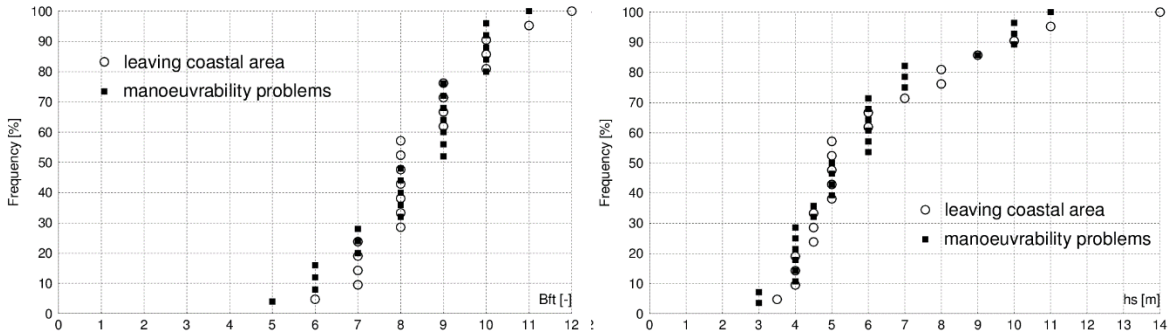


Figure 2. Wind force (top) and significant wave height (bottom) during leaving coastal areas (○) and during encountering steering and propulsion problems (●) from interviews of ship masters

### 2.1.1.2. Wind Speed

For practical assessment, it is convenient to use a unified wind speed-wave height relationship (perhaps different for the open sea and coastal areas) rather than use wind speed as an additional standard. The problem in the derivation of such a unified relation is that the relation between wind speed and wave height strongly depends on the fetch, wind duration and relation between the wind sea and swell. Because these factors depend on location, the relation between the wind speed and wave height is location dependent, even when considered in a statistical sense.

The well-known semi-empirical formula by Bretschneider for the wind sea (taken from Michel, 1999),

$$h_s = 0.243\frac{v_w^2}{g}\,\mathrm{th}\left(0.011\sqrt{gF/v_w^2}\right), \tag{1}$$

where $F$, m, is the fetch length, and wind speed $v_w$ is assumed at 10 m height above the free surface, gives for the unlimited fetch (open sea) an expression $h_s = 0.0248v_w^2$, or

$$v_w = 6.354\sqrt{h_s}, \tag{2}$$

denoted as Unlimited Fetch in Figure 3. This figure shows also a recommendation for the wind speed-wave height relationship for fully developed seas in the open areas according to NATO (1983), denoted as STANAG 4194, and hindcast data for two open-sea locations, West Shetland (generated by Oceanweather Inc. for the period from 1988 to 1998) and South-East of Iceland (generated by MET Norway for the period from 1955 to 2009, denoted SE Iceland). Both these locations are characterised by severe wind and are strongly affected by swell, representing typical North Atlantic met-ocean climate.

The semi-empirical relation (2) agrees well with the hindcast data for both locations and provides slightly conservative estimation of the required wind speed for a given significant wave height, which might be due

to the presence of swell in the hindcast data, which increases wave heights at moderate wind speeds and has less influence at greater wind speeds. The recommendation NATO (1983) agrees well with the semi-empirical formula at moderate wind speeds, but under-estimates wave heights at wind speeds greater than 12 m/s. Formula (2) is recommended by SHOPERA for the open sea.

For coastal areas, the influence of limited fetch for offshore wind can be very significant. Figure 4 shows wind speed as a function of significant wave height for 10, 20 and 30 miles fetch in comparison with the relation (2) for unlimited fetch (denoted as Unlimited Fetch). For comparison, the wind speed-wave height relationship is shown also according to the following sources:

- 2013 Interim Guidelines for Determining Minimum Propulsion Power to Maintain the Manoeuvrability of Ships in Adverse Conditions (denoted 2013 Guidelines);
- SHOPERA accident statistics (denoted Accidents);
- Hindcast data for a North Sea location off Dutch coast (simulated by Oceanweather Inc. for the period from 1964 to 1995, denoted Hindcast SNS).

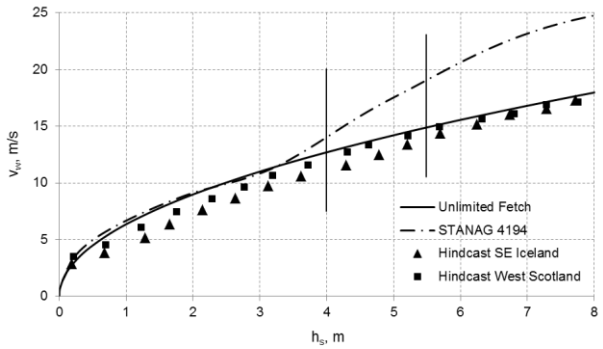


Figure 3. Wind speed-significant wave height relationship in open sea

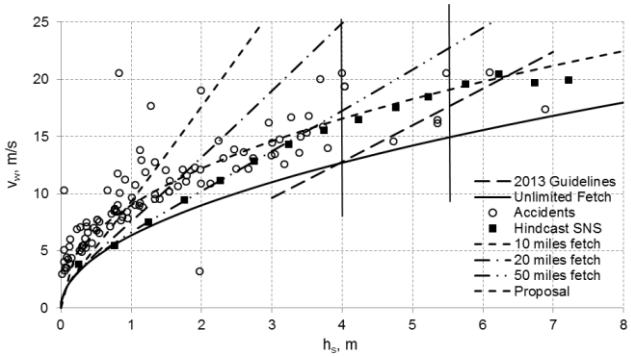


Figure 4. Wind speed-significant wave height relationship in coastal areas

The accident data show a considerable number of accidents in strong wind and under-developed waves; in such conditions, wind force at a given significant wave height increases considerably compared to eq. (2). The hindcast data for the south coast of North Sea agree well with accident data in the relevant region of significant wave heights, but show significantly smaller wind speeds in low to moderate seaways. The 2013 Interim Guidelines provide a good estimation for the wind speed in more severe seaways, but under-predict the wind speed in moderate to severe conditions. As a recommendation, agreeing with both accident data and hindcast in the relevant region of significant wave heights, and also providing a fair average of the accident data in low to moderate sea states, the following formula is proposed for coastal areas (shown as Proposal in Figure 4):

$$v_w = 9 \cdot h_s^{0.44}. \tag{3}$$

### 2.1.1.3. Other Sea State Parameters

In severe to extreme sea states, the influence of swell is usually negligible compared to the wind sea, whereas in small to moderate seaways, the influence of swell may be significant. Figure 3 shows that for the significant wave heights relevant in the assessment of manoeuvrability in adverse conditions, the influence of swell is small, therefore, a unimodal spectrum can be assumed for simplicity.

For the open sea, it is feasible to assume a situation of a ship weather-vaning for a prolonged time until the storm finishes, i.e. a developed storm situation is relevant for the assessment of the weather-vaning ability in the open sea. For a developed sea state, the Bretschneider spectrum (also referred to as a two-parameter Pierson-Moskowitz spectrum or a two-parameter ITTC spectrum) is generally recommended,

$$S_{\zeta\zeta} = 5\frac{\pi^4}{\omega^5}\frac{h_s^2}{T_p^4}\exp\left(-\frac{20\pi^4}{T_p^4\omega^4}\right), \tag{4}$$

where $T_p$, s, is the wave period corresponding to the modal wave frequency $\omega_p$, rad/s, and $\omega$, rad/s, is the wave frequency.

For coastal waters, following from the practice and confirmed by the interviews of ship masters undertaken by SHOPERA, the assumed scenario is that ship masters do not remain near the coast in a growing storm until it escalates, but either search for shelter or leave to the open sea. Therefore, the feasible scenario to be applied with the steering and propulsion criteria is a developing storm. For a developing storm a general recommendation is to use the JONSWAP spectrum with the peak parameter of 3.3, i.e. as used in the 2013 Interim Guidelines for the evaluation of ship manoeuvrability in coastal areas,

$$S_{\zeta\zeta} = \frac{\alpha g^2}{\omega^5}\exp\left(-\beta\frac{\omega_p^4}{\omega^4}\right)\gamma^a, \tag{5}$$

where $a = \exp\left\{-\left(\omega-\omega_p\right)^2 \Big/ \left(2\omega_p^2\sigma^2\right)\right\}$, $\sigma = 0.07$ if $\omega \le \omega_p$ and $\sigma = 0.09$ if $\omega > \omega_p$, $\beta = 5/4$, and the peak parameter $\gamma = 3.3$.

As a realistic assumption, directional spreading of wave energy with respect to mean wave direction is recommended; as the spreading function, $\cos^2$-spreading was used in SHOPERA. An assessment of steering and propulsion abilities in short-crested waves with $\cos^2$-wave energy spreading in comparison with assessment in long-crested irregular waves for a VLCC tanker and 14000 TEU container ship showed that assuming long-crested seaway makes assessment results negligibly to moderately conservative, thus performing assessment in long-crested waves is also acceptable, as it is more practicable for designers.

The range of characteristic wave periods (for clarity, peak wave period $T_p$ will be used) used in the assessment has a significant influence on the assessment results. For the propulsion ability criterion, as well as for the weather-vaning criterion, the upper (long waves) boundary of the used peak wave periods defines whether and how much of the added resistance peak is taken into account, whereas the lower boundary (short waves) is important for larger, especially blunt, vessels for which a significant part of added resistance comes from short wave components. For the steering ability criterion, external excitation increases with increasing wave frequency, therefore, it is important how the lower boundary (short waves) of the peak wave periods is defined.

Note that the recommended spectra are applicable in the range of peak wave periods $T_p$, s, from about $3.6h_s^{0.5}$ to about $5.0h_s^{0.5}$, marked in Figure 5 as Tpmin-JONSWAP and Tpmax-JONSWAP, respectively. The 2013 Interim Guidelines use the range of the peak wave periods from 7.0 (marked as Tpmin 2013 Guidelines) to 15.0 s. Figure 5 shows also the most likely peak wave periods from measurements for West of Scotland and Belgium coast, and the theoretical maximum storm steepness boundary, Michel (1999), marked as Max. Steepness, $T_z = 8\sqrt{h_s/g}$ or, for JONSWAP spectrum, $T_p = 3.282\sqrt{h_s}$.

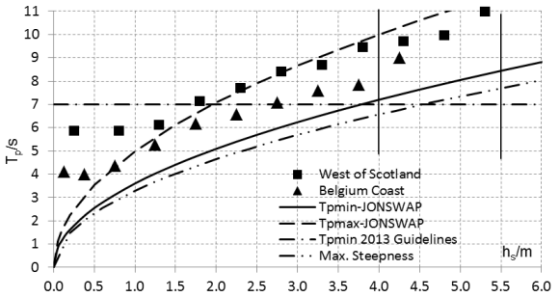

Figure 5. Peak wave periods recommended for the assessment

The lower boundary of peak wave periods used in the 2013 Interim Guidelines, 7.0 s, is slightly conservative, because it crosses the theoretical maximum storm steepness boundary in the relevant range of significant wave heights. The upper boundary, 15.0 s, although theoretically possible, is unnecessary large, because such large wave periods are not critical for propulsion or steering ability.

As the lower boundary of peak wave periods (short waves),

$$T_p^{min} = 3.6h_s^{0.5} \tag{6}$$

seems appropriate: this and larger peak wave periods are assumed suitable for the JONSWAP wave spectrum; besides, the theoretical maximum storm steepness boundary is not violated. For the upper boundary of peak wave periods,

$$T_p^{max} = 5.0 \cdot h_s^{0.5} \quad (7)$$

(or slightly higher) can be used, as this will cover the peak wave periods important for added resistance.

### 2.1.2. Identification of ships and risk analysis of relevant marine accidents

Available detailed investigations of accidents related to insufficient manoeuvrability in adverse weather conditions were studied. The most frequent cause of heavy weather-related grounding accidents is waiting at anchor in heavy weather and too late starting of the engine. In several accidents, *MAIB (1996, 2009, 2012)*, *ATSB (2008)*, vessels were not able to move away from the coast or turn into seaway despite full engine power applied. Table 1 summarises corresponding criteria, relevant for insufficient propulsion or course-changing abilities, as well as the corresponding weather conditions.

Table 1. Summary of accident reports

| Ref. | Relevant criteria | Environmental Conditions |
|---|---|---|
| MAIB (2009) | Course changing | Bft 9-10 (20.8 to 28.4 m/s), $h_s$ > 10 m |
| MAIB (1996) | Course changing | gale force wind (17.3 to 20.8 m/s), low waves |
| MAIB (2012) | Propulsion | $v_w$ = 40 knots (20.6 m/s), $h_{max}$ = 4 m |
| ATSB (2008) | Propulsion | $v_w$ = 38-46 knots (19.5 to 23.7 m/s), $h_s$ = 6.0-6.6 m |
| MAIB (2002) | Propulsion | Bft 5-7 (8.0 to 17.1 m/s), low waves |
| MAIB (2009a) | Propulsion | Bft 10 (24.5 to 28.4 m/s) |
| MAIB (2012a) | Course changing | $v_w$ = 38-45 knots (19.5 to 23.2 m/s) |

The well-known statistics of the HARDER project indicate that more than 80% of the collisions happened at significant wave height below 2 m, whereas significant wave heights exceeding 4 m were practically not recorded. Similar results were obtained from a comprehensive statistical analysis of ship accidents[1] in adverse sea conditions, conducted in SHOPERA by Ventikos et al (2014). Two main sources were used for the collection of the necessary information, namely the IHS Sea-Web marine casualty database and the public area of the marine casualties and incidents database of the International Maritime Organization (IMO) Global Integrated Shipping Information System (GISIS). The information collected from these sources was cross-checked, wherever possible, with accident reports acquired from other sources (various National Maritime Safety authorities). A characteristic sample of the results of this analysis is given in the following. From these statistics it is evident that:

1. The most vulnerable ship types with respect to navigational accidents in adverse conditions are general cargo ships, followed by Ro-Ro ferries, bulk carriers and tankers, Figure 6.
2. For these ship types, the accident location varies between port areas (almost exclusively for Ro-Ro ferries) and generally limited waters, such as port and restricted waters (for general cargo vessels and bulkers); for tankers, we observe some increased sensitivity in en route (open seas) conditions, Figure 7.
3. Inclusion in the statistical analysis of very rare abnormal weather events (hurricanes, typhoons etc.) does not significantly alter the statistics, Figure 8 and Figure 9.
4. Observed mean wind speeds of about 10 m/s and significant wave heights of 1.49 m are remarkably low, Figure 10 and Figure 11; this also applies to the statistical quartiles, Table 2, with lower values observed for collisions and groundings and the highest recorded values related to contacts.
5. There is a statistically significant difference in mean wave height between ship types, which means that some ship types are more affected by wave height than the others, Figure 12.

[1] Accident period 1980-2013; ships over 400 GT built after 1980; analysed accidents were related to adverse and heavy weather conditions, excluding poor visibility (e.g. fog).

6. The calculated accident rates, related to the Fleet at Risk, are in the range of $10^{-5}$ to $10^{-3}$ accidents per ship per year, Table 3, i.e. by one order of magnitude lower than accident rates calculated in Formal Safety Assessments, which do not consider the prevailing weather conditions.
7. Among the three navigational accident types, groundings exhibit the highest rates for cargo carrying ships in general, whereas for Ro-Ro ships contacts are associated with the highest rates, Table 4.
8. Based on the available information, hull damage was selected as a main consequence variable for the risk analysis.
9. The risk analysis implemented the concept of risk triplets, defined by Scenario, Frequency, and Consequence, (Kaplan and Garrick, 1981), and enabled the generation of three distinct types of risk-related curves, based on accident frequencies per ship type, per ship type and size class, and per ship and accident type.
10. Overall, groundings and contacts in heavy weather conditions are the accident types with the highest risk across all ship types.
11. Comparison of risk levels between ship types shows that Ro-Ro Ferries and RoRo Cargo ships exhibit high risk values due to high accident frequency and medium level of consequences, whereas Gas Carriers, Tankers and Bulk Carriers exhibit high risk values due to the observed high level of accident consequences.

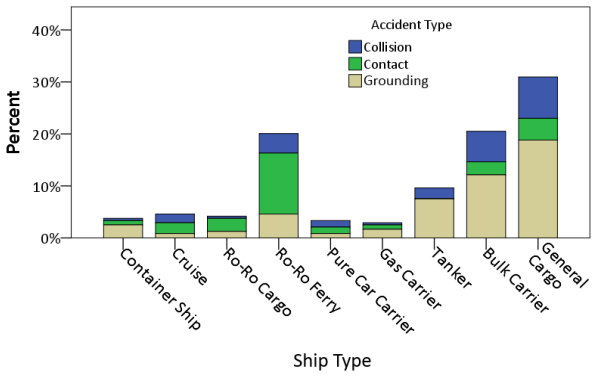


Figure 6. Percentage of ship types involved in navigational accidents under adverse weather conditions by accident type

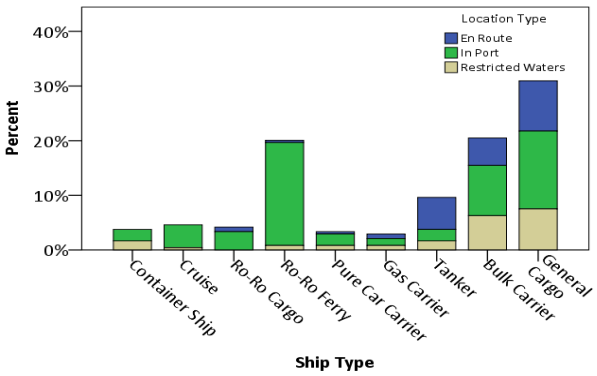


Figure 7. Percentage of ship types engaged in navigational accidents under adverse weather conditions by accident location

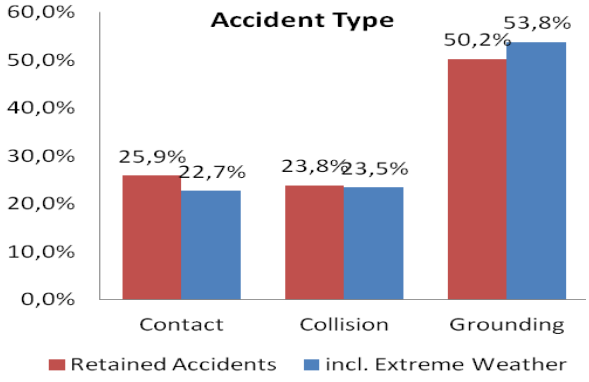


Figure 8. Distribution of accident types when including very extreme (abnormal) weather conditions

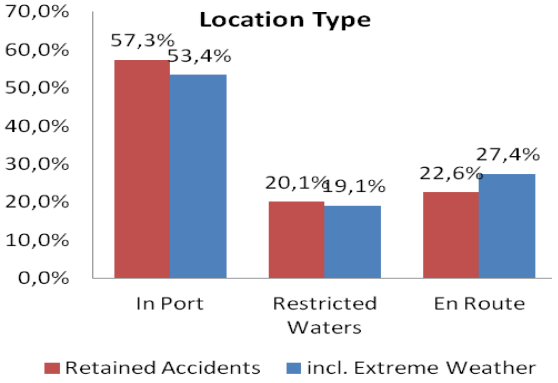


Figure 9. Comparison of accident location when including very extreme (abnormal) weather conditions

Table 2. Mean and quartiles for wind speed and wave height per accident type

| | WIND SPEED (m/s) | | | WAVE HEIGHT (m) | | |
|---|---|---|---|---|---|---|
| | Collision | Contact | Grounding | Collision | Contact | Grounding |
| Mean | 9.48 | 11.49 | 8.76 | 1.28 | 1.95 | 1.28 |
| 25th | 6.69 | 8.45 | 4.86 | 0.35 | 0.80 | 0.14 |
| 50th | 8.63 | 11.64 | 7.62 | 0.78 | 1.52 | 0.81 |
| 75th | 11.00 | 14.04 | 13.33 | 1.57 | 2.64 | 2.00 |

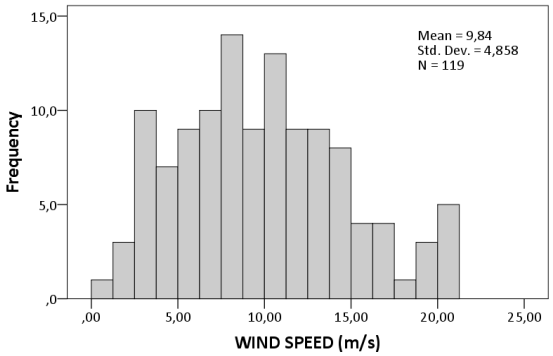


Figure 10. Frequency histogram for wind speed

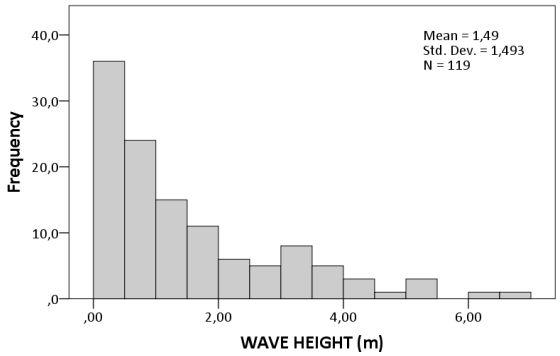


Figure 11. Frequency histogram for wave height

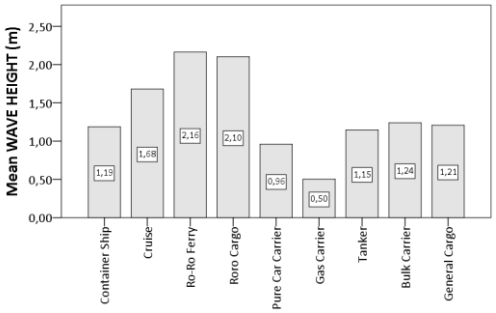


Figure 12. Mean wave height per ship type

Table 3. Fleet at Risk and accident rates per ship type

| Ship Type | Period | Fleet at Risk | Acci-dents | Rate |
|---|---|---|---|---|
| Container Ships | 1996-2013 | 63594 | 8 | 1.26E-04 |
| Cruise Ships | 1996-2013 | 5252 | 11 | 2.09E-03 |
| Ro-Ro | 1996-2013 | 19173 | 56 | 2.92E-03 |
| Pure Car Carriers | 1996-2013 | 9814 | 8 | 8.15E-04 |
| Gas Carriers | 1996-2013 | 22195 | 6 | 2.70E-04 |
| Tankers | 1990-2013 | 145159 | 23 | 1.58E-04 |
| Bulk Carriers | 1990-2013 | 143158 | 49 | 3.42E-04 |
| General Cargo | 1996-2013 | 23462 | 74 | 3.15E-03 |

Table 4. Rates of accidents in database per ship and accident type

| | Container Ships | Cruise Ships | Ro-Ro | Crude Oil Tankers | LNG | LPG | General Cargo | Bulk Carriers |
|---|---|---|---|---|---|---|---|---|
| Collision | 1.57E-05 | 7.62E-04 | 5.22E-04 | 3.44E-05 | - | - | 7.67E-04 | 9.78E-05 |
| Contact | 1.57E-05 | 9.52E-04 | 1.72E-03 | - | 4.51E-05 | 5.77E-05 | 4.26E-04 | 4.19E-05 |
| Grounding | 9.43E-05 | 3.81E-04 | 6.26E-04 | 1.24E-04 | 4.51E-05 | 1.73E-04 | 1.83E-03 | 2.03E-04 |

## 2.1.3. EEDI and safety criteria

### 2.1.3.1. Scenarios and Criteria

#### *2.1.3.1.1. Terminology*

To facilitate understanding, the following terminology is used throughout the report:

- The term *criterion* refers to a characteristic of the ship, such as ability to turn, ability to keep course etc., by which ship's abilities, considered relevant for the considered problem, are judged.
- Corresponding *measure*, e.g. turning diameter or overshoot angle, quantifies numerically the performance of ship with respect to the considered criterion. For manoeuvrability in adverse conditions, an obvious and frequently used measure is the marginal (maximum) weather severity, up to which the ship is able to fulfil the criterion (e.g. maximum wave height at which the ship can change course).
- The term *standard* (sometimes called *norm*) refers to the prescribed acceptance limit on the measure for the ship to be considered as fulfilling the defined criterion. Here, it is the specified significant wave height (and the related wind force) at which the ship should be able to fulfil the corresponding criterion.

#### *2.1.3.1.2. Existing Regulations*

Manoeuvrability of ships is presently normed by *IMO Standards for Ship Manoeuvrability*, *IMO (2002)*, which address turning, initial turning, yaw checking, course keeping and emergency stopping abilities, evaluated in simple standard manoeuvres in calm water. These Standards have been often criticized for not addressing ship manoeuvring characteristics at low speed, in restricted areas and in adverse weather conditions; the importance of the latter increased after the introduction of EEDI.

In *EE-WG 1/4 (2010)*, IACS put together the requirements of classification societies related to the redundancy or duplication of the propulsion system to indicate relevant criteria and environmental conditions for steering and propulsion in adverse weather conditions; a summary of these requirements in Table 5 ($v_d$ means design speed, $v_w$ wind speed, $h_s$ significant wave height) indicates, basically, two requirements: to change (or keep) heading and to maintain some minimum advance speed (or to keep position, i.e. zero speed).

Studies by IACS on minimum power requirements for manoeuvrability in adverse weather conditions started with analysis of functional requirements to manoeuvrability in the open sea and coastal areas, *MEPC 62/5/19 (2011)* and *62/INF.21 (2011)*, concluding that manoeuvring in coastal waters is more challenging than in the open sea; the resulting criteria for ship propulsion and steering abilities were formulated in *MEPC 64/4/13 (2012)* and *64/INF.7 (2012)*: the ship should be able, in seaway from any direction, to (1) keep course and (2) keep advance speed of at least 4.0 knots. The corresponding weather conditions are not too severe, because ship masters do not stay near the coast in an increasing storm and either search for a shelter or leave to the open sea and take a position with enough room for drifting. The standard environmental conditions defined by IACS (wind speed 15.7 m/s at significant wave height 4.0 m for ships with $L_{pp}$=200 m to 19.0 m/s and 5.5 m, respectively, for $L_{pp}$=250 m and greater) were derived by benchmarking of tankers, bulk carriers and container ships in the EEDI database against these two criteria.

Table 5. Criteria and weather conditions for redundancy and duplication of propulsion system according to requirements of classification societies, EE-WG 1/4 (2010)

| **Class** | **Criteria** | **$v_w$** | **$h_s$** |
|---|---|---|---|
| GL | Change and keep heading (weather-vaning) | 21 m/s | 5.4 m |
| GL | Advance speed ≥ min(7 knots, $0.5v_d$ ) | 11 m/s | 2.8 m |
| LR | Steering ability; advance speed ≥ 7 knots | - | - |
| BV | Advance speed ≥ 7.0 knots | Bft 5 (8.0 to 10.7 m/s) | corresp. to $v_w$ |
| ABS | Weather-vaning without drifting | 33 knots (17.0 m/s) | 4.5 m |
| DNV | Weather-vaning at advance speed ≥ 6 knots | Bft 8 (17.2 to 20.7 m/s) | corresp. to $v_w$ |

#### *2.1.3.1.3. Interviews of Ship Masters*

Interviews of masters of about 50 container ships, bulk carriers and tankers conducted in the projects PerSee and SHOPERA indicate that in the open sea, the captain usually has more freedom and can decide what severity of weather conditions is acceptable for his ship, depending on the freeboard, cargo, stability and propulsion and steering characteristics of the vessel. On the other hand, when caught in most violent storms, steering against seaway may be impossible for any vessel; in such circumstances, drifting with seaway was considered as an acceptable option for a limited time if there is enough room for drifting. However, the available power is important for escaping the storm and bringing the ship into safe weather conditions.

Manoeuvring in coastal areas was reported as more challenging than manoeuvring in the open sea, because, in principle, any manoeuvre, sometimes in unfavourable seaway direction with respect to the ship, may be required. Environmental conditions are, however, less severe than in the open sea, because ship masters do not remain near the coast in a growing storm, but either search for shelter or leave to the open sea.

As relevant manoeuvring problems, steering problems were mentioned in the interviews insignificantly more often than propulsion problems (83% vs. 60% of cases, respectively); insufficient engine power was mentioned more frequently for bulk carriers and tankers, whereas insufficient rudder capability more

frequently for container vessels. As a very specific manoeuvring problem in restricted waters, manoeuvrability at limited speed (due to navigational restrictions, e.g. during approaching ports) was mentioned, in strong wind and, sometimes, strong current, but usually without large waves because of protected areas.

#### *2.1.3.1.4. Proposal for Scenarios and Criteria*

*Shigunov and Papanikolaou (2014)* proposed to differentiate three scenarios, in which steering and propulsion abilities of ships are challenged in a different way and which require, therefore, specific criteria: open sea, coastal areas and restricted areas at limited speed. For the open sea, the ability of ship to weather-vane, i.e. keep heading in head to bow-quartering seaway, was proposed as a criterion. Regarding corresponding environmental conditions, it was noted that none of the existing ships can steer against waves and wind in most severe possible storms, therefore, benchmarking of the existing world fleet with respect to the weather-vaning criterion was proposed to define the standard wave height. For the coastal areas, two criteria were proposed: the ability of the ship to perform any manoeuvre and the ability to maintain some speed over ground to enable leaving the coastal area before the storm escalates; due to navigational restrictions, both criteria should be possible to fulfil in seaway from any direction. The corresponding environmental conditions are less severe than in the open sea and should also be defined by benchmarking of existing ships against these criteria. Manoeuvrability at limited speed in restricted areas refers to situations where the ship master has to reduce the applied engine power (and thus forward speed) significantly below available power because of navigational restrictions, e.g. during approaching to or entering ports, navigation in channels and rivers etc. Because full available power cannot be applied in this scenario, the corresponding manoeuvrability criteria will not impose any restrictions on minimum propulsion power, thus this scenario is not considered here.

Based on this, SHOPERA proposed the following three criteria for manoeuvrability in adverse weather conditions: weather vaning ability in heavy weather in the open sea and steering and propulsion abilities in increasing storm in coastal areas.

In the practical assessment, weather-vaning ability was treated in a simplified way, as the *ability of the ship to keep position in bow to bow-quartering seaway*; this simplification follows from the observation, confirmed by model tests, that the ship (with the traditional steering devices at the stern) will not be able to keep heading under the action of environmental forces if the forward speed is not sufficiently large, because of significantly reduced manoeuvring reactions on the hull and steering force on the rudder.

The steering ability in increasing storm in coastal areas is understood as the *ability of the ship to perform any manoeuvre in seaway from any direction*. An equivalent, but easier to verify in practice criterion is proposed, that the *ship should be able to start or continue course change in seaway from any direction*. This formulation should be distinguished from the traditional *course-keeping problem*: the steering ability is understood here as the ability of the steering system to overcome environmental forces and start (or continue) course change during an arbitrary manoeuvre (i.e. capability of the steering system); for this ability, it does not matter whether each intermediate state during manoeuvre is stable or not, thus the stability of the ship on each particular course is not addressed, whereas the traditional definition of course-keeping addresses stability of straightforward motion. Note that the proposed criterion does not exclude the ship's ability to perform also straightforward motion (which is one of "all" required manoeuvres): even if a ship is directionally unstable on some course, it will still be able to follow this course using rudder for continuous course corrections (which is an operational drawback and not a safety issue, and is relevant in few situations per operational life).

The propulsion ability in increasing storm in coastal areas ensures that the ship is able to leave coastal area in a sufficient time before the storm escalates. As the minimum required advance speed, 6.0 knots was chosen by SHOPERA, instead of 4.0 knots used in 2013 Interim Guidelines, to take into account possibly strong currents in coastal areas.

The corresponding environmental conditions for these three criteria need to be defined by benchmarking of existing vessels.

## 2.2. Development and refinement of numerical hydrodynamic tools

### 2.2.1. Potential flow methods for Seakeeping and Loss of Stability in Extreme Seas

An existing numerical model of the calculation added resistance and speed loss in waves, developed by Prpić-Oršić and Faltinsen (2012) has been improved by accounting for the effect of air resistance. The total wind velocity is a combination of a steady-state or mean velocity and a turbulent (gust) component. The mean speed is calculated as a function of significant wave height, according to the one-parameter Pierson-Moskowitz spectrum. The gust component is a random process with zero mean, represented by a gust spectrum. The wind direction is assumed to be the same as the wave direction. The numerical model has been extended to consider the effect of various dynamic phenomena (slamming, deck wetness, bow acceleration and propeller emergence) on voluntary ship speed reduction and so arranged to allow the prediction of ship's behaviour for the whole range of ship speeds and heading angles, which is an essential part of weather routing systems (Vettor and Guedes Soares, 2015). Averaged results for the six main North Atlantic routes shown in Figure 13 (Vettor and Guedes Soares 2014) were analysed for the case of involuntary and voluntary speed reduction (Prpić-Oršić et al., 2015), with respect to CO2 emissions and the specific fuel consumption (Figure 14). Figure 15 and Figure 16 show sailing time and $CO_2$ emission increase in percentage caused by waves and wind.

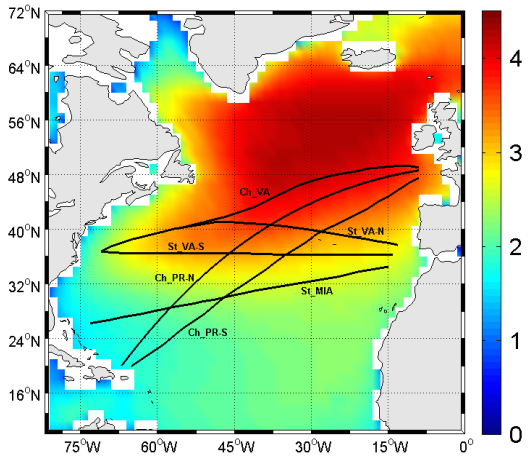


Figure 13: Main North Atlantic Routes (Vettor & Soares, 2015)

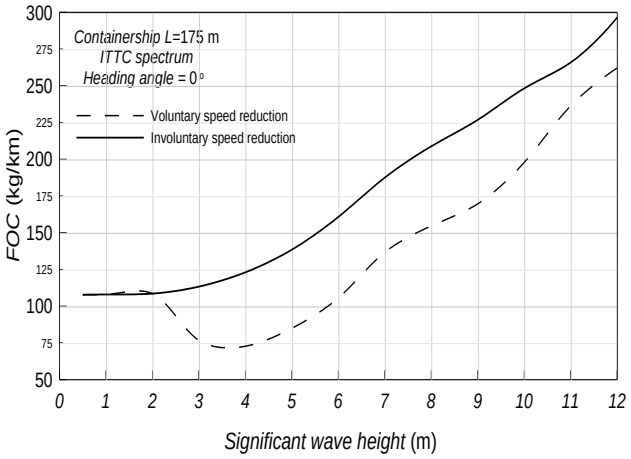


Figure 14: Fuel consumption for following sea (Prpic-Oršic, 2015)

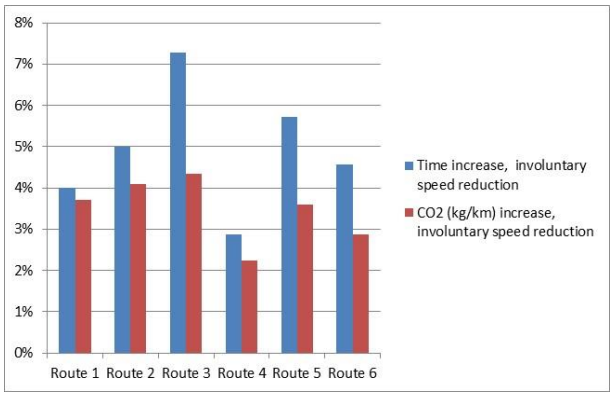


Figure 15: Time increase and $CO_2$ emmission increase (involuntary speed reduction).

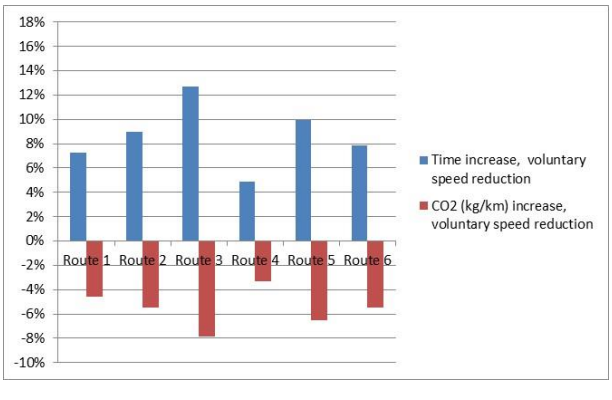


Figure 16: Time increase and $CO_2$ emmission increase (voluntary speed reduction).

With reliable weather (wind/waves) data and the performance simulation of ships in a seaway, it is possible to decrease fuel consumption and $CO_2$ emission by identifying the best possible route. It has to be done by taking into account other criteria like estimated time of arrival, safety of ship, crew, passengers and cargo, etc. The optimization problem is obviously multi-objective, non-linear and constrained and a suitable compromise has to be found between opposing targets.

The 3D seakeeping code HYBRID of NTUA has being further developed for simulating the 6 DoF nonlinear ship motions in adverse sea states and for studying the parametric rolling. The code has been used to study of parametric rolling of the ITTC-A1 ship and to calculate the drift forces and added resistance of three ships: a RoPAX ship, the KVLCC2 tanker, and the DTC container ship. HYBRID is a nonlinear time domain computer code based on the impulse response function concept and incorporates the nonlinear Froude-Krylov force and hydrostatic force to simulate the six DoF ship motions (Liu et al., 2014). For validation purpose, the code has been applied to the simulation of the parametric rolling of the ITTC-A1 containership (Umeda et al, 2000), for which the tank tests are available from the SAFEDOR project (SAFEDOR, 2008), showing satisfactory agreement with experimental results. For the calculation of drift forces and added resistance, a far-field method and a proper semi-empirical formula for the short waves region are used. A new level-1 formula has also been developed to accurately predict the added resistance of ships sailing in waves of various headings. Figure 17 compares typical results for the drift forces acting on the KVLCC2 tanker, obtained with a) the frequency domain 3D panel code NEWDRIFT of NTUA, which implements a near filed-pressure integration, b) a far field approach (see Liu et al. 2011; Liu and Papanikolaou 2013), and c) the 3D Rankine source-patch code GL Rankine of DNVGL, also based on a near-field pressure integration method for the drift forces and added resistance (Söding et al. 2012 and 2014).

In the short wave region (incident wave/ship length less than about 0.5) the added resistance predicted by potential theory codes is generally underestimated, both for full type and fine ship hull forms. As a practical approach to this problem, a semi-empirical formula (Liu et al., 2015; Liu and Papanikolaou, 2016) has been introduced to correct the prediction of added resistance in short waves, namely $\lambda/L < 0.5$ (0.7). Typical numerical results are shown in Figure 18 and Figure 19.

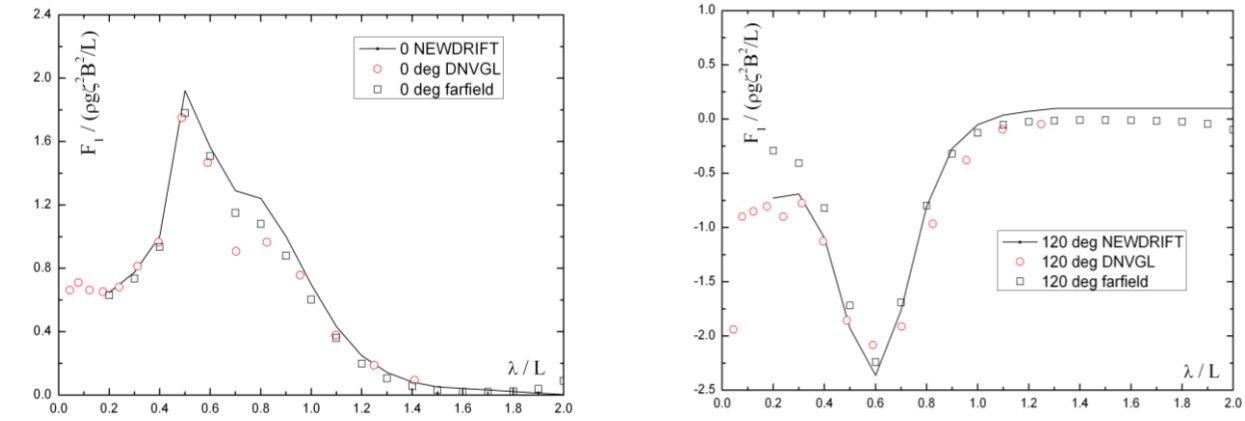


Figure 17: Drift force results on the KVLCC2 tanker in regular waves at 0° and 120° heading angles

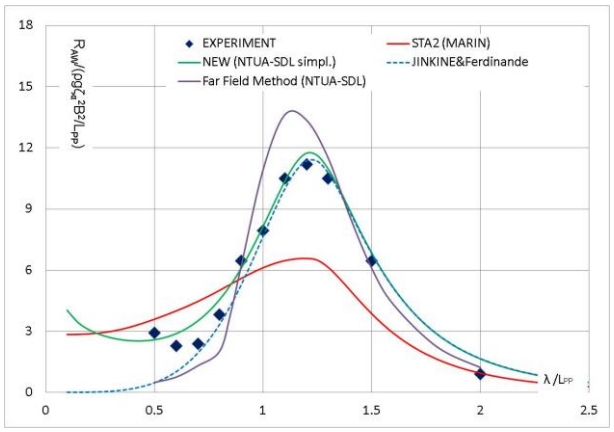


Figure 18: Added resistance of S175 containership in head waves by various methods, Fn=0.275

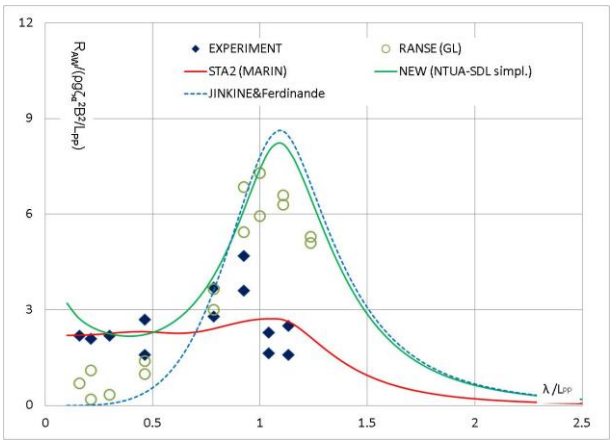


Figure 19: Added resistance of WILS II containership in head waves by various methods, Fn=0.183

DTU developed the OceanWave3D, a suite of potential flow solver tools for estimating the seakeeping and added resistance of a ship in waves. The tools are based on the high order finite difference method, see for

example (Bingham & Zhang, 2007), and two approaches have being developed and tested for representing the ship geometry: 1) overlapping boundary-fitted structured meshes, and 2) a novel immersed boundary method. The overlapping grid approach is built within the open-source Overture framework (Henshaw, Schwendeman, Banks, & Chand, 2016) and is described by (Amini Afshar, 2014). This code solves for seakeeping and added resistance using either the Neuman-Kelvin or the double body flow linearization of the problem and a pseudo-impulsive time-domain formulation. The immersed boundary technique is still in the early stages of development and is described by (Kontos S. , Bingham, Lindberg, & Engsig-Karup, 2016) (Kontos S. , Bingham, Lindberg, & Engsig-Karup, To appear). This method includes a new automated derivation procedure for implementing arbitrarily high-order Weighted Essentially Non-Oscillatory (WENO) schemes on uniform and non-uniform finite difference grids. Such a WENO treatment of the convective terms in the nonlinear, forward-speed free surface boundary conditions is shown to be robust and stable for all combinations of ship speed and wave celerity. This paves the way for extending the code to nonlinear wave-ship interaction. Significant progress has been made during this project on the development of two strategies for extending the OceanWave3D nonlinear potential flow solver strategy to treat the seakeeping and added resistance problems for ships. Convergence of the overlapping grid strategy for the Wigley hull has been demonstrated. The immersed boundary strategy has been validated for the linear response of a 2D floating cylinder. Validation results for the overlapping, boundary-fitted grid solver are shown in Figure 20 and Figure 21. The results for first order motions and added resistance are calculated for a Wigley hull at Fn=0.3 in head seas and are compared to model tests (Journee, 1992).

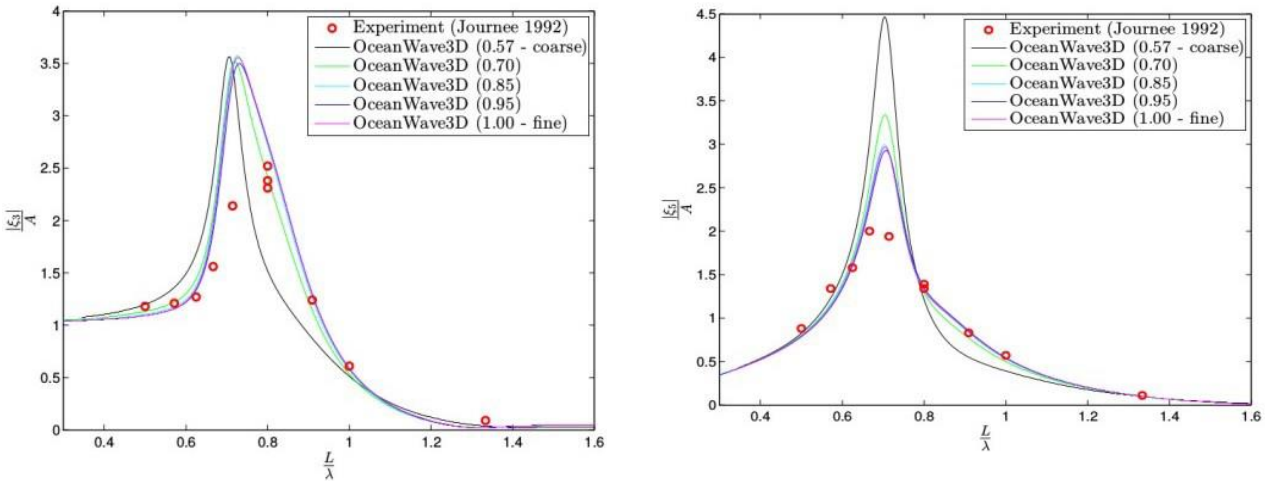


Figure 20: Convergence of the motion response amplitude. The incident wave amplitude is $\boldsymbol{A}$, the ship length is $\boldsymbol{L}$ and the wave length is λ.

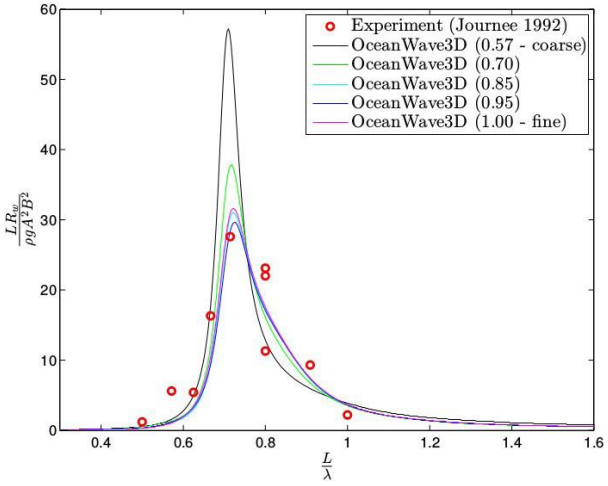


Figure 21: Convergence of the added resistance. The incident wave amplitude is $\boldsymbol{A}$, the ship has length $\boldsymbol{L}$ and beam $\boldsymbol{B}$, the wave length is λ while ρ and $\boldsymbol{g}$ are the fluid density and the gravitational acceleration.

### 2.2.2. Potential flow methods for maneuvering in waves

The potential theory code WAQUM 2 for the maneuvering of ships in waves was developed and verified in DNV legacy. WAQUM 2 is a merge of two in-house codes: WAQUM for time domain seakeeping by retardation functions and a “Life boat simulator” for the manoeuvring of a small vessel in large waves. This code combines ship manoeuvring with sea-keeping by force superposition to simulate ship responses in waves. The radiation force related to frequency dependent added mass and damping is modelled with convolution function. The transfer function of diffraction force is pre-calculated at different wave headings and wave frequencies in frequency domain, and saved as data base. WAQUM 2 interpolates the value with wave condition at each time step. Two different methods are developed to include mean added resistance in waves. The first one uses the quadratic transfer function of drift force at different wave directions and wave frequencies, which are pre-calculated at zero speed. WAQUM 2 transfers this quadratic transfer function from zero speed to small forward speed with Aranha’s empirical formula, see Aranha et al., 2001. This is only suitable for ships with low forward speed. The second method adopts the quadratic transfer function at different forward speeds. WAQUM 2 gets the real time added resistance through interpolation with ship speed at different time steps. The two methods can also be used together in the simulation. The first method is being adopted at low speed and the second method for high speed. Propeller KT, KQ curves are used for modelling the propeller, which is connected to an engine model. The engine model solves Newton’s second law equations for the crank shaft accounting for shaft speed, engine torque and propeller torque. The rudder model is implemented taking the effect of forward speed and propeller jet on the rudder force into account.

This code wass verified with the benchmark ship KVLCC2 in calm water. The verification in waves was performed for Fn =0. The comparison of the numerical simulation from the time domain code with the model tests on tuning circle with rudder angle equal to ±35 degrees are shown in Figure 22 (left). The numerical results from the time domain code are given by ‘blue line’. The ship trajectories with 35 degrees rudder from the model test is shown in ‘green line’ and trajectories with -35 degrees rudder from the model test is illustrated by ‘red line’. The diameter of turning circle from numerical simulation is larger than model test. It should be noticed that the numerical simulation is performed in full scale and the rpm of propeller is at the ship self-propulsion point. The model test is done at model self-propulsion point. The rpm of propeller and relevant rudder efficiency are hence different in this numerical simulation and the model test. This can partly explain that difference between numerical simulation and model test. In order to demonstrate this scale effect, the resistance coefficient in the time domain code was derived by CFD simulation at model scale Reynolds number, and the relevant rpm was set at model self-propulsion point. These simulation results are being compared with model tests in Figure 22 (right). The agreement has been improved. The diameter of the turning circle from the numerical simulation is now only slightly larger than that of model tests.

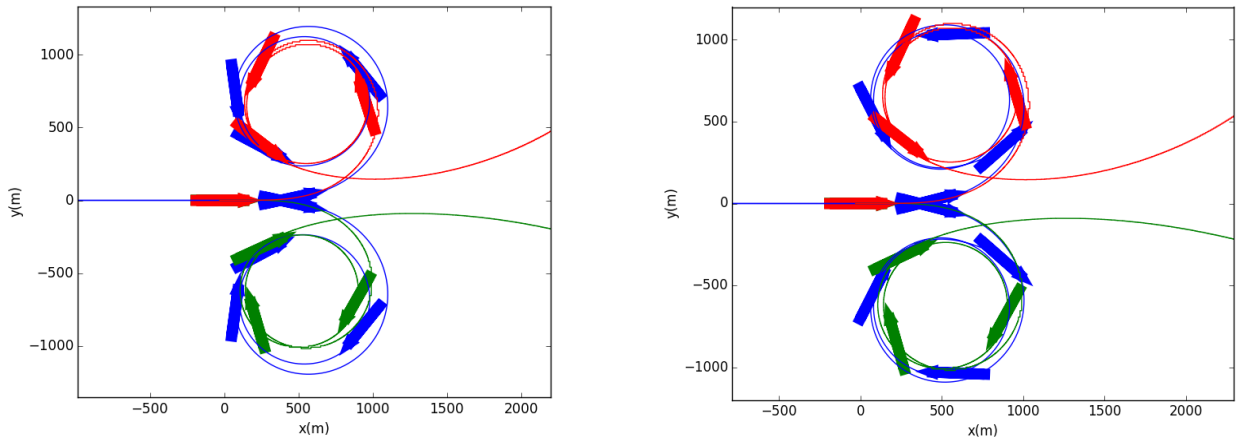


Figure 22: Comparison of turning circle between model test and numerical simulation at ship self-propulsion point (left) and at model self-propulsion point (right) - blue line is the simulation from time domain code, green line and red line gives the model test

NTUA-SDL focused on the coupling of HYBRID seakeeping code, which is a nonlinear time-domain code interfaced with the frequency-domain 3D panel code NEWDRIFT, with a manoeuvring model (HYBRID_MAN). The manoeuvring simulation model has been developed in SIMULINK and consists of two modules:

- The first module, which is based on Abkowitz's model and Nomoto's indexes, may be used for an assessment of the main ship design characteristics and features on ship stability and controllability.
- The second module, which is based on a formulation of the nonlinear equations of motion, enables the conduct of time domain simulation of different manoeuvre tests, according to IMO, such as turning circle, zig zag test etc. As a result, the characteristics of different manoeuvres can be predicted and analysed.

The set-up equations are derived by application of the Newtonian laws with respect to four degrees of freedom (surge, sway, yaw and heel), considering hull forces and moments induced by the propeller and the rudder, as well as external forces, such as wind and wave induced forces and their solution lead to a time domain prediction of the examined maneuverer. This code is also studied and verified with the model test on DTC standard containership (Figure 23, Figure 24). Hull forces and moments acting on the bare hull for DTC hull were herein estimated by CFD computations using the STAR CCM+ code (2016). The conducted research study and the shown numerical simulation results for the DTC standard containership have shown that the employed theoretical and numerical approaches to the determination of the manoeuvring equation components are satisfactory and the overall agreement of the obtained theoretical/numerical results with corresponding experimental data. The same is valid for the simulated turning circle manoeuvring trajectories, even though the effect of waves on the trajectories is less satisfactorily captured with increasing simulation time. The observed deviations, especially at following seas may be the result of the insufficiency of the second order force prediction of the DTC hull due to its peculiar hull form. It should be noted that the scale effect of the model in very short and steep waves may violate the assumption of the employed mathematical model.

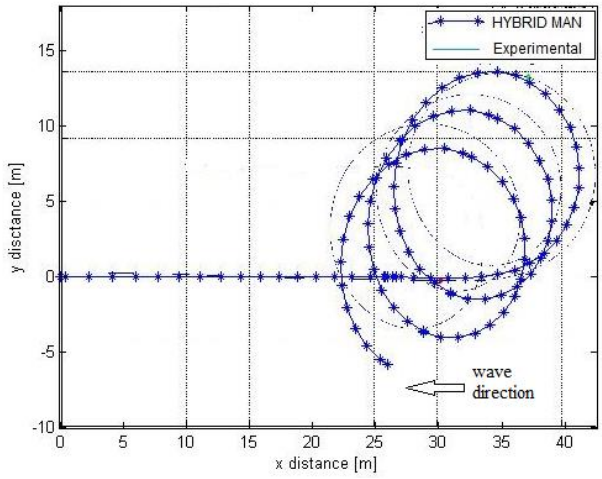


Figure 23: Test case 7080 (wave H=2m, T=12,5s)

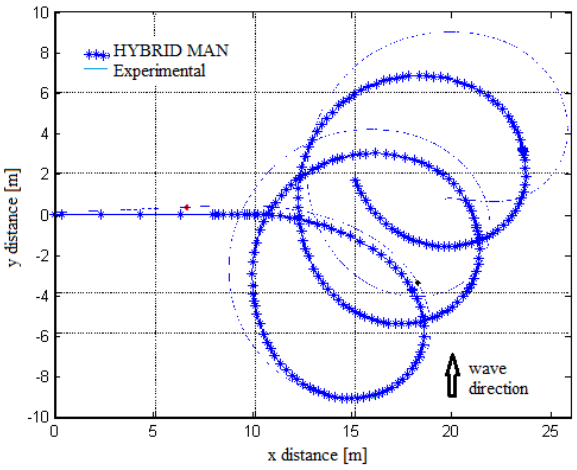


Figure 24: Test case 7010 (wave H=2m, T=10,5s, beam seas)

The existing quasi-static GLcourse computer code has been extended to time domain by including the Abkowitz model for manoeuvring. The result was a two time scale simulator, where it is assumed that the wave encounter periods are small compared to the manoeuvring time constants.

A code developed by IST for simulating the ship manoeuvring motion in regular waves has been revised and tested. The code is based on the seakeeping-type strip method fused with an empiric modular manoeuvring models. The fusion is performed in such way as to eliminate possibilities of double account of some categories of hydrodynamic forces.

RINA integrated a time domain seakeeping code, belonging to the ANSYS AQWA package, with manoeuvring models for simulating ship manoeuvring in waves. Radiation, diffraction and quadratic transfer functions derive from a frequency-domain analysis with a 3D panel code. Equations of motion (6 DOF) are solved in the time domain assuming that total forces and moments are the sum of the following contributions: diffraction, radiation (infinite-frequency coefficients and convolution integrals of impulse response functions), Froude-Krylov, hydrostatic, wave drift, hull manoeuvring (including hull lifting and cross-flow effects), resistance, propulsion and rudder (with propeller interaction).

### 2.2.3. Potential flow methods for manoeuvring in confined waters

The University of Strathclyde (SU) developed a numerical code to deal with the specific aspects of manoeuvring in shallow water as is required for port areas and channels. Given that these are restricted waters, waves are usually not important and thus an original manoeuvring code in calm water is the appropriate one for those conditions. A large number of validation studies have been carried out using the KVLCC2 ship particulars to investigate the manoeuvrability of the ship advancing in deep water and shallow water by using the in-house simulation program which is based on the Inoue model, the Kijima model, and the 3rd order polynomial model. Several CFD generated linear derivatives have been substituted to improve the accuracy of the simulations. Very satisfactory results have been obtained from comparisons with model tests and simulation results published by other organizations. For shallow water simulations, results are also reasonable when compared with a set of model test results which indicate that the shallow water effects can be clearly captured from the present simulations. Further validations on the DTC ship have also been carried out in deep and shallow water in the same manner as KVLCC2 case while the simulations apply the Kijima model and Inoue model respectively due to lack of precise nonlinear derivatives for the 3rd order model. Based on these works, an efficient way to predict the manoeuvrability of a ship navigating in shallow water while maintaining the precision has been established and the applicability of the corresponding empirical formulae to estimate the hydrodynamic coefficients is pointed out

In addition, SU proposed a methodology and developed the in-house BEM numerical program MHydro, to investigate the interaction between two vessels either overtaking or crossing each other in restricted waters. The code is based on the 3-D Rankine source method and it has been developed over a number of years. This code was originally developed to predict the hydrodynamic interaction between two ships which are stationary or advancing in waves with the same forward speed. It has been validated through two pairs of models in head seas (Yuan et al., 2014b; Yuan et al., 2014c). Based on the framework of MHydro, the University of Strathclyde has proposed an uncoupled method to predict the hydrodynamic interaction between two ships during encounter or overtaking operations in calm water and also in waves. The proposed method has been validated using a considerable body of experimental measurement data. Based on the findings from this stud, some guidelines for maximum speed and distance between two ships are provided to ship operators and designers.

The Instituto Superior Técnico (IST) continued the development and improvement of a double-body potential hydrodynamic interaction code based on the Havelock hypothesis and suitable for online simulations. The interaction code developed by IST initially was only dealing with the cases of deep water and flat bottom. In the latter case the mirror-image method was used with success. However, in practice the bathymetry can be arbitrary and the mirror-image method fails in this case. To deal with this situation the so-called moving patch method had been developed by IST. However, some preliminary tests performed prior to SHOPERA showed that while this method was adequate to the problem, its numerical behaviour presented some problems caused by the dynamic re-pavement creating additional numerical noise especially noticeable at coarse grids typically used for online simulations. To improve performance of the moving patch method, first, comparative computations aiming at establishing optimum size of the patch and optimum number of the underneath panels were carried out. Then, substantial efforts were invested in the development of a robust algorithm for dynamic automated pavement. This was achieved through combination of the Laplacian smoothing with the Blacker and Stephenson paving algorithm. Also, special measures were taken to avoid creation of “bad” elements. The new algorithm for fusion, stitching

and dynamic re-panelling of moving patches was developed and tested on scenarios of oblique crossing of a dredged channel with two ships. An alternative approach of the method avoiding dynamic re-panelling was also implemented and tested.

Independently of this, IST also developed a quite new variant of the potential panel method where dihedral panels are used instead of orthodox flat quadrilaterals. The non-penetration condition is then fulfilled in the integral sense with various degree of accuracy using Gauss integration. Internal validation of the new method demonstrated its advantages over the classic Hess and Smith algorithm providing substantially better accuracy at reduced number of panels especially in predicting the surge interaction force. As development of a reliable system identification procedure is important for estimating ship manoeuvring hydrodynamic characteristics from free-running tests, IST has also performed an advance in that direction having improved the earlier developed method based on the genetic global optimization in use of the Hausdorff distance as discrepancy measure.

### 2.2.4. Field Methods

Several simulations were performed for different ships in waves using the RANS solver OpenFOAM. Drift forces were computed for different heading angles and compared with available experimental data. Ships under investigation were the Wigley hull III, the Duisburg Test Case (DTC) containership, described by el Moctar et al. (2012) and a Cruise-Vessel. During these first studies, influencing parameters such as discretization, numerical setups and modes of motion were investigated. Achievements have been obtained with respect to the following aspects: Grid and convergence study, preliminary validation study for the calculation of second order wave forces and comparison between fixed and spring constrained surge motions on added resistance (Ley et al. 2014). The final objective is to develop off-line databases for second order wave forces, approximations of manoeuvring forces in shallow water, rudder forces behind the propeller in waves, a simplified unsteady model for a screw propeller and peculiarities of hull-propeller interaction coefficients in waves, obtained by a RANS solver.

The RANS code Neptuno developed by TUB (Cura Hochbaum & Voigt, 2002) has been enhanced with a new body force propeller model, allowing a better approximation of the rudder inflow and propeller torque. The code will be used to calculate forces on the hull due to waves, current and wind to derive a coefficient set including these environmental effects. The new body force model is based on a large set of RANS calculations for the isolated propeller rotating in homogenous inflow. The present calculations were made for a stock propeller with six blades, seen in Figure 25 on the left. The advance coefficient $J$ and the angle of incidence $\alpha$ were varied in a range from 0.1 to 0.9 and 0° to 30°, respectively. For each time step of the calculated case – which corresponds to a specific rotation angle of a considered propeller blade – the resulting pressure and shear stresses in each cell of a triangular grid on both the suction and pressure side of the blade are saved. The propeller disk is then discretized with a polar grid (right-hand side of Figure 25) and for each cell of this grid the three components of the mean force per unit area caused by all propeller blades over a complete revolution are calculated and stored in a database for each considered pair $J$ and $\alpha$. In addition, the corresponding induced velocities of the propeller in an upstream reference plane are saved as well. When setting up the RANS calculation of a forced motion test, each cell of the polar grid on the propeller disk gets mapped to a cell in the computational domain and vice versa. The individual inflow condition at this cell is then evaluated from the total local wake field.

There are three inflow parameters considered – the inflow speed and two angles, the first angle corresponding to the angle $\alpha$ mentioned above and the second one, which allows for turning back the current situation at the considered cell to the general situation assumed when generating the database, where the oblique propeller inflow was always horizontal. This makes it possible to take into account any inflow condition to the propeller as occurring for instance during sway and yaw motions of the ship. The body forces for each cell within the propeller region foreseen in the computational grid for the RANS simulation of virtual captive model tests are obtained from the database depending on the current inflow condition using a two-dimensional interpolation on $J$ and $\alpha$.

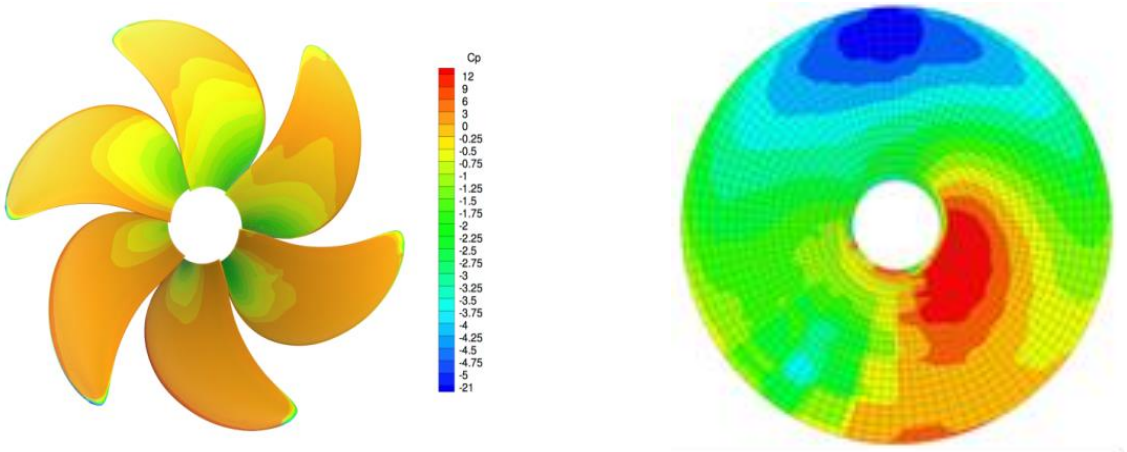


Figure 25: Pressure on blades during RANS calculation and mean axial force distribution on propeller disk

UDE developed an off-line database for mean second order wave forces. The motion and force RAOs are calculated for the DTC and the KVLCC2 in waves at a large range of encountering angles and wave lengths using the RANS solver OpenFOAM and other RANS methods. Calculated drift forces for different encountering angles were compared with available experimental data. To identify the effect of spring stiffness during the numerical tests, a stiffness study was performed. In addition, rudder deflection tests in bollard pull condition were performed in order to derive the resulting rudder forces.

Another approach that is being pursued by VTT is the simulation of ships in manoeuvring conditions by coupling a potential flow method for the representation of the propeller with a RANS solver, which simulates the bulk flow around the hull. The objective is to find a correction factor for the propeller wake in varying inflow conditions, in this way having the real wake field and propeller forces during manoeuvres. The correction factor approach is explained in detail in (Sánchez-Caja, et al., 2014) for straight ahead motion. In the present research the propeller suction is modelled as the suction of an equivalent actuator disk with angular varying loads. Only a one-cell layer of body forces is used in the propeller axial direction, even though more layers could be used if needed. The RANS code FINFLO was coupled with a propeller lifting line method for the prediction of the effective wake. The correction factors were calculated for a relatively light loaded propeller condition using circumferentially averaged values. Future work will consist of applying the correction factor approach to ship flow in manoeuvring conditions.

IST used OpenFOAM to calculate calm water resistance and drift velocity dependant forces for the KVLCC2 and the RoPax ferry, employing the morphing mesh technique to allow ship motions. Results for the free surface wave elevation along the hull and at y/Lpp=0.0964 obtained with OpenFOAM are presented in Figure 26 and Figure 27 respectively and compared with experimental measurements. From these forces, the sway dependant force coefficients are derived and compared to values available in international literature. A study on shallow water influence on the ship resistance was performed for the KVLCC2 and the added resistance in head seas was computed.

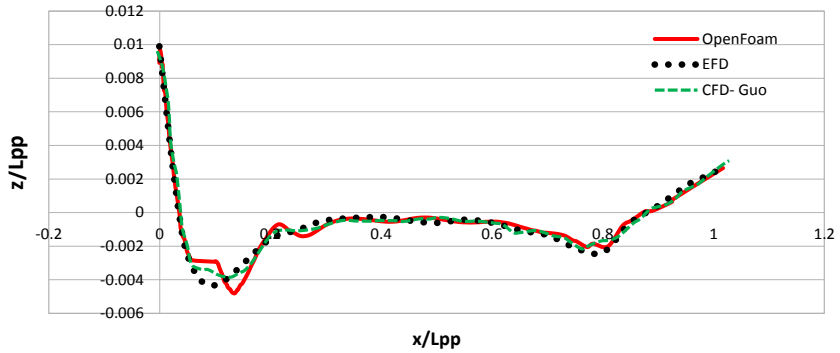


Figure 26: Free surface wave elevation along the hull

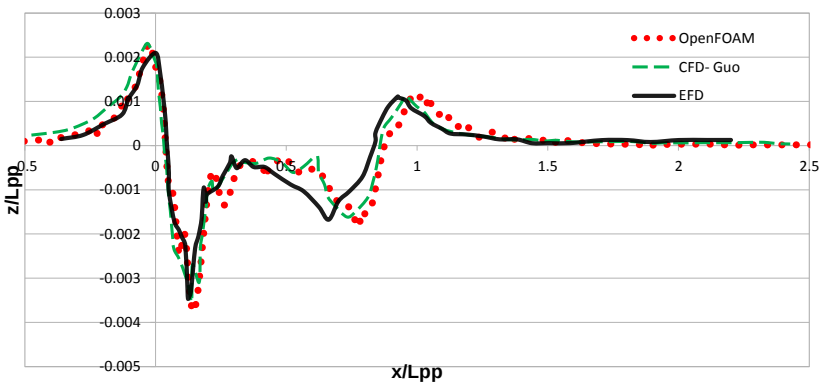


Figure 27: Wave profile at y/Lpp=0.0964

SU carried out selected simulations of the case study vessel KVLCC2 in order to validate the used numerical field method. Simulations were performed at model scale for direct comparison with tank model tests and linear and nonlinear manoeuvring coefficients were predicted. For the coefficients prediction, linear and large amplitude PMM tests were performed. The obtained coefficients were also used within SU's activities, to enhance potential flow method based predictions in confined waters.

LR calculated RAOs of added resistance in head seas at 6kn and 16kn with the code StarCCM+. The obtained results were compared with experimental data and several numerical methods.

Finally, NTUA also worked with StarCCM+ and calculated calm water resistance, drift forces and added resistance in waves for the DTC and KVLCC2 hulls (Figure 28, Figure 29). Obtained results were compared with experimental data and were found in good agreement (Papanikolaou et al, 2016).

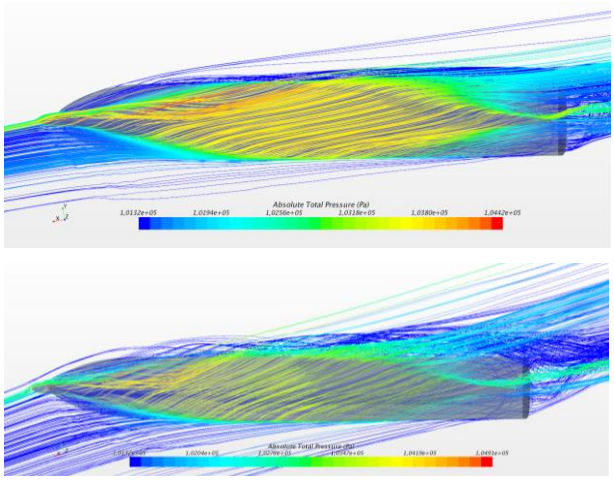

Figure 28: Flow streamlines around the DTC hull exposed to static drift for β=10, 20 deg, at 20kn. Colours refer to total pressure

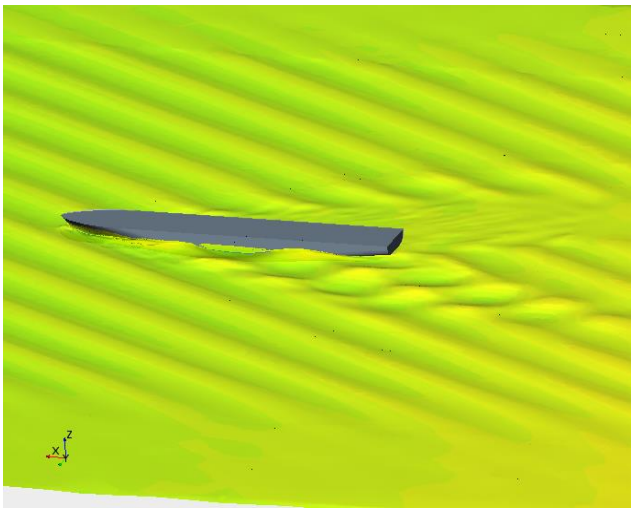

Figure 29: Wave patterns for the DTC 2270 case after 3 wave periods, at 0kn and λ/L=0.21

## 2.3. Experimental Studies

The SHOPERA model tests specification included more than 1,300 different tests, distributed among the partners for three hull designs of different hydrodynamic characteristics (DTC post-panamax container vessel, KVLCC2 tanker and a RoPax ferry, which is not part of this publication). The workload is shared with CEHIPAR, Flanders Hydraulics Research (FHR) and Technische Universität Berlin (TUB). The aim of the model tests in SHOPERA is to close gaps in available benchmark data and broaden the database test results for manoeuvring in waves and seakeeping.

### 2.3.1. The Ship Models

The KVLCC2 is a VLCC-type vessel, representing the second variant of a modern tanker design developed by the Korean Institute of Ship & Ocean Engineering (KRISO) with bulbous bow and U-shaped stern lines (see Figure 30 and SIMMAN Homepage, 2008). The hull lines have been exclusively developed for testing and benchmarking and no full scale ships of that type exist. The main particulars of this vessel and the loading conditions of the model for scantling draught and heavy ballast are given in Table 6 in full scale. Within the SHOPERA project, the KVLCC2 design has been tested in deep water at CEHIPAR (scale 1:80) and in shallow water at Flanders Hydraulics (scale 1:75).

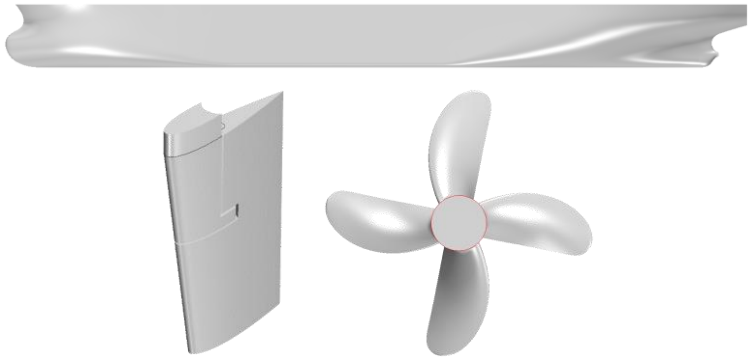

Figure 30: View of the KVLCC2 hull (top), the rudder (bottom, left) and the propeller (bottom, right)

The Duisburg Test Case (DTC) design is a post-panamax 14000 TEU container vessel, developed at the Institute of Ship Technology, Ocean Engineering and Transport Systems (ISMT) of the University of Duisburg-Essen for benchmarking and validation of numerical methods and its lines are available to the public (see Figure 31). The main particulars of this vessel and the loading conditions of the model for the design draught and light ballast are given in Table 6 in full scale. Within the SHOPERA project, the DTC design has been tested in deep water at MARINTEK (scale 1:63.65) and in shallow/intermediate water at TUB and FHR (scale 1:89.11).

Table 6: Main particulars and loading conditions for the KVLCC2 and DTC (all values refer to the origin located at [AP/CL/BL])

| | | KVLCC2 | | DTC | |
|---|---|---|---|---|---|
| $L_{pp}$ | [m] | 320.0 | | 355.0 | |
| B | [m] | 58.0 | | 51.0 | |
| $C_B$ | [-] | 0.8098 | | 0.661 | |
| | | Scantling Draught | Heavy Ballast | Design Draught | Light Ballast |
| $T_{FP}/T_{AP}$ | [m] | 20.8/20.8 | 8.2/11.5 | 14.5/14.5 | 7.8/11.0 |
| $\nabla$ | [t] | 320438 | 133186 | 173468 | 104102 |
| LCG | [m] | 171.1 | 169.0 | 174.059 | 170.460 |
| VCG | [m] | 18.56 | 11.17 | 19.851 | 16.56 |
| $GM_T$ | [m] | 5.71 | 21.4 | 5.1 | 12.4 |
| $r_{xx}$ | [m] | 23.2 | 23.2 | 20.3 | 20.1 |
| $r_{yy}$ | [m] | 80.0 | 80.0 | 87.3 | 95.9 |
| $r_{zz}$ | [m] | 80.0 | 80.0 | 87.4 | 96.9 |

### 2.3.2. Added Resistance and Drift Forces

The added resistance and drift force tests have been conducted in steep regular waves and selected irregular sea states. At MARINTEK, the wave climates have been generated along the limiting curves of the wave makers in a range of $0.1 \leq \lambda/L_{pp} \leq 1.2$. Due to the high wave steepness and the extension of the testing range into oblique seas and the short relative wave length region (diffraction dominant domain), the results

obtained at MARINTEK offer valuable insights and contribute to an enhanced benchmark and validation database compared to the currently available state-of-the-art.

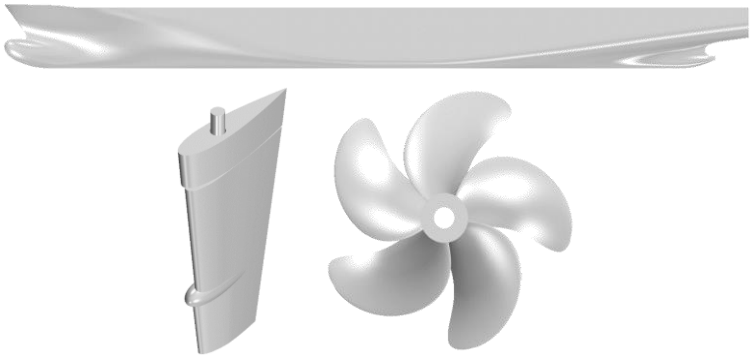

Figure 31: View of the DTC hull (top), the rudder (bottom, left) and the propeller (bottom, right)

### 2.3.2.1. Experimental Setup DTC, Deep Water

For the added resistance tests in deep water at MARINTEK, the DTC model was captive in a soft-mooring arrangement as visualized in Figure 32. Lightweight lines were used and the spring stiffness has been chosen such that the eigenfrequency of the mooring in the relevant direction is less than 1/6th of the lowest wave encounter frequency. A supplementary set of force transducers was installed in the aft and fore joints of the lines to ensure consistency in the measurements. For the drift force tests in deep water, the DTC model was captive in a soft-mooring arrangement as visualized in Figure 32 and held at position/towed by the gondola at constant speed. Light weight lines were used and the spring stiffness has been chosen such that the eigenfrequency of the mooring in the relevant direction is less than 1/6th of the lowest wave encounter frequency. At the same time, the aim was to minimize the yaw drift angle (it was kept within ±2°).

A transverse beam was mounted to the gondola and the lines were deflected by low friction pulleys to align and attach the springs vertically. Force transducers were mounted forward of the bow and behind the stern at CL and KG. A supplementary set of force transducers was installed in the lines to ensure consistency in the measurements. The model was fitted with segmented bilge keels, rudder (fixed at 0° rudder angle) and rudder box during this set of tests.

All wave environments have been measured without the presence of the model for reference. For drift force tests, the gauge was located at the model position and for added resistance in a representative location between starting position and wave maker.

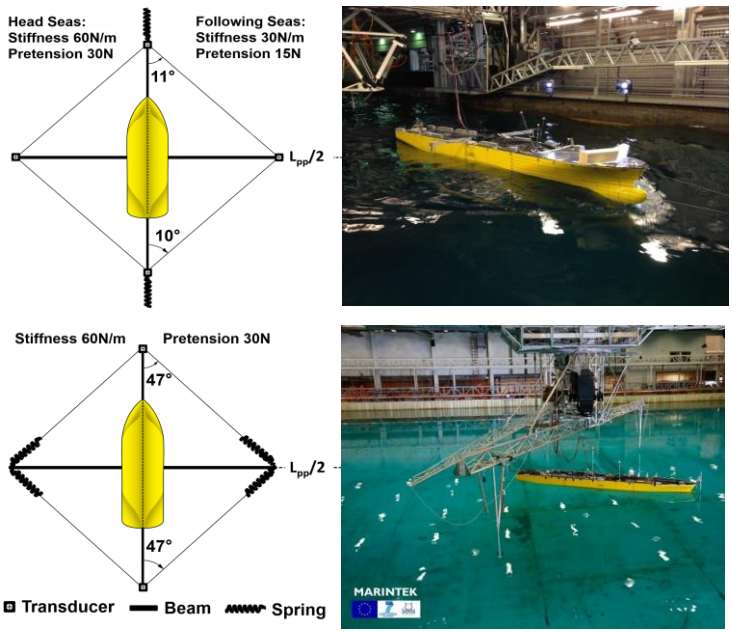


Figure 32: DTC model in soft-mooring arrangement for added resistance (top) and drift force tests (bottom) at MARINTEK (left: schematic sketches, right: impressions from model tests)

### 2.3.2.2. Experimental Setup KVLCC2, Deep Water

To measure the mean drift forces in regular waves and deep water conditions at CEHIPAR, the model was restrained with a soft mooring system consisting in four lines arranged in the shape of a diamond in the horizontal plane. The geometry of the system is given in Figure 33 (left). The objective of the soft mooring is

to be able to measure the drift forces while keeping the orientation of the model and influencing its motions the minimum possible. To this purpose, the mooring was designed such that the natural resonance periods in surge, sway and yaw were well above the period of the largest wave to be tested. The arrangement allows to easily change the orientation of the model with respect to the waves just by slowly rotating the turret of the CPMC. The same arrangement was used for the added resistance tests in regular and irregular waves by moving the carriage at the desired speed. The incoming wave has been measured by a wave probe forward of the model. This measurement is affected by the wave reflections from the model. The undisturbed reference wave height was also measured in absence of the model.

The vessel motions in 6 DOF were measured by an optical tracking system (Krypton). Wave forces were measured by two six component dynamometers, one at the bow and one at the stern at the points of attachment of the mooring lines. Additional load cells were mounted in each line.

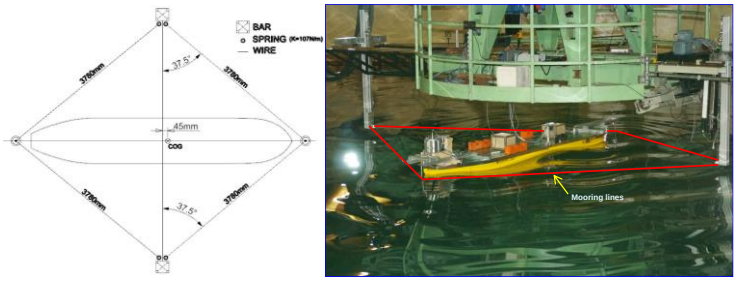


Figure 33: Mooring arrangement for the drift force tests with the KLVCC2 model at CEHIPAR

Both the dynamometers and the load cells can be combined separately to give two different estimates of the surge and sway forces and the yaw moment so giving some redundancy. The results from the load cells gave similar results to those of the dynamometers except that they are slightly lower due, probably, to friction at the pulleys used to connect the wires to the springs and load cells. All results presented in the following are direct measurements from the dynamometers.

### 2.3.2.3. Experimental Setup KVLCC2 & DTC, Shallow Water

At FHR, captive model tests have been performed with a 1:75 scale model of the KVLCC2 and a 1:89.11 scale model of the DTC in the Towing Tank for Manoeuvres in Shallow Water (co-operation with Ghent University, see Figure 34). The KVLCC2 was tested at scantling and heavy ballast draught and the DTC at design loading condition, see Table 6. The considered under keel clearances are expressed as a percentage of the draft at the aft perpendicular and have the following magnitude:

- 30% and 20% for the KVLCC2, the latter only at scantling draft;
- 100% and 20% for the DTC.

The sailing speeds were 0, 6 and 12 knots full scale for the KVLCC2 and 0, 6 and 16 knots for the DTC. At 0 kn, the drift angles were varied for the KVLCC2 (30% ukc only) to investigate various incoming wave angles (0 to 150° in steps of 30°, which corresponds with the interval from head to stern quartering waves).

At FHR the tests have been performed with fully restrained surge, sway and yaw, while heave, roll and pitch were free. During the tests the wave climate was measured at the four positions in the Towing Tank. Waves were varied in length between 0.2 and 1.2 $\lambda/L_{pp}$.

Figure 34: Impression of the KVLCC2 (top) and DTC model (bottom) in the captive test setup at FHR

The possible wave height is strongly dependent of the shallow water effects, which put a limit on the maximal wave height that can be tested. Moreover, in order to avoid transient effects, the ship velocity

may further reduce the maximal achievable wave height. For a selection of wave lengths, 50% and 70% of the wave heights listed in Table 7 were also tested. The movement of the vessel in the vertical plane (heave, pitch, roll) is measured using four gauges, connected to the fixed frame of the towing tank carriage. These four gauges are located at four fixed positions, which enables to compute the ship's heave, pitch and roll during the tests. The force and moment components which are mentioned in the output file (X,Y,N) are also calculated based on the results of four separate force gauges.

The total X-force can be simply calculated as the sum of the fore and aft longitudinal force measurement. Similarly, the Y-force is obtained by addition of the fore and aft (lateral force measurement. The yaw moment is calculated based on the longitudinal positions of the Y-force measurement gauges. A useful time window is then determined based on the following constraints:

Table 7: Base prototype wave heights at FHR

| Ship | ukc | Velocity [kn] | Wave height [m] |
|---|---|---|---|
| KVLCC2 - scantling | 30% | 0 – 12 kn | 2.25 |
| | 20% | 0 – 12 kn | 1.50 |
| KVLCC2 – ballast | 30% | 0 – 12 kn | 1.50 |
| DTC | 100% | 0 – 16 kn | 5.00 |
| | 20% | 0 – 6 kn | 2.00 |
| | | 16 kn | 1.20 |

- Constraint 1: The velocity of the vessel is constant;
- Constraint 2: A fully developed regular wave system is present;
- Constraint 3: The transitional effects, which are present when the ship moves from calm water to waves, have disappeared;
- Constraint 4: The reflected waves (on ship model, tank wall and wave generator) have not yet reached the ship model.

Within this time window, a Fourier analysis is applied to determine the mean value $a_0$ and the harmonic coefficients $a_1...a_4$ and $b_1...b_4$ of each measurement:

$$f = a_0 + a_1 \cdot cos(\omega \cdot t) + b_1 \cdot sin(\omega \cdot t) + a_2 \cdot cos(2 \cdot \omega \cdot t) + b_2 \cdot sin(2 \cdot \omega \cdot t) + a_3 \cdot cos(3 \cdot \omega \cdot t) + b_3 \cdot sin(3 \cdot \omega \cdot t) + a_4 \cdot cos(4 \cdot \omega \cdot t) + b_4 \cdot sin(4 \cdot \omega \cdot t)$$

The added resistance is then the $a_0$ value in a regular wave climate minus the $a_0$ value in calm water for the same ship model sailing the same trajectory (straight-line, same velocity).

#### 2.3.2.4. Experimental Setup DTC, Intermediate Water Depth

Added resistance and drift force tests have been performed in the seakeeping basin of TUB. The DTC model was tested at scale 1:89.11 at a water depth of 1 m leading to a UKC of 613% (corresponding to a water depth to draught ratio of 7.13) in the design condition. Due to the very slow forward speed considered, no shallow water effect is expected in calm water. However for waves longer than 2 m a certain influence of the bottom on the waves will be present due to the finite water depth. During all performed model tests at TUB, the DTC model was equipped with segmented bilge keels and rudder. The propeller was not present. The performed tests consisted in added resistance tests in regular head waves with two model speeds corresponding to 8 kn and 16 kn in full scale and zero speed drift force tests, where mean forces and moments are measured. In the latter case, the incident wave angle was varied in 30° steps from head to following seas in order to obtain wave forces from all directions for manoeuvring prediction purposes. Seven wave lengths ranging between 0.35 λ/Lpp and 1.2 λ/Lpp were selected for all testing conditions. The wave steepness was kept constant at H/λ=0.02 for all waves. Note that for this steepness the Airy (linear wave) theory is not completely valid any more. To investigate the influence of the wave steepness, two additional tests with a modified wave amplitude were performed in each condition for the shortest wave and for the wave length leading to the maximum RAO value of the most relevant force involved.

In the scope of this research project a new measurement platform has been developed at TUB, especially designed to determine hydrodynamic forces and moments acting on a ship model in waves. Thereby the 6-DOF motions of the model are measured as well. The new device, shown in Figure 35, has been designed such that the model motions are constrained as far as possible in order to minimize influences on the registered time traces and mean values of forces and moments. The measurement platform is coupled with the towing carriage and consists of two nested slides (front and back). Each slide consists of a Δy-slide for

transversal motion and a nested Δx-slide for longitudinal motion, both displacing with low friction linear ball bearings on steel rails. The slides are softly hold at a mean position by springs connected to each slide. Due to the motions of the slides, the model can move in the horizontal plane, only restricted by spring stiffness and a maximum motion amplitude of each slide of 0.2 m. Each Δx-slide has a vertical “heave rod” connected to the model via a rod end to allow free heave, roll and pitch motions. Between each rod end and the model a force gauge is placed to measure the forces at these two points. With these measured forces and knowing the position of the force gauges, the global longitudinal and transversal force on the model in ship fixed coordinates as well as the yaw moment are obtained. If the pure hydrodynamic forces are sought, i.e. for direct comparison with CFD results, they can be obtained from these forces after deduction of weight and inertial force contributions. The model motions are measured with a set of ten cable actuated distance sensors with low friction. This redundant arrangement has been chosen for minimum motion interference. With the signals of six distance sensors the motion parameters can be determined in real time during the tests allowing for an accurate calculation of all inertial contributions.

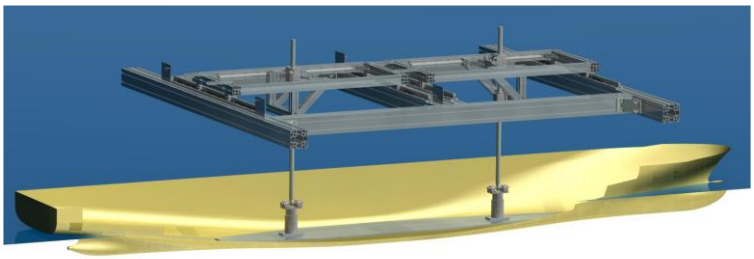

Figure 35; Measurement platform developed and used for added resistance and drift force tests at TUB

### 2.3.2.5. Selected Results DTC

The added resistance of the DTC hull was measured in a range of $0.1 \leq \lambda/L_{pp} \leq 1.2$. The shortest waves were measured at MARINTEK, with the wave maker operating at its lower limit and the wave time series reveal that the waves are not as stable as for the other periods. While the measured total longitudinal forces are very similar for the three investigated wave heights at $\lambda/L_{pp} = 0.1$, the RAO data is scattered. This is caused by the normalization with very small values (squared wave amplitudes) that amplify the uncertainties of the experimental data. However, there is a tendency that the RAO values for the added resistance increase for shorter relative wave lengths. This range is of particular interest for large vessels since it covers normal operating sea states (for the DTC, $\lambda/L_{pp} = 0.1$ is equal to a wave length of 35.5 m or a wave period of 4.77 s in deep water). Three different water depths, under keel clearances (ukc) and wave steepness have been considered for the added resistance tests with the DTC hull at design draught at 6 kn and 16 kn forward speed. For 6 kn, the measured normalized added resistance values are increasing with increasing water depth and ukc (see Figure 36, left). While the magnitudes of the RAOs are different, the overall tendencies are similar (as far as evaluable from the data points), the peak of the RAO is located around $\lambda/L_{pp} = 0.8$. For the 16 kn case, as presented in Figure 36 (right), the normalized added resistance RAO values for deep water (636.5 m water depth at full scale, blue), intermediate water depth (89.11 m water depth at full scale, purple) and the 100% ukc condition (29.0 m water depth at full scale, red) are very similar without a clear trend regarding the influence of the water depth. The normalized added resistance at 20% ukc (17.4 m water depth at full scale) is significantly higher for all investigated wave conditions. However, looking at the actual forces presented in full scale in Figure 37, it becomes evident that the values measured for 20% ukc are the smallest. There are several effects that lead to the high normalized values as shown in Figure 36: The static ukc for these runs is 20% (or 3.25 cm at model scale). The sinkage measurements from these runs however reveal squat effects leading to a dynamic ukc of only 10.7% (or 1.75 cm) in calm water and 0.9% (or 0.15 cm) in the presence of waves. This is certainly an extreme condition where the vessel is sailing in the boundary layer of the bottom flow of the towing tank, which is estimated to be 7.6 cm thick, according to Prandtl's law. The effect of this on the added resistance is not known.

Due to the very low ukc, the wave amplitudes had to be very small (0.6 m full scale, or 6.7 mm at model scale) in order to avoid that the heave and pitch motions cause bottom contact of the ship model. For very

small wave amplitudes, measurements and accuracies are challenging, but also the amplitude-squared relation between incident wave and mean added resistance seems to be questionable. This well-established relation has been found to be valid in the longer wave regime in deeper water, as deducible from Figure 36 and Figure 37. The different force levels in Figure 37 are resulting from different wave amplitudes (steepness) in the tests. At $\lambda/L_{pp} = 1$, the full scale wave amplitudes at MARINTEK (blue dots) are 6.25 m, 4.7 m and 3.1 m. The full scale amplitude at TUB is 3.1 m (purple dots) and at FHR 2.5 m (100% ukc, red dots) and 0.55 m (20% ukc, green dots). The two measured force values for the same wave amplitude are very similar, and the forces for different amplitudes are clearly increasing with the squared-amplitude of the wave. Further added resistance tests with a lighter loading condition for the DTC (light ballast, c.f. Table 6) have been performed at TUB for 8 kn and 16 kn forward speed. As expected, the non-dimensional added resistance increase with increasing forward speed, accompanied by a shift of the peak towards longer waves (see Figure 39). Systematic experimental data for added resistance in oblique seas is not easily available. Series of tests with the DTC at design loading condition have been performed at MARINTEK, with varying encounter angle from head (0°) to following seas (180°) in 30° intervals. The results are summarized in Figure 38. The highest forces have been measured in head seas and bow quartering seas (waves 60° off the bow), where the peak of the RAO is shifting towards shorter waves for increasing wave encounter angles. In shorter waves $\lambda/L_{pp} < 0.3$, the added resistance is similar for headings from 0° to 60°. At 120°, the measured added resistance is small, changing sign at $\lambda/L_{pp} = 0.25$. From 150° to 180° (stern quartering to following seas), the added resistance becomes negative, i.e. the vessel experiences a pushing effect rather than a resistance caused by the presence of the waves. The results of the added resistance tests at 16 kn forward speed are shown in Figure 40.

The added resistance coefficient measured with the wave steepness H/λ=0.02 mentioned above, plotted over the wave length (red curve), behaves as expected. This force RAO has a peak at about $\lambda/L_{pp} = 0.85$ and decreases towards long waves. The variation of the wave amplitude (green dots in Figure 40) shows that the added resistance varies slightly, decreasing for larger wave steepness. For the shortest wave length $\lambda/L_{pp} = 0.35$ the steepness of waves W11 and W12 were 0.029 and 0.037, respectively. For the wave length $\lambda/L_{pp} = 0.85$ the steepness of waves W51 and W52 were 0.014 and 0.026, respectively. In addition, the pure hydrodynamic mean force from tests with constant steepness (orange line in Figure 40) is up to 20% larger than the measured force (including inertial effects) for wave lengths above $\lambda/L_{pp} = 0.6$. Figure 41 shows the non-dimensional longitudinal and transversal mean forces as well as the mean yaw moment measured for all considered encountering angles and wave lengths for the DTC at zero speed. In the diagrams especially short wave phenomena are noticeable, e.g. the longitudinal force $F_X'$ at μ=90° has a significant negative value for wave lengths up to $\lambda/L_{pp} = 0.4$, whereas wave lengths above $\lambda/L_{pp} = 0.5$ yield almost no mean value. Also for the yaw moment $M_Z'$, the short waves generate a mean moment at μ=90° and the zero-crossing angle is shifted towards μ>100°. Note that during a large number of tests, the DTC experienced stern slamming, even in very short bow quartering waves of moderate steepness. This may explain the very high non-dimensional side forces shown in Figure 41.

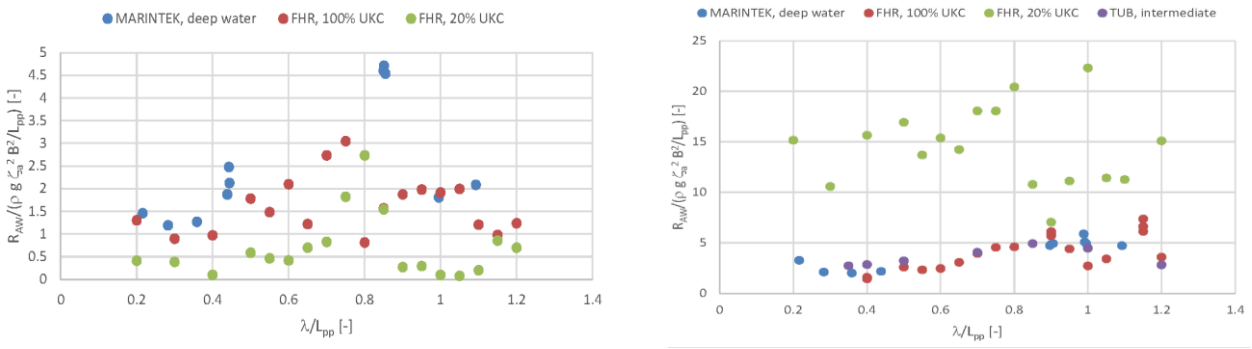


Figure 36: Comparison of normalized added resistance data measured with the DTC model at design draught at 6kn (top) and 16kn forward speed (bottom) in different water depths

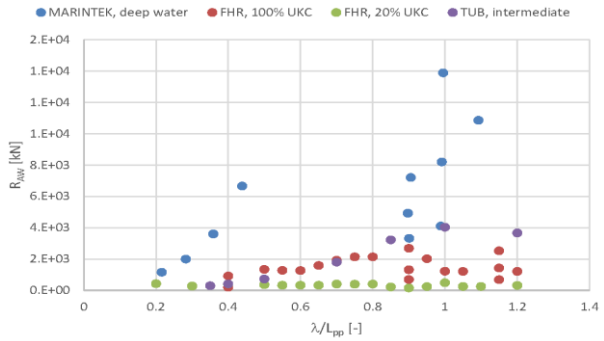


Figure 37: Full scale added resistance for the DTC model at design draught at 16kn forward speed

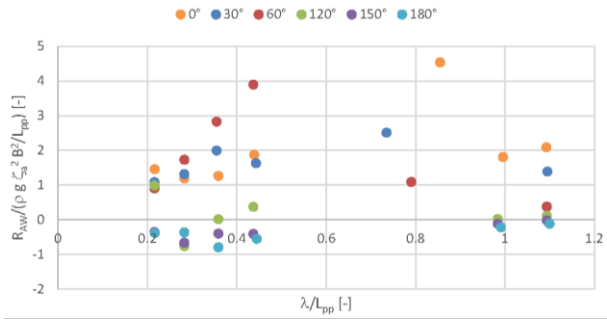


Figure 38: Added resistance data for the DTC model at design draught and 6kn forward speed in deep water and different wave headings (0° denotes head seas)

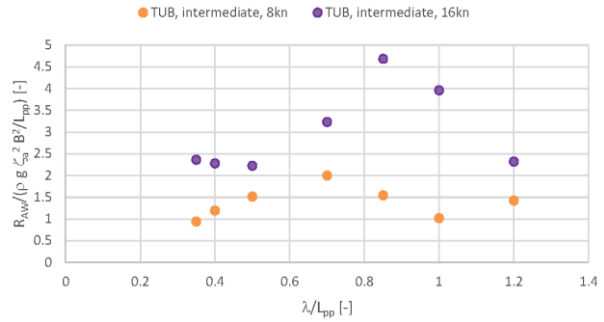


Figure 39: Added resistance for the DTC model at light ballast with 8 and 16kn forward speed in intermediate water depth

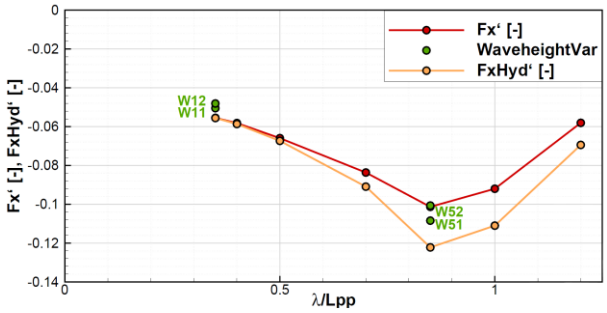


Figure 40: Measured added resistance for the DTC at 16 kn (TUB)

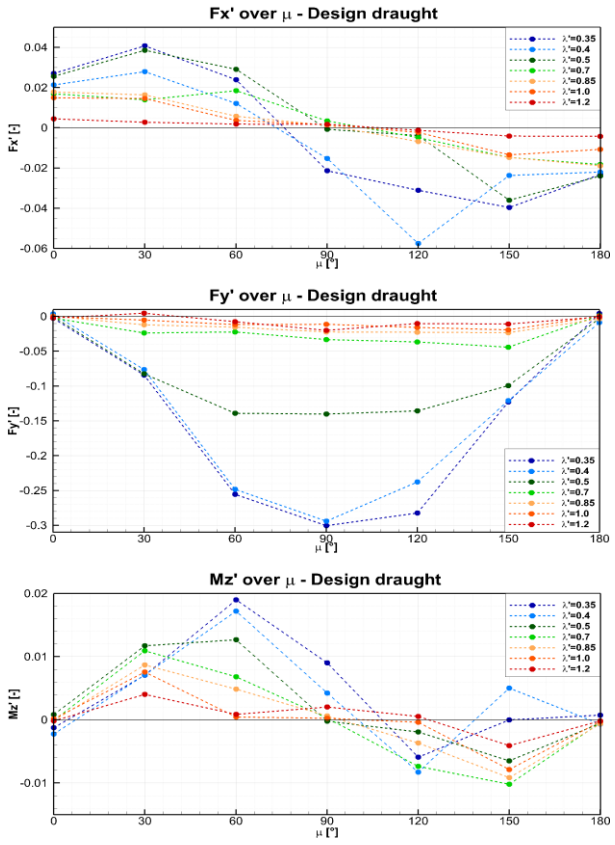


Figure 41: Longitudinal force, transversal force and yaw moment (from top to bottom) due to waves at zero speed (TUB)

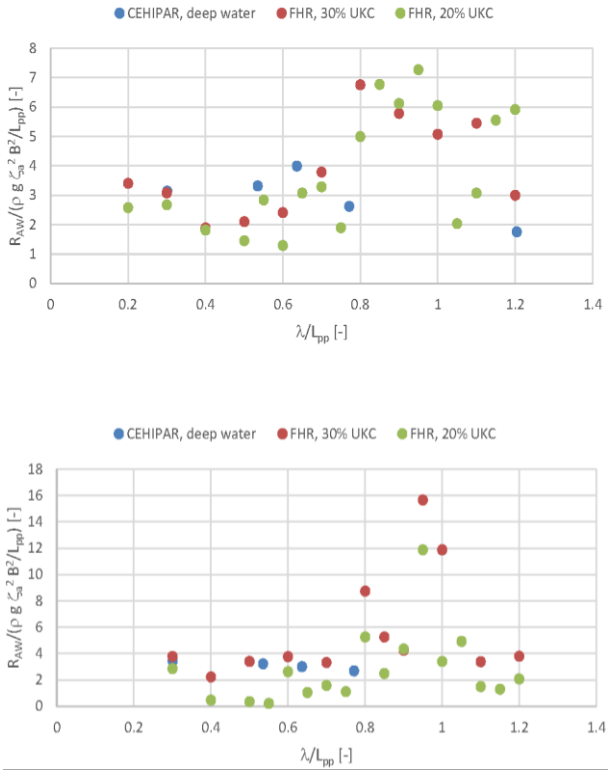


Figure 42: Comparison of added resistance data measured with the KVLCC2 model at scantling draught at 6kn (top) and 12kn forward speed (bottom) in different water depths

#### 2.3.2.6. Selected Results KVLCC2

For the added resistance tests with the KVLCC2 at scantling draught, three different water depths and under keel clearances (ukc) have been considered as well. In Figure 42 (left), the measured normalized added resistance values for 6 kn forward speed are shown. A similar tendency as for the DTC results can be observed: the RAO values are increasing with increasing water depth and ukc – apart from the last data point in deep water. In shallow water, the peak of the RAO is located around λ/Lpp = 0.8, while it appears to be at λ/Lpp = 0.65 in deep water. For the 12 kn case, as presented in Figure 42 (right), the added resistance RAO values for deep water (400 m water depth at full scale, blue) and 30% ukc condition (27.0 m water depth at full scale, red) are very similar in the range $0.3 \leq \lambda/L_{pp} \leq 0.8$. The lowest added resistance values are obtained for the 20% ukc condition (25.0 m water depth at full scale, green).

Another focus of the experimental program of the SHOPERA project lies on the measurement of drift forces in regular waves. For the KVLCC2, numerous drift force tests have been conducted both in deep water at CEHIPAR and in shallow water conditions at FHR. The tendencies for the longitudinal forces are similar as for the added resistance results: the RAO values for deep water and 30% ukc condition are very similar in the range $0.3 \leq \lambda/L_{pp} \leq 0.8$. For longer waves the forces in shallow water are increasing towards a peak around $\lambda/L_{pp} = 0.9$ while they are decreasing in deep water. The normalized lateral forces for both water depths are very similar for $\lambda/L_{pp} \geq 0.4$. For shorter waves, the RAO values in deep water are increasing while they are almost constant in shallow water. The tendency of the yaw drift moment is very similar for both water depths, with changing signs between $0.2 \leq \lambda/L_{pp} \leq 0.6$. The magnitude of moments in shallow water is larger than in deep water conditions.

#### 2.3.2.7. Selected Results DTC

The first step of testing was the establishment of the propeller open water characteristics. The open water characteristics of the DTC propeller have also been established in SVA Potsdam at a different scale (1:59.406). Both measurement agree quite well. For the propulsion tests in waves, the DTC model has been tested at design draft and parameters of variation were the propeller rpm and the wave period. One calm water reference run, ten runs in regular waves and three runs in irregular waves have been conducted. However, the iterative approach to find the correct setting to obtain a mean speed of 6 kn and 10 kn, respectively, in each wave condition led to a higher number of runs. For each wave period, two wave heights have been tested. Despite the well-tuned and operated online autopilot, severe course-keeping problems have been encountered for all regular waves with periods higher than 5 s (full scale) after a certain number of encountered waves. During the tests, it became clear that a free-running model is not controllable in regular waves with an encounter period close to the vessels natural periods in heave and pitch. The motions become very high and the vessel is in a 'locked' situation, where an increase of propeller revolutions does not lead to an increase of forward speed until a certain threshold is passed and the vessel speed suddenly 'jumps' up and the motions decrease again. The overall behaviour in regular waves with an encounter period close to the vessels natural period in pitch can be characterised as instable. Therefore, the tests in longer waves have been run with 10 kn mean forward speed against the waves instead of 6 kn. A maximum rudder angle of 2-4° was require to keep course.

From the results it became clear that the propulsion characteristics such as propeller thrust, torque and revolutions are influenced by the present waves. While the measured values for the a mean speed of 6 kn in the shortest wave (5 s full scale) are very close to the calm water values for the same, the measured values for 10 kn forward speed and longer regular waves (10-15 s full scale) are clearly higher than for the associated calm water case. Thrust, torque and rpm reach a maximum for a full scale period of 13.9 s (11.2 s encounter period), which is close to the vessels natural period in pitch, where added resistance is very high. An increase in wave height for the same period leads to a clear increase in thrust, torque and revolutions to maintain the same mean forward speed.

Figure 43 show the results of the bollard pull tests with the DTC at model scale: The graphs show the longitudinal rudder force, the lateral rudder force, the rudder moment and the pull force for three different propeller revolution settings, corresponding to 30%, 75% and 100% MCR. As typical for model tests at

Froude identity where viscous effects are not scaled correctly, rudder stall occurs already for lower rudder angles than at full scale. This is observable by a decrease of the longitudinal rudder force for rudder angles greater than 20°, for the lowest RPM setting even from 15°.

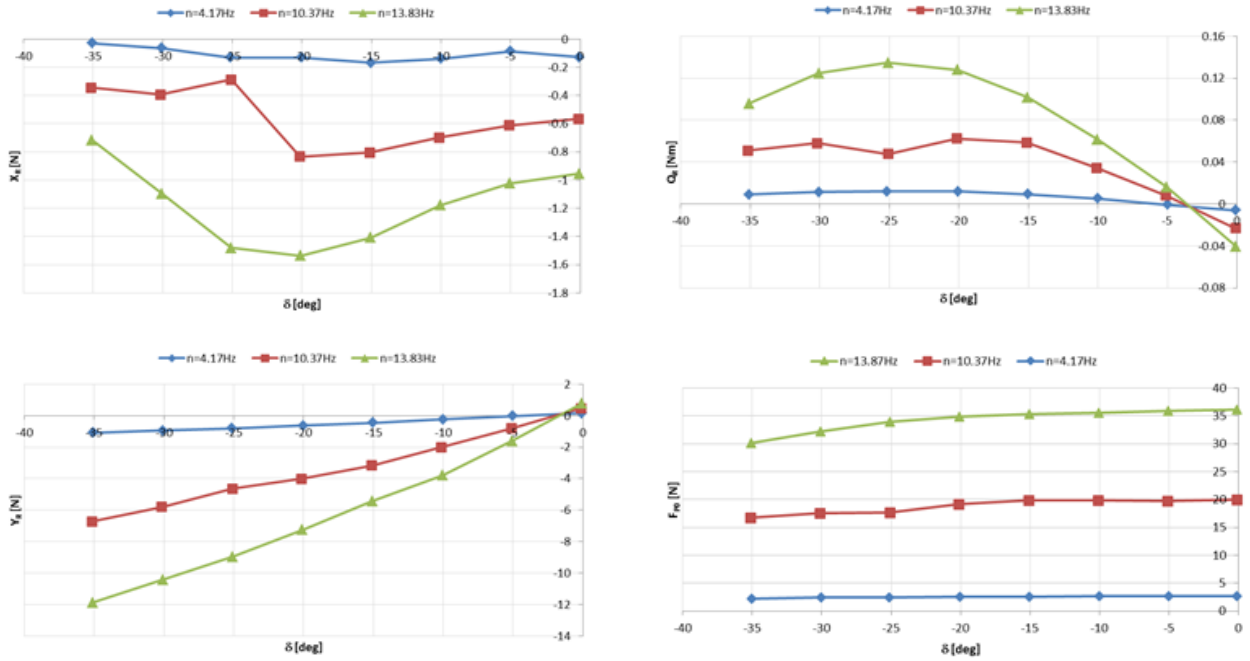


Figure 43: Selected results of bollard pull tests with the DTC model in calm water from top to bottom: longitudinal rudder force, lateral rudder force, rudder moment and pull force for three different propeller revolution settings (corresponding to 30%, 75% and 100% MCR).

### 2.3.2.8. Selected Results KVLCC2

Rudder forces where measured during test in calm water and in waves at CEHIPAR. In Figure 44 a comparison in between transversal forces for a test in calm water and in waves is shown. The vessel speed is 9 kn and the wave is 4 m high and 10.13 s of period. The forces for the case of 60° of heading is the closest one to the calm water case, while the case for 120° of heading present higher values. There is an asymmetry in between both sides of the curve caused by the asymmetry of the propeller flow and the wave velocity field.

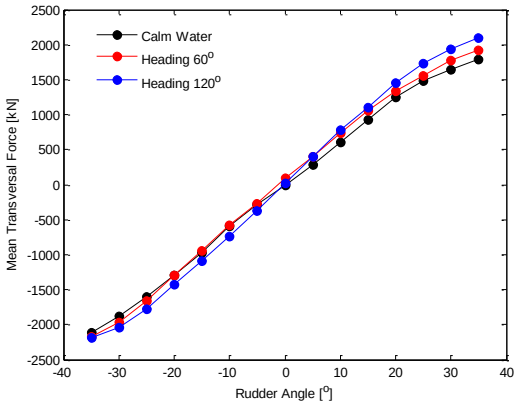


Figure 44: Comparison of rudder forces for the KVLCC2

## 2.3.3. Manoeuvring in waves

The manoeuvrability of ships is addressed by IMO Standards for Ship Manoeuvrability, adopted in 2002 (see IMO 2002), which assess turning ability (the ability of ship to turn using hard-over rudder), initial turning ability (i.e. the course-changing ability), yaw-checking ability, course-keeping ability and emergence stopping ability, which are evaluated in simple manoeuvres in calm water. These standards have been often criticized for not addressing ship manoeuvring characteristics at low speed, in restricted areas and in adverse weather conditions. The availability of both, experimental benchmark data and validated numerical methods to assess manoeuvrability in waves in limited. Therefore, special attention has been paid to this test type in the compilation of the model test matrix for the research project SHOPERA. Calm water manoeuvres such as turning circles and zig-zags have been performed in regular waves of different periods

and height with different initial headings. It should be noted that these are not defined IMO conform manoeuvres and the results are not comparable to calm water results in classical quantities such as e.g. the tactical diameter or the overshoot angle. The purpose of these tests is to gain insight into the manoeuvrability of vessels in the presence of waves in a broader and more general sense.

#### 2.3.3.1. Experimental Setup DTC

Turning circle (35° rudder angle) and 20°/20° zig-zag manoeuvres in calm water and regular waves have been performed with the free-running DTC model (connected by an umbilical to a manually controlled gondola following the model). The majority of tests have been performed with the rudder set to starboard. Additional runs have been conducted to investigate the differences in manoeuvring behaviour when the rudder is set to portside, caused by the single screw propeller and twisted rudder setup of the DTC. The evaluation of the test data revealed that the rudder of the DTC model was mounted approx. 3° off the true zero angle towards portside, leading to pronounced differences between manoeuvres over portside and starboard side. Repetitions of the calm water turning circle manoeuvres showed a deviation of less than 1% in tactical diameter and advance.

#### 2.3.3.2. Experimental Setup KVLCC2

The set up for the evolution circles in waves is performed by attaching the model to a six component dynamometer, which is fixed to the carriage, setting the model in a fully captive way (no sink, trim or heel). The forces due to the turning and waves influence can be measured. Special care was taken to avoid the wave reflected influence during the test.

#### 2.3.3.3. Selected Results DTC

The test matrix comprises a total of 17 turning circle manoeuvres, two calm water reference runs, 14 runs in regular waves (parameters of variation: initial heading, rudder direction, wave period, wave height) and 1 run in irregular seas. In addition, five 20°/20° zig-zag manoeuvres have been performed, one calm water reference run and 4 runs in regular head waves (parameters of variation: wave period and timing of rudder execution relative to crest/trough). The comparison of the phasing of the rudder execution revealed a negligible influence on the characteristics of the manoeuvres with differences of 2-3% for overshoot angles and timing. These differences are in the range of accuracy of manoeuvring tests in waves and it is difficult to draw conclusions with respect to the influence of phase shift on the manoeuvring characteristics.

In Figure 45, examples of the influence of the initial wave heading on the trajectory during the manoeuvre is shown. The tests have been conducted in regular waves with H = 2.0 m and T = 10.6 s (full scale). The vessel trajectories in the x-y-plane in waves are compared to a reference run in calm water (black trajectory). The approach speed for all cases is 6 kn (full scale) and the results are synchronized with respect to rudder execution (35° to starboard). In head sea conditions (red trajectory), the first circle requires less space compared to the calm water reference run, and as apparent from Figure 45, it takes the vessel approximately the same time to change heading by 90° as in calm water, while a turn over 180° takes less time than for the calm water case. The head waves push against the bow and thus amplify the effect of the moment produced by the rudder. The vessel is drifting oblique with the direction of wave propagation. This is caused by the wave moment acting against the rudder moment when the ship is turning from 180° to 270°. In following sea conditions, the (blue) trajectory of the vessel is strongly distorted by the pronounced drift motion between consecutive turns, here the wave moment amplifies the effect of the rudder moment when the ship is turning from 180° to 270°. In this condition, it takes approximately the same time to turn 90° as in calm water, while it takes significantly longer to turn by 180° (see Figure 46). When the vessel approaches the manoeuvre in beam seas and initially turns the bow into the waves (green trajectory), it takes slightly longer to turn 90°, while the time required to turn by 180° is approximately the same as in calm water (see Figure 46). An example of the influence of regular head waves on the course changing ability of the DTC vessel is presented in Figure 47, where three 20°/20° zig-zag manoeuvres with 6 kn approach speed are compared.

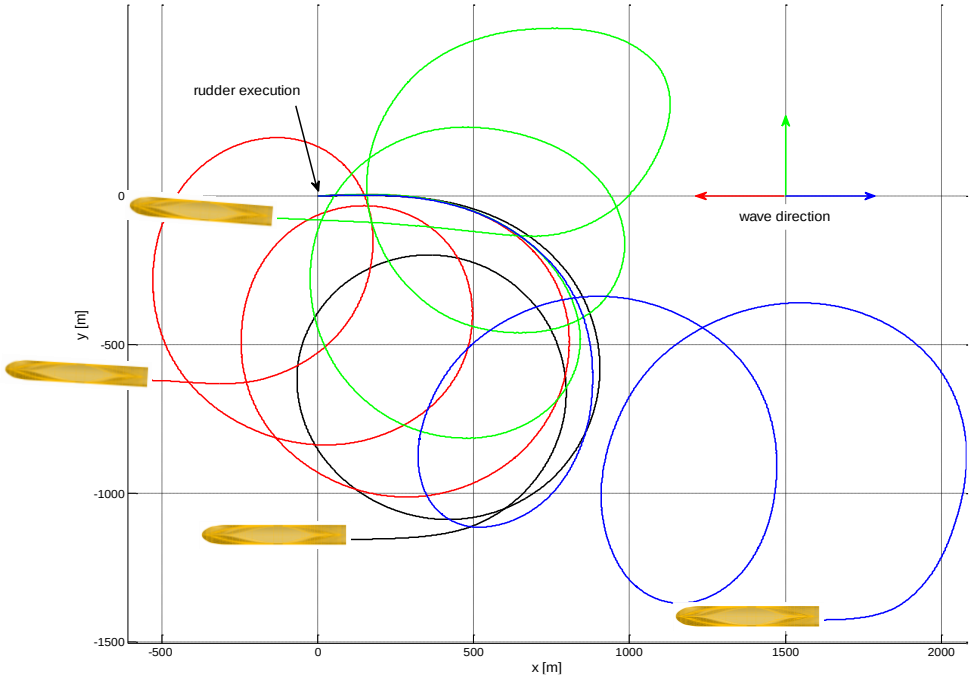


Figure 45: Trajectories of the DTC performing turning circle manoeuvres (rudder 35° to starboard) in MARINTEK's Ocean Basin in calm water (black), head waves (red), beam waves (green) and following waves (blue)

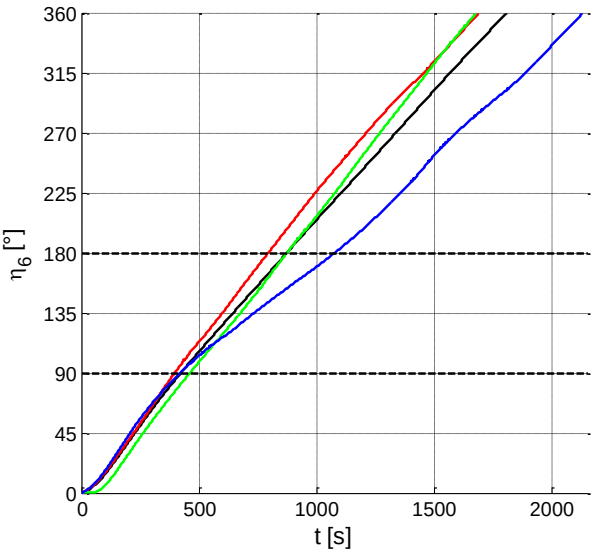


Figure 46: Time series of the vessel heading during the turning circle manoeuvres in calm water (black), head waves (red), beam waves (green) and following waves (blue)

The black lines show the yaw angle (solid) and rudder angle (dashed) as a function of time in calm water (full scale), the red and blue lines represent the regular head wave cases (red: H = 2.0 m/T = 10.6 s, blue: H = 2.0 m/T = 13.94 s). All three cases are synchronized with respect to first rudder execution, which has been performed with wave crest at Lpp/2 (FP) for the cases with waves.

While the first (and second) overshoot angle and initial turning time is similar for all three cases, the differences become more pronounced for reach and time for the complete cycle. In head waves, the vessel requires less time to reach zero heading after the first and third rudder execute. The shortest duration for the completion of the manoeuvre is observed for the longer wave period (T = 13.94 s).

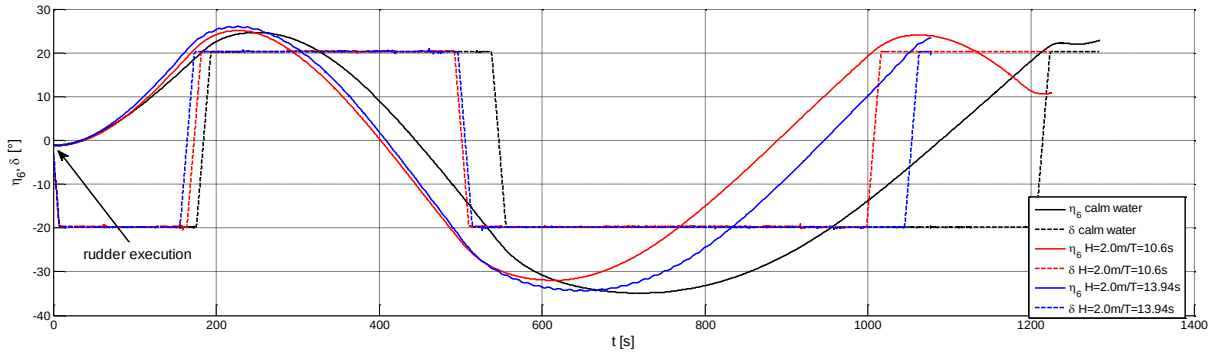


Figure 47: Yaw and rudder angle of the DTC performing 20°/20° zig-zag manoeuvres in MARINTEK's Ocean Basin in calm water (black) and regular head waves with H = 2.0m/T = 10.6 s (red) and H = 2.0m/T = 13.94 s (blue), full scale

### 2.3.3.4. Selected Results KVLCC2

Test circle of evolution in waves were performed at CEHIPAR for different combination of wave frequency, circle radius, drifting angle and velocities. Figure 34 shows an example of the measured Fx and Fy forces on the model during the test. The colour scale represents the force magnitudes. The polar plot displays the ship heading, 180 degrees means that the ship is in head seas. From the distribution of colours, it is possible to notice how the forces magnitude and encounter frequency are varying with the ship heading. For instance, in head seas the change in between colours is faster than in following seas meaning that the encouter frequency is higher. Also, the gradient of change of colour is high as the amplitude of the forces magnitude is changing more in head seas than in following seas as it was expected. Furthermore, it is possible to notice two important areas, bow quartering and stern quartering and beam seas for the Fy force. These areas show a high variation of the force magnitude as in these cases the ship is showing almost or its entire lateral surface to the waves.

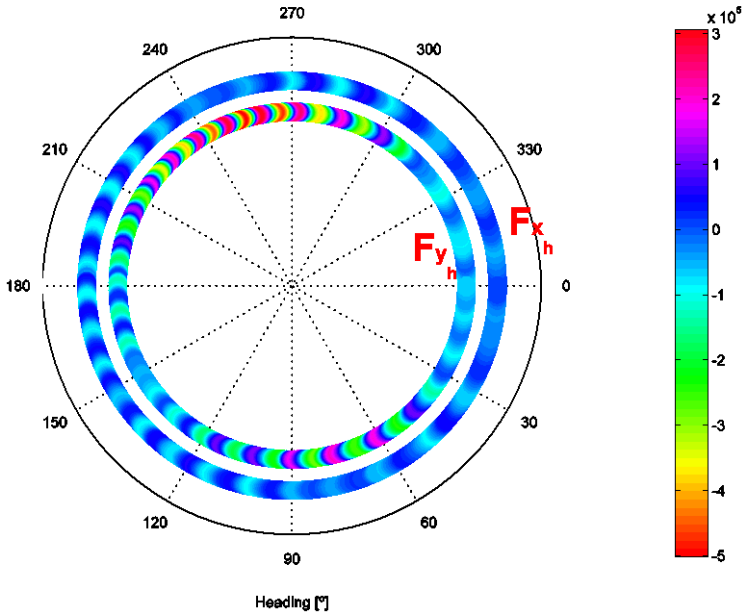


Figure 48: Example of longitudinal and lateral forces during a captive circle in wave

## 2.4. Validation, Sensitivity Studies and Level 1 Methods

The results of the experimental investigations have been used to validate the developed and fine-tuned methods and software tools presented in the previous sections. Selected test cases have been used in an open-call benchmarking of SHOPERA with external participants to evaluate the state-of-the-art of numerical methods for the proposal of new regulations. Further on, simplified models of propulsion, steering devices and engine dynamics have been developed and implemented in the numerical simulation tools.

Finally, addressing intact stability problems can be done with the available state-of-the-art numerical tools for intact stability assessment. However, the requirements of intact stability have been so far never considered in a coupled way with other safety aspects of ship sailing in adverse weather conditions. For example, safe combinations of ship course and speed with respect to dynamic stability in waves may be not possible from the point of view of achievable advance speed or course-keeping. On the other hand, reduction of installed power and thus deterioration of manoeuvrability in adverse conditions will increase the likelihood of unfavourable courses and speeds and thus the danger of undesirable ship motions and stability failures. This coupling has been investigated in detail.

### 2.4.1. Validation

Figure 49 (Ley et al. 2014) shows computed and measured (dimensional) added resistance values of a cruise vessel in regular waves for Fn=0.23. $R_{TAW}$ denotes the total added resistance, $R_{FAW}$ the frictional added resistance $L$ the ship length between perpendiculars, and $\lambda_w$ the wave length. The computations were performed using a Reynolds-averaged Navier Stokes (RANS) equations solver. Numerical results agreed fairly well with model test measurements.

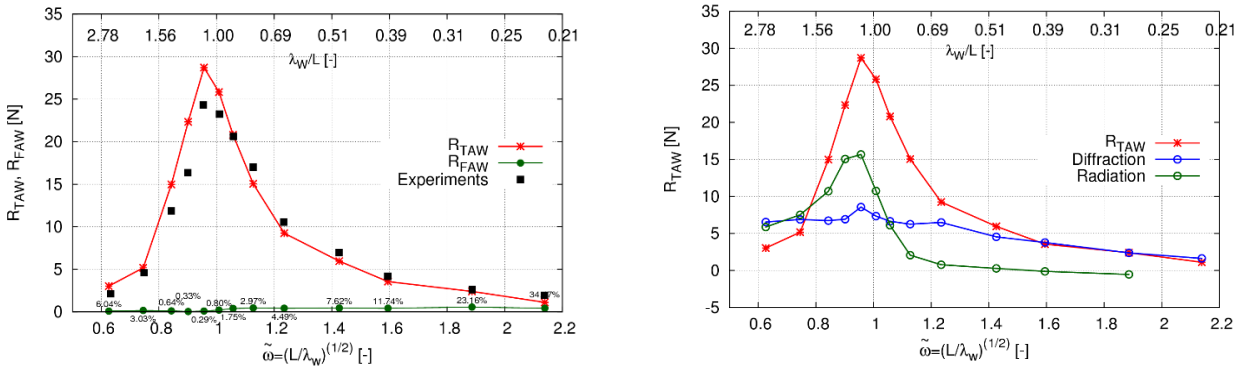


Figure 49: Computed and measured added resistance in waves

In Figure 49 (left) the percentage of the total added resistance $R_{TAW}$ attributed to viscous effects $R_{FAW}$ is included, which is steadily increasing when moving to higher wave frequencies. Figure 49 (right) shows the components of the aided resistance related to radiation and diffraction effects. To determine the diffraction part, simulations were conducted in waves with the ship totally restrained at its dynamic equilibrium sinkage and trim position. To compute the radiation part, simulations were performed in calm water with the ship executing forced heave and pitch motions. As expected, the radiation component is the predominant part of total resistance in waves of $\lambda/L$ ratios from about 0.8 to 1.1 (around heave-pitch resonance), whereas in short waves radiation effects die out.

In longer waves radiation and diffraction components are nearly equal. It should be noted that the sum of radiation and diffraction force components does not yield the total resistance, because the interaction effects between radiation and diffraction are herein not shown separately, see Ley et al. (2014).

### 2.4.2. Added Resistance in Short Waves

With the continuous increase of ship sizes (in view of the economy of scale), the range of relative wave length to ship length $\lambda/L$ of practical interest is being shifted to lower values. This makes the prediction of

added resistance of ships in such regions increasingly important. For instance, if the upper limit for a short wave approximation is set at $\lambda/L$=0.5 (for head seas conditions) and assume ships of length larger than about 100m, this means that we can satisfactorily calculate the added resistance for these ships in waves up to about 50m in length, with a corresponding period close to 6s, which is a typical peak period of waves in many coastal and even pelagic open seas (like the Aegean Sea in East Mediterranean). When considering ships of length over 250m, the limiting wave period for short waves rises to about 9s, which practically means that we could cover by the short wave approximation not only all coastal areas, but even a significant portion of open seas.

Recent IMO regulations and guidelines call for simplified approaches, namely *Level 1 methods*, able to estimate the added resistance and required powering of ships in waves at low speed (in the range of 4kn). The determination of the minimum powering for safe operation in adverse weather conditions is therefore inherently related to the estimation of ship's added resistance *in short waves and at low speed*.

Revisiting briefly the scientific work in this area we recall first the work by Havelock (1940), who derived a formula to calculate the steady force acting on a fixed vertical circular cylinder in waves. Later on, Fujii and Takahashi (1975) proposed a semi-empirical formula for the added resistance due to diffraction using Havelock's theory by introducing two coefficients, one for the forward speed and the other for the draft. Takahashi (1988) and Tsujimoto et al. (2008) worked on the fine-tuning of the two coefficients based on experimental data. In parallel, Faltinsen et al. (1980) developed an asymptotic formula for the added resistance on wall-sided hull forms in short waves as a by-product of their 'near filed' method for the calculation of the 2nd order wave induced forces and moment, namely by integrating the pressure over the hull surface using an approximate velocity potential near the bow. It was pointed out by Fujii (discussion to Faltinsen et al. (1980)) that for full ships the results based on this formula agree well with experimental data. Despite that for fine hull ships there are still considerably large deviations from the experimental data, the introduction of the base flow based on slender body theory into the formula was a significant improvement. As pointed out by Sakamoto and Baba (1986), for a ship symmetric about midship section advancing in beam seas, the added resistance predicted according to Faltinsen et al. (1980) does not go to zero because the advance speed makes the wave field asymmetrical with respect to midship. On the other hand, those methods based on the concept of correcting Havelock's formula for forward speed effect will yield zero results as they are essentially a zero speed approach. For developing practical and reliable best practice for conducting and analysing speed/power trials, MARIN developed the STA1 and STA2 empirical methods (ITTC, 2012) utilizing seakeeping model test results. Our experience shows that the short wave formula of STA2 tends to yield an overestimation.

As revealed by CFD simulations (Ley et al., 2014), the viscous effects, which cannot be captured by potential flow theory, play a significant role in the prediction of added resistance in short waves. Hence it is necessary to use experimental data to fine-tune relevant semi-empirical coefficients resulting from potential theory considerations. Liu et al. (2015) revisited Faltinsen's formula and reconsidered the effects of local and global ship's hull form, bow flare and local draft, to derive an improved formula:

$$
\begin{aligned}
F_1 &= \int_C \bar{F}_n \sin\theta \, d\ell \\
\bar{F}_n &= \frac{1}{2}\rho g \zeta^2 \sec\alpha_{WL}\alpha_d \left(\frac{0.87}{C_B}\right)^{\cos\alpha\left(1+4\sqrt{Fn}\right)} \\
&\left\{\sin^2\left(\theta+\alpha\right)+\frac{2\omega_0 U}{g}\left[1-\cos\theta\cos\left(\theta+\alpha\right)\right]\right\}
\end{aligned}
\tag{8}
$$

where $C$ is the non-shadow part of the waterline, $\zeta$ is the incident wave amplitude, $\alpha$ is the wave propagation direction ($\alpha=\pi$ in following seas), $\vartheta$ is the inclination angle of a line segment and $U$ is the ship's speed of advance, $\alpha_{WL}$ is the sectional flare angle at the ship's still waterline ($\alpha_{WL}$ =0 in case of a vertical wall) and $\alpha_d$ is the local draft correction coefficient. This formula has been validated for wave headings ranging from head to beam waves. Furthermore, in response to the ongoing discussions about Level 1 and

Level 2 methods for the estimation of minimum powering in waves, the newly derived formula is simplified to using only main ship particulars and fundamental wave characteristics. Extensive validations of the simplified formula were carried out by applications to different types of ships and results show that the following simplified formula well captures the added resistance of ships in short head waves:

$$F_1 = \frac{2.25}{2}\rho g B \zeta_a^2 \sin^2 E \left(1+5\sqrt{\frac{L}{\lambda}}Fn\right)\left(\frac{0.87}{C_B}\right)^{1+4\sqrt{Fn}} \quad (9)$$

where $E=atan(B/2/L_E)$ and $L_E$ is the entrance length of the waterline. Figure 50 to Figure 52 show typical result derived by this formula in comparison with experimental data.

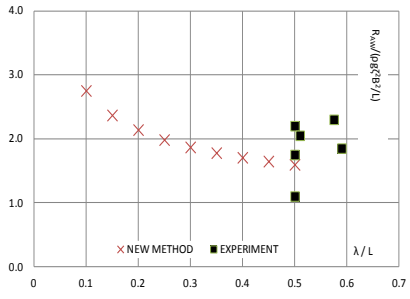


Figure 50: Added resistance of the S175 container ship in head seas, α= 180°, Fn=0.20

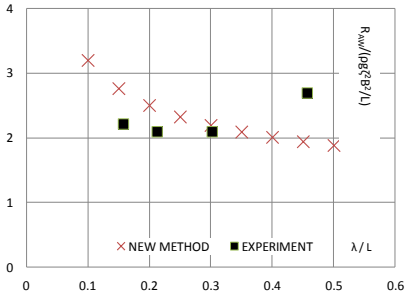


Figure 51: Added resistance of the WILS2 ship in head seas, $C_B$=0.602, Fn=0.183

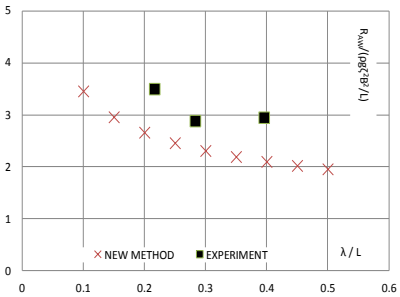


Figure 52: Added resistance of the PerSee cruise ship in head seas, $C_B$=0.654, Fn=0.23

### 2.4.3. Benchmark Study

To evaluate the world-wide availability of methods that can be used in the practical assessment, SHOPERA conducted an international benchmark study of numerical and empirical methods for the time-average wave-induced forces and moments and simulation of ship manoeuvres in waves. The benchmark study was completed in April 2016, when a summary of the benchmark results was presented in a public workshop held in London. This study aimed to contribute to the international state of the art in the assessment of the operation of ships in adverse sea conditions by:

1. Recording numerical methods employed for the prediction of time-average wave-induced forces and moments (including added resistance) and manoeuvrability of ships in waves, and
2. Assessing the current level of accuracy and efficiency of the relevant numerical prediction methods by comparison with model experiment data.

Eventually sixteen (16) institutes participated by submitting results based on numerical simulations by use of codes of various levels of complexity. They can be roughly classified into the following main categories:

1. Potential theory-quasi 2D strip theory method with possible viscous flow corrections;
2. Potential theory-Boundary Element Method(BEM) or 3D panel method with possible viscous flow corrections;
3. Viscous Flow-RANS methods

For the calculation of mean forces and moments, the methods can be classified into the following categories:

1. semi-empirical methods;
2. far field/momentum methods;
3. near field/pressure integration methods.

The participating software/codes employed sometimes a mix of various methods and the finally chosen methods for generating the submitted results were not always exactly known to the study organizer. For

the simulation of a ship's manoeuvring behaviour in waves (motion trajectories), it is noted that presently, there is not a unified mathematical formulation for the subject, despite some efforts for standardization. Hence, various modelling methods for the manoeuvring equations were adopted by the participants.

#### 2.4.3.1. Conclusions from the benchmark study

The benchmark study concerned two large ships, the DTC containership and the KVLCC2 tanker, both well over 300m in terms of length. For such large ships, the encountered waves in actual sea conditions are mostly 'short', namely $\lambda/L < 0.5$, where the benchmark study focused on. The study delivered a good insight into a complicated hydrodynamic problem on the basis of experimental and numerical studies. It provided also valuable benchmark data to the international scientific community related to a subject with strong engineering background linked to international maritime regulations. Some essential aspects of the subject were noticed and should be further studied in the future. In particular, examining the numerical methods in comparison to model experimental data, the following may be concluded:

1. The predictability of the time-average wave-induced surge force, including added resistance, is generally decent to good. The performance of the tested methods is better for moderate speeds and worsens with decreasing speed. Also, the agreement is better for the tested full type ship (KVLCC2) than for the DTC containership hull form.
2. The time-average wave-induced sway force is predicted very well, generally better than the surge force, consistently for DTC and KVLCC2 ships, whereas agreement for the yaw moment is generally worse.
3. For the manoeuvrability simulations, the behaviour of the employed numerical methods is not consistent. Despite the large spreading among the numerical methods and deviation from experimental results, some methods, performing well in one case, were not good for another case, thus conclusions could not be drawn, except for some qualitative effects of the impact of incoming waves.
4. The overall impression of the submitted results based on strip theories was not satisfactory. This is mainly due to its insufficiency in accounting the 3D and end effects (bow and stern) of the hull form, which are significant in the present study subject.
5. BEM methods implementing various theories performed as a category of methods best in the present benchmark due to their essential merits: comparatively easy to use, when the code is properly programmed and validated and with decent results for non-extreme designs and loading/environmental conditions. Interesting that a group of a few 3D panel methods can be identified, results of which are close to each other and to experiments throughout all considered cases. However, spreading between these methods and their deviations from experiments increase in difficult cases.
6. Herein employed CFD/RANSE methods have proved their ability to provide accurate results even in difficult cases, although they sometimes delivered irrational results, for instance, in Figure 3. Because of the differences between different sets of results (while based on fundamentally the same solution methods), this is likely due to improper setups (treatment of sway and yaw, influence of free drift on time-average forces etc.) and perhaps sometimes improper use of tools, leading to the conclusion that they are highly dependent on their usage, rather than on the physics of the studied problem.
7. There was also one empirical method participating in the benchmark study by submitting results on the prediction of time-average surge force and yaw moment. For the studied cases, the empirical method delivered good results, showing a promising performance.

Some additional general comments may be concluded:

a. Limitations of the numerical methods: CFD tools are highly dependent on the end-users' skills (background, experience with the type of problem, etc). The empirical formulas, on the other side, are not dependent on the end-user. However, the quality of predictions is solely dependent on the code developer's know-how and the code user's experience.
b. The particularity of hull form: The scattering of the numerical results appears to be larger for the DTC ship than for the KVLCC2 ship. This can be credited to the effect of their hull form. The DTC ship disposes

a relatively small draft (in comparison with other main particulars), an extended bulbous bow close to the free surface and a transom stern with long overhang near the calm water free surface. It is well known that for an emerging bulbous bow and immersing transom stern, with the associated complex wave phenomena and rapid change of the wetted part of the ship, are critical issues for potential flow codes. Potential flow panel methods are not performing well in these conditions due to their essential limitations. However, even RANSE methods are challenged under similar conditions and may fail, if not properly used.

c. The tested waves: As the size of the tested ships is large (>300m), representative sea states fall into the relatively short waves. In order to measure the small absolute values during model tests, quite steep waves were generated and tested. This may have created additional uncertainty in the benchmarked results, independently of the specific hull form. This uncertainty can only be partially controlled by using larger ship models for testing or applying full scale CFD simulations in future work.

d. Uncertainties related to experimental results should be bore in mind. Both maneuvering tests and mean forces/moment tests are subject to the influence of the mean second order forces. During the tests, which had a focus on relatively short waves, rather steep waves have been generated. The impact of wave steepness should be investigated in future studies.

e. In several cases, large relative spreading of numerical results and large relative deviations from the experiments are partially explained by the smaller absolute values than for other cases.

### 2.4.4. Steering Devices

**Simplified Rudder Force Model**

The forces of the rudders can be approximated based on the following equations:

$$Y_R = \frac{1}{2}\rho v_r^2 A c_L(\delta) \tag{10}$$

$$X_R = \frac{1}{2}\rho v_r^2 A c_D(\delta) \tag{11}$$

where $Y_R$ denotes the rudder side force, $X_R$ the rudder longitudinal force, $\rho$ the water density, $v_r$ the mean axial velocity in the propeller slip stream, $A$ the projected rudder area, $c_L$ the lift coefficient, $c_D$ the drag coefficient and $\delta$ the rudder angle. Coefficients $c_L$ and $c_D$ may be taken from literature (e.g. Abott and Doenhoff (1959), Brix (1993)) and may be assumed as linear functions of the rudder angle $\delta$. The maximum rudder angle is assumed to be 35° for seagoing ships. $v_r$ may be calculated as follows:

$$v_r = (1-w)v\sqrt{1+\frac{A_S}{A}C_{th}} \tag{12}$$

where $w$ denotes the wake fraction number, $v$ the ship speed, $A_S$ the projected area in the propeller slip stream and $C_{th}$ the propeller loading coefficient. An empirical formula for the estimation of the wake number is given in the following:

$$w = 0.75 \cdot C_B - 0.24 \tag{13}$$

where $C_B$ denotes the block coefficient. The thrust loading coefficient is defined as:

$$C_{th} = \frac{8T}{\rho\pi(1-w)^2 v^2 D^2} \tag{14}$$

where $T$ is the propeller thrust and $D$ the propeller diameter.

## 2.4.5. Engine Dynamics

### 2.4.5.1. Engine Model

The available delivered power on the propeller $P_D^{av}$, W, can be calculated as:

$$P_D^{av} = \eta_s \eta_g P_B^{av} - P_{PTO} \quad (15)$$

The assumptions used in the project for the non-dimensional shaft efficiency, non-dimensional gear efficiency and power take-off were $\eta_s = 0.98$, $\eta_g = 1.0$ for directly connected engines and $\eta_g = 0.98$ for single-stage geared engines, and $P_{PTO} = 0.0$ W in emergency situations; these values can be used as default, unless less conservative parameters are available from the manufacturer.

Within the comprehensive and simplified assessment procedures, a steady engine model can be used to define $P_B^{av}$ as a function of the engine rotation rate, defined by the *engine diagram*. Figure 53 shows an example of the engine diagram for a two-stroke low-speed turbocharged diesel engine, the type used on the majority of modern merchant ships. The horizontal axis corresponds to the rotation speed as percentage of rotation speed at the maximum continuous rating (MCR), and the vertical axis shows shaft power as percentage of MCR (note logarithmic scales used for both axes). Line 1 corresponds to the *maximum rotation speed* (*minimum rotation speed limit*, or *idle limit*, corresponding to 25%-30% of the nominal rotation speed, is not shown).

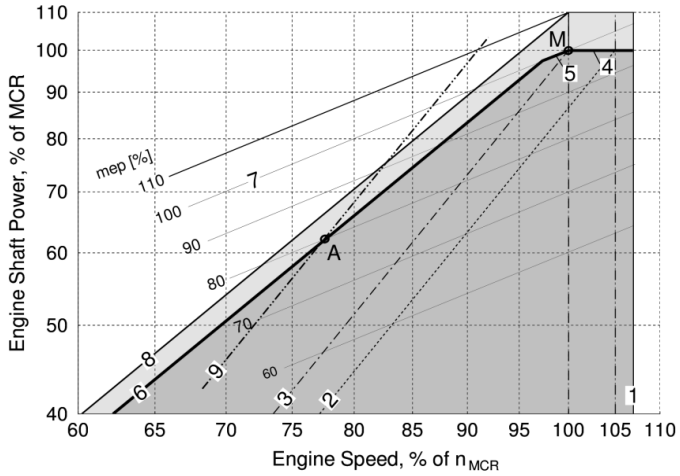


Figure 53. Diesel engine diagram

Curve 2 is called the *light propeller curve* and corresponds to resistance and propulsion characteristics of a clean hull and propeller in calm water. Along this line, shaft power is defined by the hull resistance curve, open-water propeller characteristics and hull-propeller interaction coefficients. Curve 3 is referred to as the *heavy propeller curve*, and is assumed in design as propeller curve corresponding to fouled hull in heavy weather. This curve corresponds to shifting the light propeller curve upwards by a *sea margin* up to point M; point M corresponds to MCR and is the layout point for the engine.

In the assessment of the sufficiency of the installed diesel engine for manoeuvrability in adverse conditions, it is necessary to take into account that the maximum continuous output of a diesel engine is bounded, depending on its rotation speed, by several limits:

- *Power limit*, line 4, at the maximum rotation rates. At the power limit, maximum power continuously provided by the engine is constant and equal to MCR).
- *Maximum torque limit* (also called *maximum mep limit*), line 5, defined by the shafting system bearing strength, at the moderately reduced rotation rates. At the maximum torque limit, torque is constant and thus the maximum engine output is proportional to rotation speed.
- *Surge limit* (also called *air limit*), line 6, at low rotation rates. To the left of line 6, the engine will lack air from the turbocharger for the combustion process. Surge limit depends on the

turbocharging technology used; thus, manufacturer data should be referred to for its exact definition.

Diesel engine is controlled by changing pressure in cylinders; *constant mean effective pressure* (mep) lines are the lines parallel to line 7, which corresponds to the mep limit of 100%; along these lines, shaft power is proportional to the rotation speed, and, correspondingly, the torque is constant.

Line 8 is the engine *overload limit*: whereas the area between lines 2, 4, 5 and 6 is available for continuous operation in adverse conditions or during manoeuvres without time limitation, the area between lines 4, 5, 6 and 8 is available for overload running for limited periods (1 hour per 12 hours); this area should not be considered available for manoeuvring in adverse conditions.

Due to increased resistance in adverse conditions or during manoeuvres, line 2 shifts upwards, for example, up to line 9, and the maximum engine output is defined by the intersection point A of line 9 with one of the engine limit curves 5 or 6. At low added resistance, e.g. in normal operation in low to moderate sea states, maximum torque line 5 is relevant, whereas for propulsion and manoeuvring in heavy weather, i.e. at a greater added resistance, surge limit line 6 becomes the limiting curve.

In any case, it is important to take into account that the available shaft power in adverse conditions is reduced compared to MCR.

#### 2.4.5.2. Other Types of Engine and Propulsion

SHOPERA has performed case studies for vessels with various types of engine and propulsion besides the low-speed two-stroke diesel engine working directly on a fixed-pitch propeller. Although in the practical approval, verified manufacturer data describing engine limit curves and propeller characteristics should be used, a summary of approaches used to consider other types of the engine and propulsion in the SHOPERA case studies is given below for information:

- For 4-stroke diesel, the air-surge limit curve is much more restrictive than the air-surge limit curve for 2-stroke engines. In SHOPERA, measurement data were used for 4-stroke diesels.
- For a diesel-electric propulsion, it was assumed that the power output of an electric motor is independent from the rotation speed, i.e. the output of the engine was assumed constant at all rotation speeds. In emergency situation, 100% of MCR can be considered as the maximum available power.
- For a vessel equipped with a controlled-pitch propeller, it was assumed that the propeller operates at a constant rotation rate, and the pitch of propeller blades was varied to adjust the propeller to the actual forward speed and required thrust.

#### 2.4.5.3. Propeller Model and Hull-Propeller Interaction

The propeller thrust $T$ was found from the equilibrium equation in the x-direction (1). Using the known thrust, the advance ratio J was found from the nonlinear equation $T = \rho u_a^2 D_P^2 K_T(J)/J^2$ using known open-water propeller characteristic $K_T(J)$ and the propeller advance speed $u_a$. From the found advance ratio J, the torque coefficient $K_Q(J)$ was found using the open-water propeller characteristic. After that, the propeller rotation speed $n_P$ was found from the equation $n_P = u_a/(JD_P)$ and then the required delivered power to the propeller was calculated as $P_D = 2\pi\rho n_P^3 D_P^5 K_Q(J)$. The open-water propeller characteristics can be defined using methods summarized in Table 8.

### 2.4.6. Assessment Procedures

#### 2.4.6.1. General

The general assessment concept proposed by SHOPERA is to allow free choice of assessment procedures of different complexity (similarly to 2012 Interim Guidelines), ranging from simple empirical formulae to advanced assessment procedures, so that the designer can select the most suitable procedure depending

on the particular design needs. Simple assessment procedures are sufficient for the majority of conventional vessels, whereas more accurate assessment procedures and evaluation methods are required for cases with large uncertainties, such as innovative propulsion and steering solutions, which are intended to be promoted by the EEDI regulations.

SHOPERA proposes three alternative assessment procedures:

- Comprehensive Assessment allows the best accuracy, solving coupled nonlinear motion equations. Still, the designer does not have to use tedious/expensive evaluation methods for different assessment components, but can choose between numerical, experimental or empirical methods for different elements. This type of assessment is anyway necessary for ships with innovative propulsion and steering arrangements.
- Simplified Assessment, a first-principle assessment with reduced number of considered situations and reduced complexity of motion equations, also allowing choosing between experimental, numerical or empirical methods to evaluate force components, and having complexity of a spreadsheet calculation.
- Sufficient Propulsion and Steering Ability Check is based on pure empirical formulae to define the required installed power as a function of main ship parameters (deadweight, block coefficient, windage area, rudder area, engine and propulsion type), of a complexity of a pocket calculator.

#### 2.4.6.2. Comprehensive Assessment

Compliance with the IMO Manoeuvrability Standards, *IMO (2002)*, is demonstrated in full-scale trials, which is impossible for ship manoeuvrability assessment in adverse weather conditions. Alternatively, the proposed criteria (weather vaning, steering and propulsion abilities) can be evaluated, in principle, directly in transient model experiments with self-propelled ship models in simulated irregular waves and wind, for all required combinations of wave directions and periods. This is, however, presently unfeasible for practical purposes for several reasons: First, providing reliable statistical predictions in irregular seaway requires repeating tests in multiple long realisations of each seaway, which is too expensive. Besides, few facilities exist worldwide, which are able to perform such tests, which makes such tests impractical for routine design and approval. Third, verification of such tests by the Administration is impossible (unless the test program is repeated), which makes this approach impractical for approval. Finally, results of such tests very much depend on the time history of steering, which causes too large variability and uncertainty of test results, which therefore cannot be reliably verified especially in marginal cases (i.e. cases near the failure boundary, which are the actual cases of interest in approval). Alternative to such model tests, direct numerical simulations of transient manoeuvres in irregular seaway are not mature enough yet for routine design and approval, *ITTC Manoeuvring Committee (2008)*. The approach proposed by SHOPERA is based on separate evaluation of different acting forces (waves, wind, propeller, rudder etc.) using simple model tests, numerical simulations or empirical formulae, and combination of the defined forces in a simple numerical model. Whereas the resulting procedure is based on first principles and takes into account all relevant physics, it is at the same time:

- verifiable by Administrations or Recognised Organisations,
- based on technology presently available in the industry,
- inexpensive and as accurate as presently practicable,
- flexible, in that designers and administrations are free to choose alternative methods (experimental, numerical or empirical) depending on designer needs,
- open for updates when new numerical or experimental methods are developed, without the need to revise the Guidelines.

The Comprehensive Assessment procedure proposed by SHOPERA is based on neglecting oscillatory forces and moments due to waves and thus considering only time average forces and moments, assuming that the time scale of such oscillations is shorter than the time scale of manoeuvring motions. This effectively reduces the evaluation of manoeuvrability criteria to a solution of coupled motion equations in the horizontal plane under the action of *time-average* wave-induced forces, as well as wind forces, calm-water

forces, rudder forces and propeller thrust. Projecting forces on the $x$- and $y$-axes and moments on the $z$-axis of the ship-fixed coordinate system, **Error! Reference source not found.**, leads to a system of equations, converging to a steady state described by the following system (note that achieving converged solution can be realised in different ways, including time-domain simulation):

$$X_s + X_w + X_d + X_R + T(1-t) = 0 \quad (16)$$

$$Y_s + Y_w + Y_d + Y_R = 0 \quad (17)$$

$$N_s + N_w + N_d - Y_R l_R = 0 \quad (18)$$

Indices d, w, s, and R denote, respectively, wave, wind, calm-water and rudder-induced forces and moments; T is propeller thrust. The coordinate system has an origin *O* in the main section at the water plane; *x*-, *y*- and *z*-axes point towards bow, starboard and downward, respectively (positive rotations and moments with respect to *z*-axis are clockwise when seen from above). The ship sails with the speed $v_s$; its heading deviates from the course by the drift angle $\beta$. The mean wave and wind directions are specified by angles $\beta_e$ and $\beta_w$, respectively (0, 90 and 180° for waves and wind from the north, east and south, respectively); rudder angle $\delta$ is positive to port; $l_R$ is the lever of the yaw moment due to rudder. A converged solution, described by system (16)-(18), provides the required propeller thrust (from which, advance ratio *J*, rotation speed *n* of the propeller and required $P_D$ and available $P_D^{av}$ delivered power are found), drift angle $\beta$ and rudder angle $\delta$.

The evaluation of steering ability and propulsion ability criteria is performed as follows:

- According to the steering ability criterion, the ship should be able to overcome environmental forces to start or continue course change in waves and wind from any direction. To evaluate this criterion, the ratio of the required brake power $P_B$ to the available brake power $P_B^{av}$ is computed along the line $[\delta = \delta_{max}]$; the maximum of the ratio $P_B/P_B^{av}$ should not exceed 1.0.
- According to propulsion ability criterion, the ship should be able to keep speed of at least 6.0 knots in waves and wind from any direction. To evaluate this criterion, the ratio of the required brake power $P_B$ to the available brake power $P_B^{av}$ is computed along the line $v_S$=6.0 knots; the maximum of the ratio $P_B/P_B^{av}$ should not exceed 1.0.

Figure 54 shows examples of converged solutions and application of the steering and propulsion criteria in polar coordinates ship speed (radial) – seaway direction (circumferential, head waves and wind come from the top): along line A, the required delivered power is equal to the available delivered power, line B corresponds to the required advance speed (here 4.0 knots), and line C limits the highlighted area, in which the required steering effort exceeds the available one (here, rudder angle exceeds 25°). The left plot illustrates a seaway in which the vessel fulfils both criteria (line A does not cross lines B and C); in the middle plot, the installed power is marginally sufficient to provide advance speed of 4.0 knots in head seaway, where line A crosses line B; in the right plot, the installed power is marginally sufficient for steering in nearly beam seaway, where line A crosses line C.

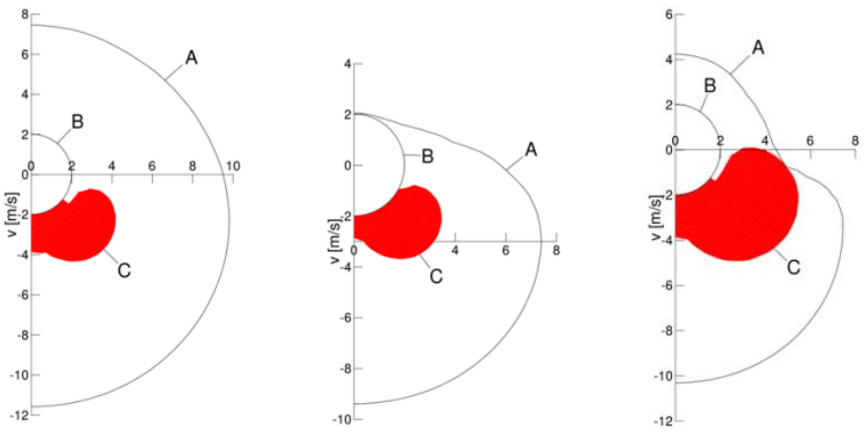


Figure 54. Result examples of Comprehensive Assessment

The advantage of the proposed Comprehensive Assessment, and the main difference from the Comprehensive Assessment in the 2012 Interim Guidelines is that the different effects (wind, waves, calm water, rudder, propeller and engine) can be measured or computed separately, if necessary with different methods (experimental, numerical or empirical). Note that even if model tests or complex numerical computations are used for some of contributions, they are done in stationary setups under well-controlled conditions and combined in a simple mathematical model.

### 2.4.6.3. Evaluation Methods for Components of Forces and Moments

The terms of the equation system (16)-(18) can be defined with different methods: empirical formulae, numerical methods or model experiments. The methods that can be applied are described in Table 8.

Table 8. Methods for evaluation of components in Comprehensive Assessment procedure

| Elements | Components | Model Tests | Numerical Methods | Empirical Methods |
|---|---|---|---|---|
| Calm-water | X, Y, N | steady-drift towing tests | double-body steady-drift CFD simulations | empirical formulae |
| Time-average wave forces | X,Y,N | drift forces in regular waves at different speeds and headings | potential methods, CFD for drift forces in regular waves | empirical formulae |
| Wind forces | X,Y,N | static wind tunnel tests | CFD for static wind forces | empirical formulae |
| Rudder forces | X,Y | steady towing tests with working propeller | CFD simulations with rotating propeller | empirical methods |
| Open-water propeller characteristics | T, J, $n_P$ , $P_D$ | open-water propeller tests | potential methods, CFD for open-water propeller simulations | propeller series |
| Engine | $P_B^{av}$ | static model (engine diagram) | | |

Because the proposed assessment procedure allows definition of different forces separately, using different (experimental, numerical or empirical) methods, an important question is how much freedom we have in the definition of each force component. Table 9 shows the percentage of the change of the required installed power to fulfil propulsion and steering ability requirements due to changes of each force or moment component in turn by 10% at significant wave height of 5.5 m, obtained with the Comprehensive Assessment (maximum values over several ships of different types are shown). The figures mean, for example, the following: a change of the *x*-calm water force by 10% changes the required installed power by 3.0%. The table shows that the most important contributors (bold) are the time-average *x*- (added resistance) and *y*-forces, calm-water *x*- and *y*- forces and *z*-moment and lateral rudder force. For these forces, the error of about 15% leads to the error in the definition of the required power of 5%.

Table 9. Percentage change of required installed power due to change of components of forces and moments

| Contributions | *x*-force | *y*-force | *z*-moment |
|---|---|---|---|
| Calm-water | **3.0** | **3.4** | **3.5** |
| Wind | 2.5 | 1.6 | 0.6 |
| Wave | **3.8** | **3.0** | 0.3 |
| Rudder | 1.5 | **3.4** | - |

Opposite to the transient manoeuvring tests in simulated wind and irregular waves, the proposed procedure relies on measurements of separate forces in well-controlled steady conditions. For calm-water, wind, rudder and propeller forces, such experiments are well established and can be done in many facilities world-wide (note that calm-water resistance and propulsion characteristics, including open-water propeller characteristics and hull-propeller interaction coefficients can be taken from the model tests that are

required for EEDI verification anyway). However, measurement of the time-average wave forces requires advanced measurements in a seakeeping basin, therefore, cannot be used routinely.

Numerical methods are presently available, in principle, for the same forces (calm-water, wind, rudder and propeller) as well; however, their use in regulatory assessment needs a significant effort of administrations and recognised organisations. The availability of numerical methods for time-average wave forces is one of the most critical issues: the absence of suitable numerical methods for added resistance led to the removal of numerical methods from the 2013 Interim Guidelines. Development and validation of numerical methods for time-average wave forces and moments was one of the major tasks of SHOPERA. Model test measurements of such forces were done for three ship models (a 14000 TEU container vessel, a VLCC tanker and a RoRo) for various ship speeds and wave directions and periods (with particular emphasis on short waves); results of these measurements were used for an international benchmarking of the available numerical methods for time-average wave forces. The results of this benchmarking (will be published elsewhere) show a significant progress of numerical methods in the last years and indicate the principal availability of numerical methods for regulatory purposes, if applied correctly.

Especially important for the practical implementation of any practical procedure is the availability of empirical methods for different force components. In addition to the well established empirical methods for wind forces, *Blendermann (1993)*, *Fujiwara et al. (2006)*, extensive validation studies were carried out together with the project from Japan for calm-water reactions and rudder forces in propeller race, which indicate availability of such empirical methods for the practical use; however, designers and Administrations should ensure that empirical methods are used within their applicability limits. Again, empirical methods for the time-average wave forces and moments have required particular attention and the significant progress achieved in the project will be reported elsewhere.

An important aspect of propulsion and steering in adverse conditions is a correct description of the engine under high load. In SHOPERA, air/surge limits of diesel engines (two- and four-stroke) were verified and recommendations were provided for practical assessment procedures.

### 2.4.6.4. Simplified Assessment

#### *2.4.6.4.1. Principles*

The aim of the development of the Simplified Assessment was to have a simple enough procedure for routine use by Administrations by reducing the number of calculations (solution cases) as well as the number of terms in motion equations (16)-(18), while keeping all relevant physics. In particular, the Simplified Assessment addresses the same criteria as those enforced in the Comprehensive Assessment (weather-vaning, steering and propulsion). The simplified procedures for steering ability (ability to start or continue course change in any seaway direction) and propulsion ability (ability to keep a minimum advance speed in all seaway directions) were proposed in *Shigunov et al. (2014)*.

#### *2.4.6.4.2. Simplified Steering Ability Assessment*

The starting point is system (16)-(18), solved for all relevant forward speeds and all seaway directions to check that the ship is able to start or continue course change in seaway from any direction. Note that for the steering ability, both the steering system and propulsion (which influences steering ability) are required and should be integral parts of the assessment: e.g. ships with powerful propulsion may have a smaller rudder, whereas ships with weaker propulsion may compensate this with larger or more effective steering devices. Results of Comprehensive Assessment for many ships show that the dimensioning condition for the installed power, i.e. the condition at which the ratio of the required to available delivered power is maximised along the line of maximum steering effort (further referred to for brevity as *critical condition for steering*) is close to beam seaway, Figure 54, right. Note that from experience, as well as from the results of Comprehensive Assessment for many ships, critical conditions for steering occur most frequently in stern quartering waves, like in Figure 54, middle; however, in such situations the required power is less than the required power defined by the Propulsion Ability, i.e. by the crossing point of lines A and B. When the

Steering Ability is dominating for the definition of the installed power, i.e. when line A crosses line C, the critical conditions are always close to beam seaway situations. This allows reducing the evaluation of the time-average wave and wind forces to beam seaways.

The second simplification stems from the observation that the levers of time-average wave and wind yaw moment are negligible compared to the lever of the calm-water yaw moment in critical conditions for steering.

Note that the simplifications made restrict the Simplified Steering Ability assessment to the vessels with conventional steering devices arrangement at the stern (including azipods); vessels equipped with azipods at the bow require Comprehensive Assessment.

As a result, the system of equations (16)-(18) reduces to one equation

$$X_{\mathrm{s}} + X_{\mathrm{w}}^{90} + X_{\mathrm{d}}^{90} + X_{\mathrm{R}} + T(1-t_{\mathrm{H}}) = 0$$

and one check

$$Y_{\mathrm{R}} \geq -b\left(Y_{\mathrm{w}}^{90} + Y_{\mathrm{d}}^{90}\right)$$

where

$$b = N'_{\mathrm{s}} / \left(N'_{\mathrm{s}} + 0.5Y'_{\mathrm{s}}\right).$$

To define the components of forces and moments $X_{\mathrm{s}}$, $X_{\mathrm{w}}^{90}$, $Y_{\mathrm{w}}^{90}$, $X_{\mathrm{d}}^{90}$, $Y_{\mathrm{d}}^{90}$ and $X_{\mathrm{R}}$ in the Simplified Assessment of Steering Ability, any of the methods used in the Comprehensive Assessment can be applied; in addition, application of simplified empirical formulae seems suitable for this assessment level.

#### *2.4.6.4.3. Simplified Propulsion Ability Assessment*

The starting point is the system of equations (16)-(18), which has to be solved for all possible seaway directions to demonstrate that the ship is *able to keep forward speed of at least 6.0 knots in seaway from any direction*. Noting that bow seaways are most critical for required power at a given speed (Figure 54, middle plot), it is enough to consider only seaways from 0 to about 60° off-bow in the assessment. Further, neglecting the influence of drift on the required thrust and required power allows omitting equations (17) and (18). Thus only eq. (16) needs to be considered, and only in head waves:

$$X_{\mathrm{s}} + X_{\mathrm{w}} + X_{\mathrm{d}} + X_{\mathrm{R}} + T(1-t_{\mathrm{H}}) = 0$$

However, it is important to keep in mind that the time-average longitudinal force due to waves $X_{\mathrm{d}}$ should be taken as the maximum force in mean wave directions between 0 and 60° off-bow.

The contributions $X_{\mathrm{s}}$, $X_{\mathrm{w}}$, $X_{\mathrm{d}}$ and $X_{\mathrm{R}}$ can be found using any method from the Comprehensive Assessment (empirical, numerical or experimental). However, it seems logical to allow using also simpler approximations for these terms in the Simplified Assessment.

#### *2.4.6.4.4. Sufficient Propulsion and Steering Ability Check*

The simplest assessment procedure, *Sufficient Propulsion and Steering Ability Check*, is based on pure empirical formulae to define the required installed power as a function of main ship parameters. The formulae proposed below are based on the application of the comprehensive propulsion and steering assessment procedures to over 400 bulk carriers, tankers, container ships and general cargo vessels equipped with two-stroke low-speed diesel engines, a fixed-pitch propeller and a conventional rudder. For each ship, the maximum significant wave height was found, at which the required brake power is equal to the available brake power, separately for steering and propulsion criteria. Based on these results, MCR was approximated as empirical formulae of $h_s$, for each combination of main ship parameters, and then, the required installed power was found that satisfies the standard significant wave heights for propulsion and steering proposed in section 2.6.3.

The resulting empirical formulae are, for propulsion ability requirement

$$MCR = 0.21 \cdot C_B^{0.5} \cdot L_{pp}^2,$$

where MCR, kW, is the required installed power in terms of the maximum continuous rating of the engine, and for the steering ability requirement

$$MCR = 0.15 \cdot c_R \cdot L_{pp}^2,$$

where $c_R = L_{pp} T_m / \left(50 \cdot A_R^*\right)$, and $A_R^* = \min\left(2A_R / 3, A_R^p\right)$.

Figure 55 compares these empirical formulae with the results of the comprehensive assessment; ideally, the Sufficient Propulsion and Steering Ability Check should provide the same or slightly more conservative results than the Comprehensive Assessment. Testing of the proposed formulae by all interested stakeholders and its validation are required to approve / improve them; it should be noted that these formulae are suitable only for vessels equipped with two-stroke low-speed diesel engines, a fixed-pitch propeller and a conventional rudder; for other types of engine, propulsion and steering the simplified or comprehensive assessment should be used.

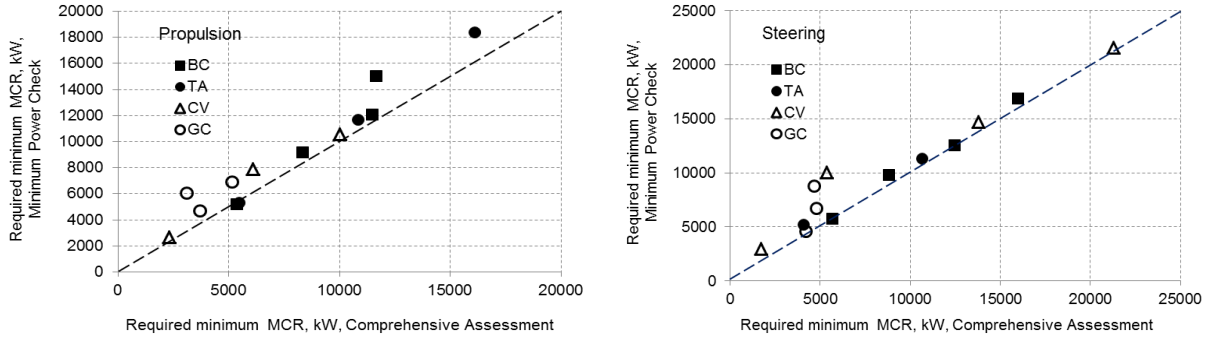


Figure 55. Required MCR according to Sufficient Propulsion and Steering Ability Check (y axis) in comparison to required MCR according to Comprehensive Assessment (x axis) for propulsion ability (left) and steering ability (right) requirements

## 2.5. Optimisation

The challenge of identifying the more suitable path between the conflicting requirements of reducing greenhouse emissions and at the same time maintaining adequate safety of ships in adverse sea conditions is the main objective of the SHOPERA project. To this end, the development of multi-objective optimization procedures are foreseen in SHOPERA, in which a ship's performance is assessed holistically, looking for the minimum powering requirement to ensure safe ship operation in adverse seaway/weather conditions, while keeping the right balance between ship economy, efficiency and safety of the ship and the marine/air environment. The planned optimization studies were implemented in two phases:

- The first phase consists of a *Global Optimization*, aiming to identify most favourable combinations of main dimensions, form parameters and other integrated characteristics of the ship, including powering and manoeuvring devices, for the selected operational profile. These studies should be carried out applying as far as possible simplified methods, developed within the project.
- The second phase consists of a *Detailed Optimization*, including hullform details. These studies should be carried out applying refined and more accurate methods.

### 2.5.1. Parametric Models for the Global Optimization of Passenger and Cargo Ships

The parametric models for the Global Optimization of Passenger and Cargo Ships, have been developed within the NAPA or the CAESES software tools. Using these models the following tasks are performed automatically without the need of any interaction with the user:

1. Hullform development
2. Resistance and propulsion estimations
3. Development of internal layout
4. Weights estimation - Definition of Loading Conditions
5. Evaluation of transport capacity (lanes length, number of cars/trucks, payload, volume of cargo holds or cargo tanks, depending on the ship type)
6. Evaluation of Stability Criteria and other Regulatory Requirements
7. Assessment of Building and Operational Cost, Annual Income and Selected Economic Indices
8. Evaluation of Energy Efficiency Design Index (EEDI)
9. Evaluation of hydrodynamic/manoeuvring performance in adverse seaway/weather conditions

The hullform and the internal layout of a medium-size ROPAX ship developed by the corresponding parametric model are shown in Figure 56 and Figure 57 respectively.

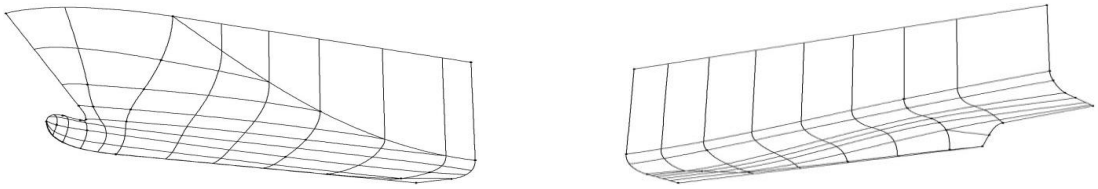

Figure 56: Typical hullform (fore and aft parts), developed by the parametric model

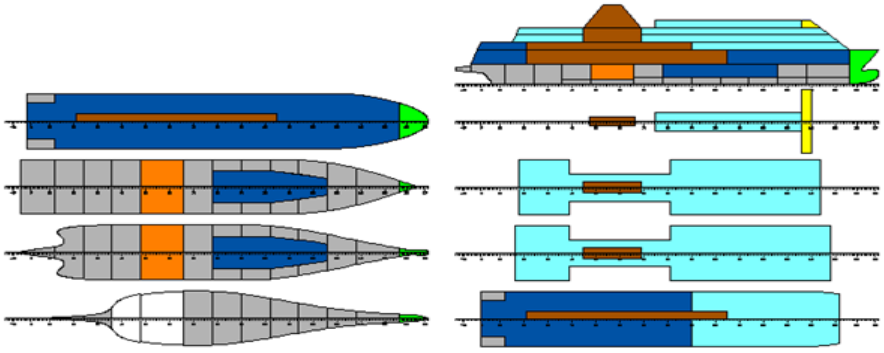

Figure 57: Internal arrangement of small RoPax developed by parametric model

### 2.5.2. Global Optimization Studies

The developed parametric models have been used for the global optimization of a series of passenger and cargo ships as shown in Table 10. In the following selected results are going to be presented. A detailed presentation of the employed methods and the obtained results from the optimization studies is given in Deliverable D5.3.

Table 10: Global Optimization Studies – Ship Types and Corresponding Software Platforms

| | Ship Type | Number of Ships | Software Platform |
|---|---|---|---|
| 1 | Bulk carriers | 2 | NAPA |
| 2 | Containerships | 2 | NAPA |
| 3 | Tankers | 2 | NAPA |
| 4 | Cruise ships | 1 | CAESES |
| 5 | RoPax Ships | 2 | CAESES |
| 6 | General cargo ships | 1 | CAESES |
| 7 | LNG carriers | 1 | CAESES |
| | TOTAL | 11 | |

#### 2.5.2.1. Optimization of a small RoPax Ship

The small RoPax ship is designed for operation between Piraeus and the Port of Rethymno at the island of Crete, with a roundtrip length of 320 sm, a transport capacity of 1,200 passengers, 200 private cars and 21 trucks and a service speed of 23.8 kn. For the above operational scenario, several studies have been performed with the optimization tool available in NAPA (i.e. the Optimization Manager), using Genetic Algorithms. The results presented in the following were obtained by varying the main dimensions as follows: Length BP from 105 m to 115 m, Beam from 18 m to 20 m and Design Draught from 5 m to 5.4 m.

Scatter diagrams of NPV vs. DWT and Propulsion Power are shown in Figure 58 and Figure 59. Only feasible designs are shown in these and the following diagrams, while the starting point of the optimization (the original design) is marked by a cross. A negative relationship between NPV and DWT is shown in Figure 58. This is because the freight rate of trucks was assumed to be constant, irrespectively of their weight. This way, ships capable of carrying the same number of trucks, but of increased mean weight, are penalised because of their increased propulsion power requirements, whereas at the same time they are not receiving any credit for their increased DWT capacity.

The obtained results indicated that compliance with the EEDI Phase II requirement was quite demanding for this study, as most of the unfeasible designs (not shown here) failed to satisfy this criterion. At the same time, only two designs were identified, marginally fulfilling the EEDI Phase III requirement. Scatter diagrams of the calculated margins with respect to the EEDI Phase II and Phase III are plotted in Figure 60. The EEDI margin is herein defined as the required EEDI minus the attained value. Therefore, a positive margin indicates a design complying with the corresponding phase, while designs with negative margin are failing to comply with the requirement. A plot of the calculated margin with respect to the EEDI Phase III requirement versus NPV is plotted in Figure 61. It is anticipated that systematic hullform and propeller optimizations, installation of energy saving devices and waste heat recovery systems, or other technological advances might help the designers to improve the performance of future ships, without the need of (significant) compromises with respect to service speed. However, with the current parametric model, it was found that, in order to obtain a significant number of designs in compliance with EEDI Phase III requirement, the design speed should be reduced down to 21.6 kn, a reduction that would have a significant impact on the specified operational scenario. For the design speed of 23.8 kn, four Wärtsilä 9V32 engines were selected for all ships presented herein. For the reduced speed of 21.6 kn, these engines were replaced by four Wärtsilä 9L26 engines. As a result, compliance with EEDI Phase III requirement was achieved by a number of design alternatives (see Figure 62).

In contrast to what was observed in the case of tankers and bulk carriers, compliance with the SHOPERA propulsion criterion in adverse weather conditions was easily achieved. The same conclusion was derived by all optimization studies for RoPax ships that were carried out, regardless of their size. This is of course

expected, since RoPax ships are highly powered in comparison with other types of ships of equal displacement. Even the designs with reduced service speed of 21.6 kn, complying with EEDI Phase III, had enough power to ensure adequate manoeuvrability in adverse weather conditions. Calculations performed with one propeller in operation (to verify redundancy of the propulsion system), and assuming a 30% reduction of the propeller thrust to account for ship motions, unsteady conditions and propeller racing, indicated that all feasible designs were able to achieve 12 kn at bow waves with a significant wave height of 4.0 m (see Figure 63). The propulsion criterion plotted in this figure corresponds to the ratio of the required to the available propulsion power; therefore, values less than 1.0 indicate compliance with the criterion.

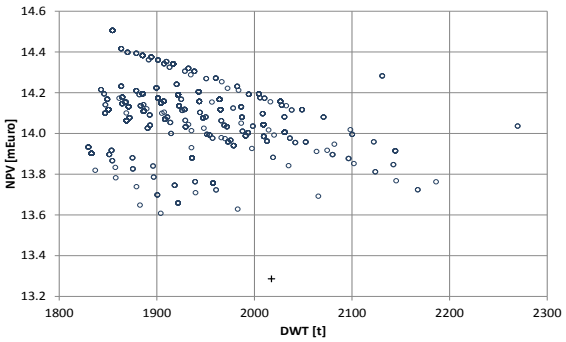


Figure 58. NPV vs. DWT

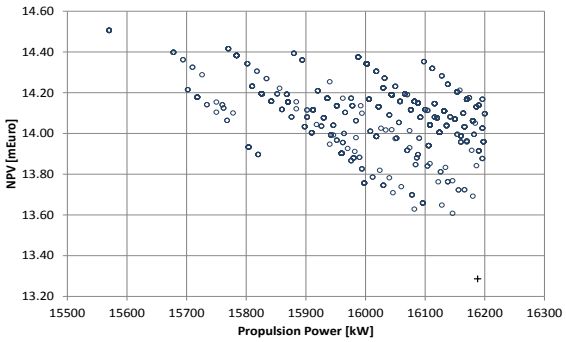


Figure 59. NPV vs. Propulsion Power

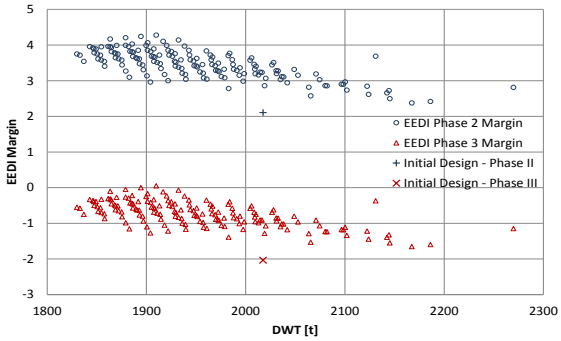


Figure 60. EEDI Phase II and III Margin vs. DWT

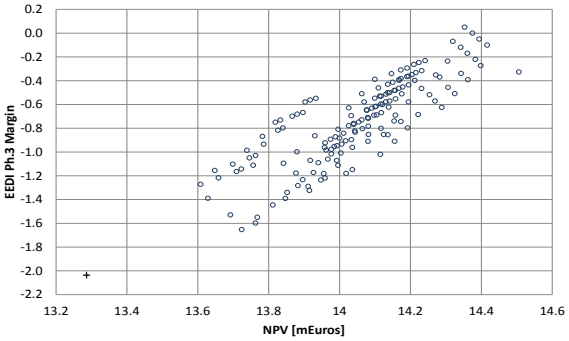


Figure 61. EEDI Phase III Margin vs. NPV

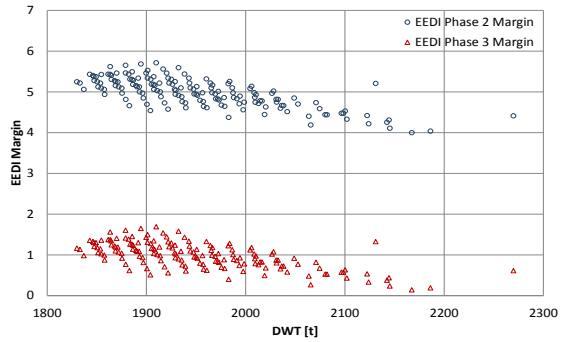


Figure 62. EEDI Phase II and III Margin vs. DWT for vessels with smaller engine

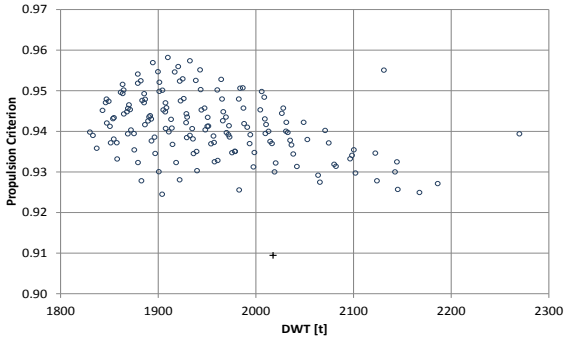


Figure 63. Propulsion Criterion vs. DWT

### 2.5.2.2. Optimization of a SUEZMAX Tanker

In the following, results obtained from the optimization of a SUEZMAX tanker will be presented. The ship is assumed to operate between Sidi Kerir and Aghioi Theodoroi, with a roundtrip length of 1,048 sm. The ship will be fitted with a main engine delivering 18,660 kW MCR at 91 RPM. The results presented in the following were obtained by varying the main dimensions as follows: Length BP from 240 m to 291 m, Beam from 44 m to 52 m and Design Draught from 15 m to 17.4 m.

A scatter diagram of NPV vs. DWT is shown in Figure 64. In contrast to the RoPax ships, in the case of cargo ships a strong positive relationship between NPV and DWT is shown. The calculated margins with respect to the EEDI Phase 0, Phase I and Phase II are plotted in Figure 65. The obtained results indicate that compliance with the EEDI Phase I requirement was easily achieved, while no design was found complying with Phase II (fulfilment of EEDI Phase I requirement was set as a constraint, therefore, all the feasible designs that are presented in the following diagrams comply with this requirement). In order to comply with the SHOPERA propulsion criterion, the ship must have enough power to achieve a forward speed of 6 kn at bow waves with a significant wave height of 5.5 m. As shown in Figure 66, all vessels comply with the criterion, with the larger margin obtained by some of the smaller ones, with DWT values bellow 164 kt. However, even in the other end of the DWT range some designs were found with a propulsion criterion bellow 0.915. A scatter diagram of EEDI margin vs. the propulsion criterion is shown in Figure 67.

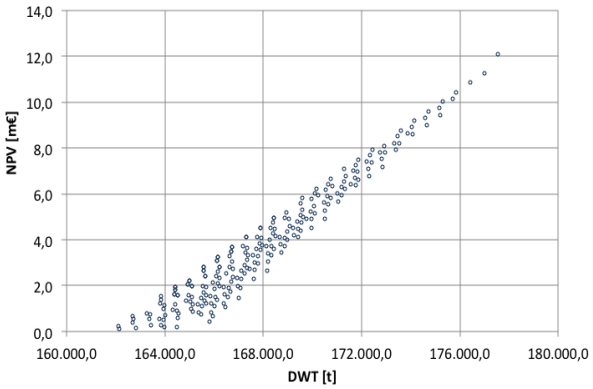


Figure 64. NPV vs. DWT

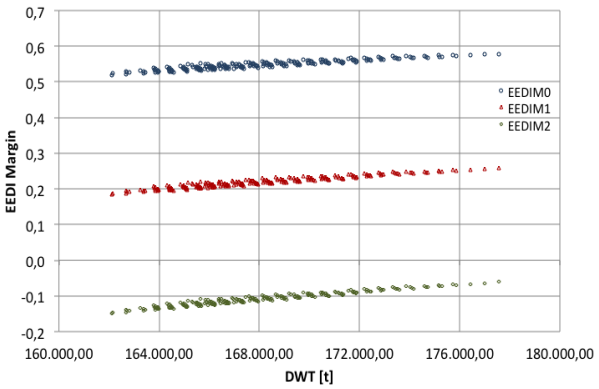


Figure 65. EEDI Phase 0, I and II Margin vs. DWT

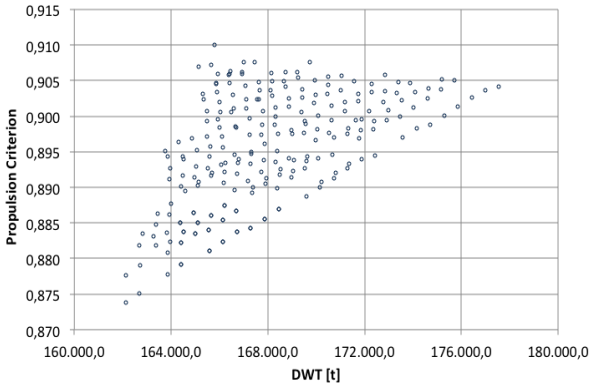


Figure 66. Propulsion Criterion vs. DWT

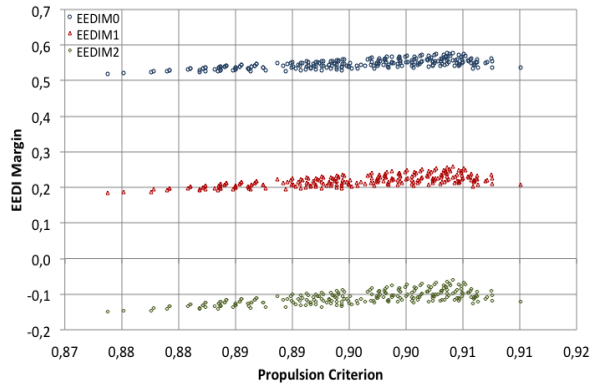


Figure 67. EEDI margin vs. Propulsion Criterion

### 2.5.2.3. Optimization of a 5,000 TEU Container Ship

Results obtained from the optimization of a 5,000 TEU Container ship will be presented next. The ship is assumed to connect the ports of Caucedo, Santos, Buenos Aires, Montevideo, Rio Grande, Itajai, Santos, Rio De Janeiro, Cartagena, Veracruz, Altamira, Houston and New Orleans, with a roundtrip length of 11,984 sm. The ship's service speed is 21.5 knots. The results presented in the following were obtained by varying the main dimensions as follows: Number of Bays from 14 to 18, Rows of containers from 13 to 17, Design Draught from 10 m to 14 m, Tiers in hold from 6 to 10 and Block coefficient from 0.56 to 0.77. The scatter diagram of NPV vs. DWT is shown in Figure 68. The calculated margins with respect to the EEDI Phase 0, Phase I and Phase II vs. DWT are plotted in Figure 69. Fulfilment of EEDI Phase II requirement was set as a constraint. Compliance with the SHOPERA propulsion criterion vs. DWT is shown in Figure 70. A scatter diagram of EEDI margin vs. the propulsion criterion is shown in Figure 71.

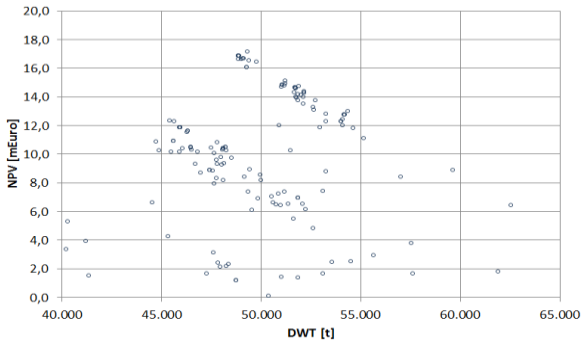


Figure 68. NPV vs. DWT

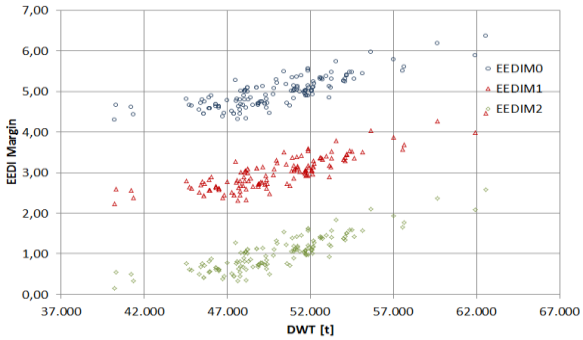


Figure 69. EEDI Phase 0, I, II Margin vs. DWT

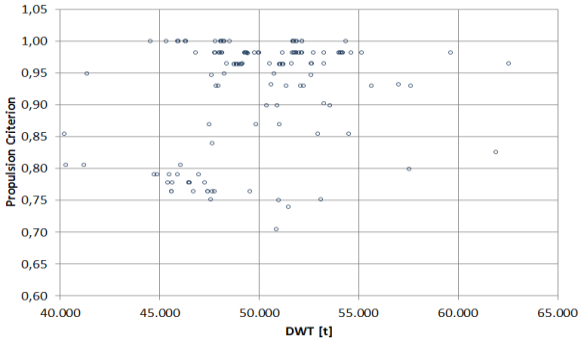


Figure 70. Propulsion Criterion vs. DWT

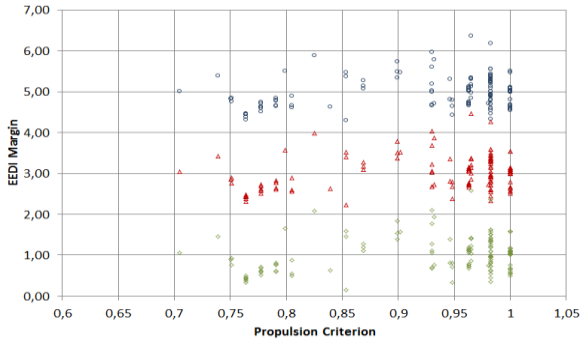


Figure 71. EEDI margin vs. Propulsion Criterion

### 2.5.2.4. Optimization of a Cruise Ship

The Cruise Ship is designed for worldwide and year-round operation following the summer season in Europe and Caribbean areas, assuming a constant number of passengers and revenue. The results presented below were obtained by varying the following design variables: Beam from 25 m to 30 m, Draught from 6.4 m to 7 m, Half Beam from 13.4 m to 15.4 m, Height from 16 m to 20 m, Position of FP (xFp) from 200 m to 250 m, Position of Main Frame (xMainFrame) from 79 m to 89 m, Position of Peak (xPeak) from 225 m to 275 m and Position of Transom (xTransom) from -12 m to -8 m. The scatter diagrams of Length Overall vs. GT and Propulsion Power are shown in Figure 72 (only feasible designs are included). The obtained results indicate that compliance with EEDI Phase II & III was easily achieved. The calculated margins with respect to the EEDI Phase II and Phase III vs. DWT and the compliance with the SHOPERA propulsion criterion are also plotted in Figure 72. The results presented are obtained with SHOPERA criteria as developed for Cruise Ships CPP propulsion.

## 2.5.3. Local hullform optimizations

Five ship types were selected for detailed hullform optimization. Three of them have been extensively studied in the other WPs of SHOPERA; the Calmac RoPax, the DTC container ship and the KVLCC2 tanker. A Cruise Ship, derived by the global optimization was the 4$^{th}$ ship selected for detailed hullform optimization studies and finally the D-Bulker of NAPA was also used by courtesy of NAPA Ltd. The Calmac RoPax represents a small Roro Passenger ferry, which is operating in area where both confined waterways and adverse open sea weather conditions prevail. Two versions were analysed: with and w/o a bulbous bow. For the KVLCC2 tanker and the D-Bulker, along with the original version, featuring a bulbous bow, two alternatives were tested, one with a bulbous bow of increased size and one w/o a bulbous bow.

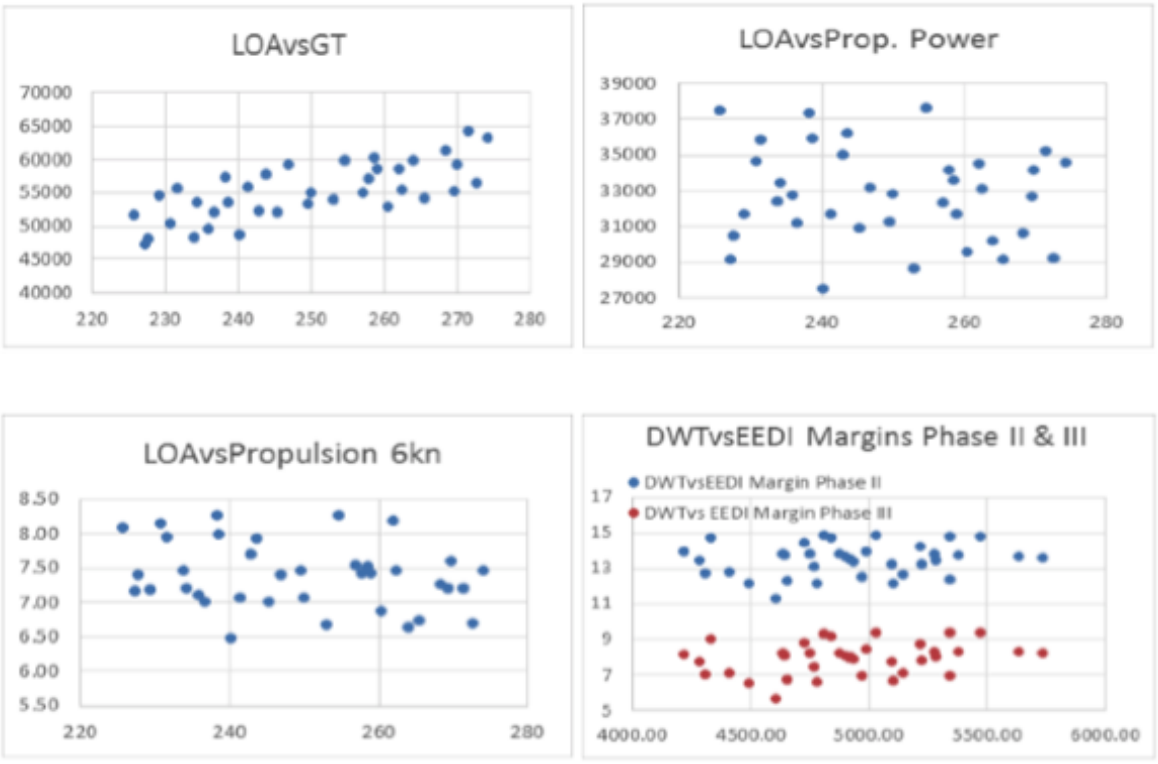


Figure 72. Obtained results from the optimization of the Cruise ship

The hydrodynamic performance analysis both for the tanker and the bulk carrier revealed that the larger bulbous bow section seemed to decrease the resistance both in shallow and deep water. The difference of resistance in shallow and deep water was significant. The versions without the bulbous bow provided the largest resistance in all conditions.

The added resistance in waves of the tanker ship was minimized with the non-bulbous bow version. This version, however, produced clearly the highest resistance values in calm water. Quite the converse trend was observed with the bulkers, as the version with no bulbous bow, had clearly the highest value for the added resistance in waves.

The bow form optimization of the Cruise ship and the Container ship has been conducted to ascertain the performance of their hull in terms of the added resistance in waves. The step-wise modifications were done on the hull and the added resistance in waves of different frequencies were calculated. An in-house code was used based on the pressure integration method. In the first stage of the work for the cruise ship optimization, a sensitivity analysis of 15 parameters was made by changing by ±10% the original values. Next the most influent parameters were identified and a response surface was fit to the results, using a linear polynomial approximation. Finally by determining the minimum value of the added resistance, the optimum combination of the parameters was obtained. In the bow form optimization of a Container ship hull, all the form parameters were used. Next a response surface was fit to the results of a systematic variation conducted by altering the hull parameters by a factor of ±10%. Finally, by determining the minimum value of the added resistance, the optimum combination of the form parameters was obtained.

## 2.6. Case Studies

### 2.6.1. Introduction

It is not realistic and not necessary to design ships for operation in the worst possible storms that can be theoretically encountered, when considering ship's economy and the fact that ships can nowadays timely avoid such stormy conditions by improved weather forecasts and satellite information systems. The *standard* operational wave heights of ships should be defined in such a way that the majority of the *existing* vessels fulfils the related requirements, because, first, present design and operational practices cannot be changed abruptly, for example, because of the introduction of EEDI and, second, the present safety level with respect to manoeuvrability-related accidents in heavy weather is satisfactory, *Ventikos et al. (2014)*. Notably, to similar conclusions comes a study by IACS, *EE-WG 1/4 (2010)*, Table 5, which identifies rather mild standard wave heights for weather-vaning (wind speed up to 21 m/s and significant wave height up to 5.4 m) and advance speed (up to Bft 8 at 6.0 knots advance speed) requirements.

Therefore, benchmarking of the existing fleet with respect to the herein proposed new criteria appears as the most rational way to define standard wave heights in relation to implementation of the EEDI requirements. Such an approach was also used in the IACS studies on minimum power requirements and led to the environmental conditions in the 2013 Interim Guidelines: wind speed 15.7 m/s at significant wave height 4.0 m for ships with $L_{pp}$=200 m to 19.0 m/s and 5.5 m, respectively, for $L_{pp}$=250 m and greater.

Therefore, case studies were undertaken in SHOPERA concerning all ship types considered in the EEDI regulations.

### 2.6.2. Comparison between Criteria

The weather-vaning ability was treated using a simplified criterion, as the ability of the ship to keep position in bow to bow-quartering seaway; this simplification follows from the observation that the ship (with the traditional steering devices at the stern) will not be able to keep heading under the action of environmental forces if the forward speed is not sufficiently large, because of significantly reduced manoeuvring reactions on the hull and steering force on the rudder. Figure 73 compares marginal significant wave heights according to comprehensive propulsion assessment (x axis, note that here 4.0 knots advance speed was used) with marginal significant wave heights according to the comprehensive position keeping (y axis) assessments for bulk carriers, tankers and container vessels. Obviously, marginal wave heights for position-keeping are consistently greater than those for 4.0 knots propulsion; the deviation between results decreases with increasing ship size, according to Froude law. Note, however, that the marginal wave heights according to these assessments are very well correlated, which means that for norming, one of the criteria is redundant. Before making the final choice, a comparison with assessment based on other weather-vaning criteria would be useful, e.g. with the more comprehensive "heading recovery" criterion proposed by the project conducted in The Netherlands.

Figure 74 compares marginal wave heights according to comprehensive propulsion assessment (x axis, here, 6.0 knots advance speed was used) with marginal wave heights according to steering assessment (y axis) for bulk carriers (BC), tankers (TA), general cargo vessels (GC) and container ships (CV). The marginal wave heights according to these two criteria are also correlated to some degree, however, with significantly more spreading than for the position keeping vs. propulsion. It can be concluded that fulfilment of the propulsion ability requirement at a certain marginal significant wave height guarantees fulfilment also of the steering ability requirement at a marginal significant wave height of about 1.0 m smaller. The difference becomes slightly greater than 1.0 m at the propulsion marginal significant wave heights above about 5.5 m, which are, perhaps, not relevant anyway. Note, however, that this correlation between the propulsion and steering abilities stems from the fact that the steering systems of the considered ships are properly dimensioned according to other requirements, e.g. IMO Manoeuvrability Standards (2002).

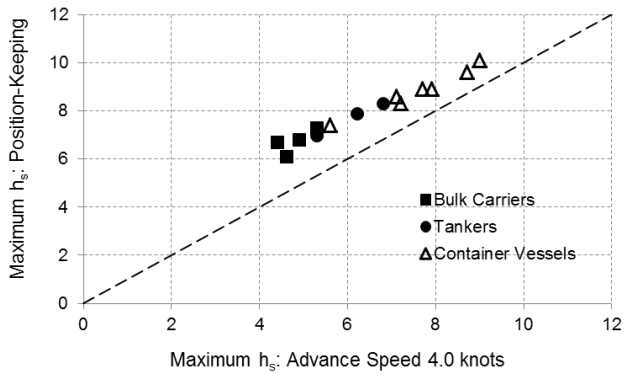


Figure 73. Marginal significant wave heights according to comprehensive 4.0 knots propulsion (x axis) and comprehensive position keeping (y axis) assessment

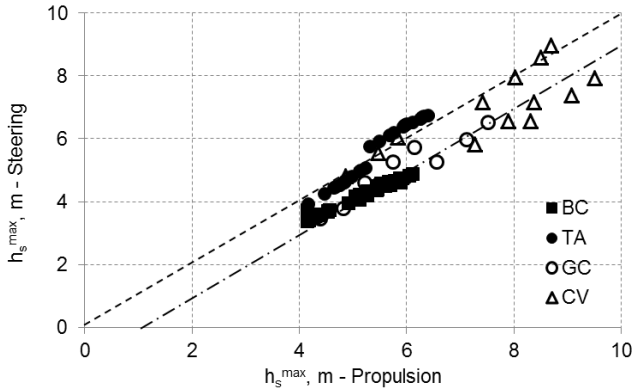


Figure 74. Marginal wave heights according to comprehensive propulsion (x axis) and steering (y axis) assessments for bulk carriers (BC), tankers (TA), general cargo vessels (GC) and container ships(CV)

### 2.6.3. Definition of Standard Wave Heights Using Comprehensive Assessment

One of the aims of the Case Studies was to provide recommendations for the standard wave heights using Comprehensive Assessment. This study was done as follows: first, a sample of representative vessels was selected; after that, the Comprehensive Assessment of Propulsion and Steering Abilities was applied to find the marginal wave height (separately for Propulsion and Steering and for different ship types and sizes); finally, a fit of the determined marginal wave heights vs. $L_{pp}$ was done to define the standard wave height per ship type and overall for all ship types; note that the marginal wave heights were considered separately for the Propulsion and Steering Abilities.

To select representative vessels, several series of designs were generated:

1. Series of bulk carriers and tankers along the defined boundary lines MCR($L_{pp}$), which exclude a certain percentage of vessels with lower power. As the "bottom line", a line corresponding to the limit of 5% of the low-powered vessels was used; besides, 10%-, 20%- and 30%-lines were defined and series of ships were generated. For comparison, low-power series were generated also for container ships and general cargo vessels. These series were generated using the IHS-FairPlay data for each of the considered vessel types.
2. Series of bulk carriers and tankers along the lines MCR($L_{pp}$) corresponding to vessels that fulfil marginally the requirements of EEDI implementation Phase 1, 2 and 3.
3. Series of bulk carriers and tankers along the Minimum Power Lines according to the 2013 Interim Guidelines, Res. MEPC.232(65), as amended by Res. MEPC.255(67) and MEPC.262(68).

These series of bulk carriers and tankers are shown in graphs of *length between perpendiculars* ($L_{pp}$, *x* axis) vs. *installed power* (MCR, *y* axis) together with the *FairPlay* data in Figure 75 to Figure 77; Figure 78 shows container ships and general cargo vessels, which were used for comparison.

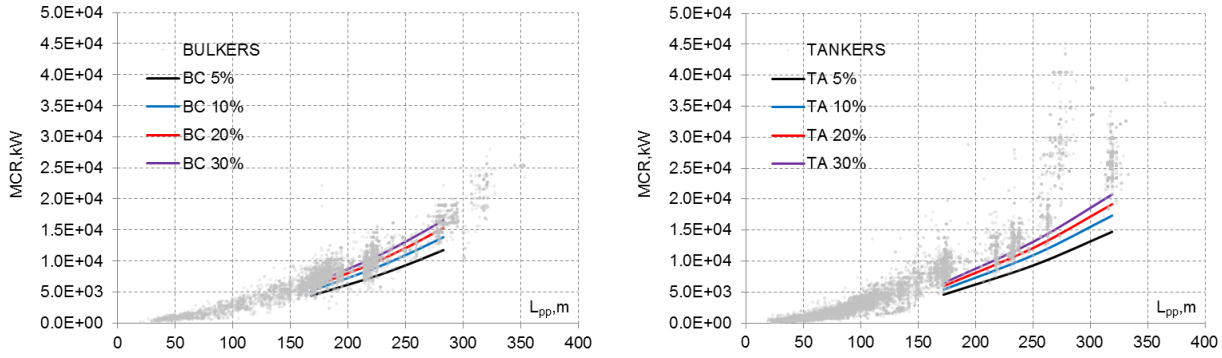


Figure 75. Series (solid lines) of bulk carriers (left) and tankers (right) corresponding to the 5% (lowest line), 10% (next line), 20% and 30% of FairPlay database (grey points) low power vessels

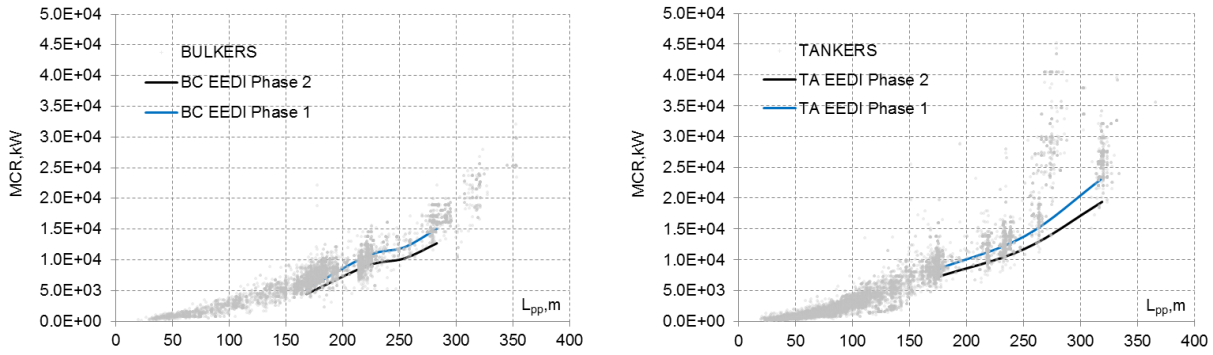


Figure 76. Series (solid lines) of bulk carriers (left) and tankers (right) marginally fulfilling requirements of EEDI implementation Phase 2 (lowest line) and 1 (top line) vs. FairPlay database (grey points)

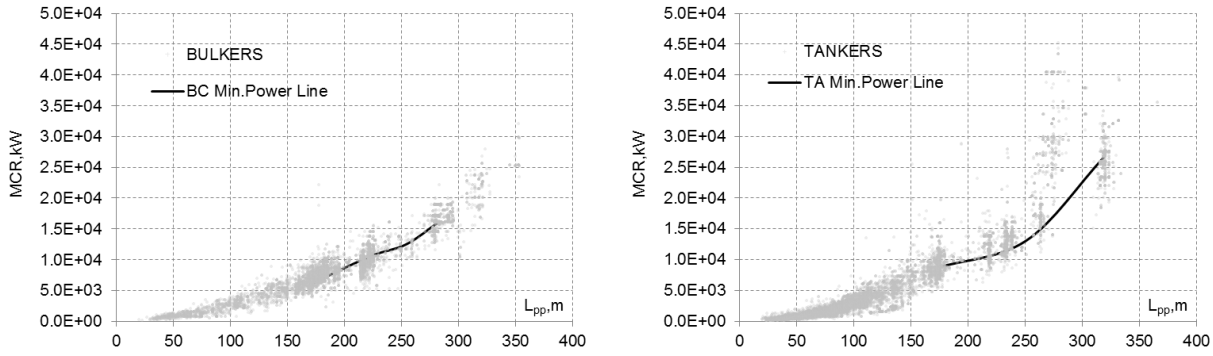


Figure 77. Series (solid lines) of bulk carriers (left) and tankers (right) marginally fulfilling requirements of (updated) Minimum Power Lines of 2013 Interim Guidelines

The marginal significant wave heights obtained with Comprehensive Propulsion and Steering assessment are shown in Figure 79, left and right plots, respectively, for the bulk carriers and tankers with the installed power corresponding to the 5% of low power vessels of the *FairPlay* database. Results for low-power container ships and general cargo vessels are shown for comparison. Bulk carriers and tankers look very similar with respect to the marginal wave heights and are significantly below container ships.

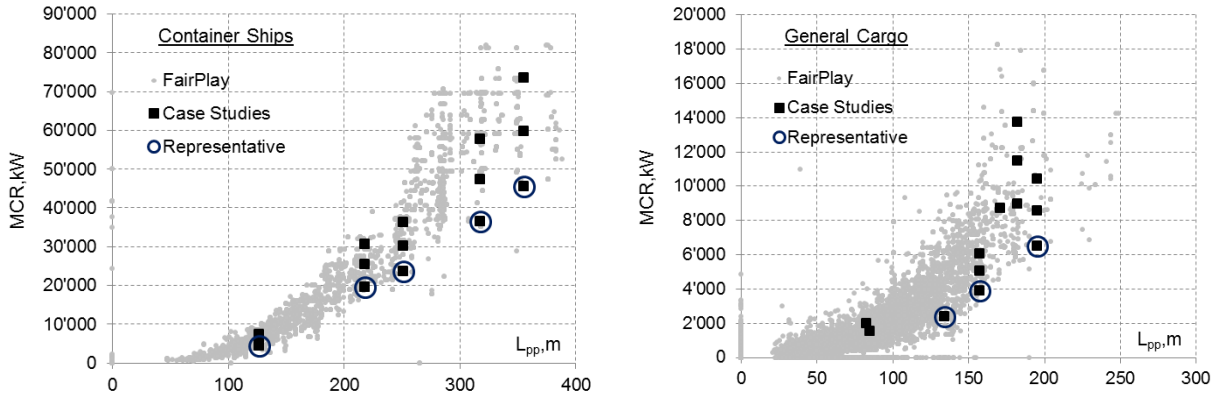


Figure 78. Series of container ships (left) and general cargo vessels (right) selected for comparison (circles) with bulk carriers and tankers along low-power boundary of IHS FairPlay database

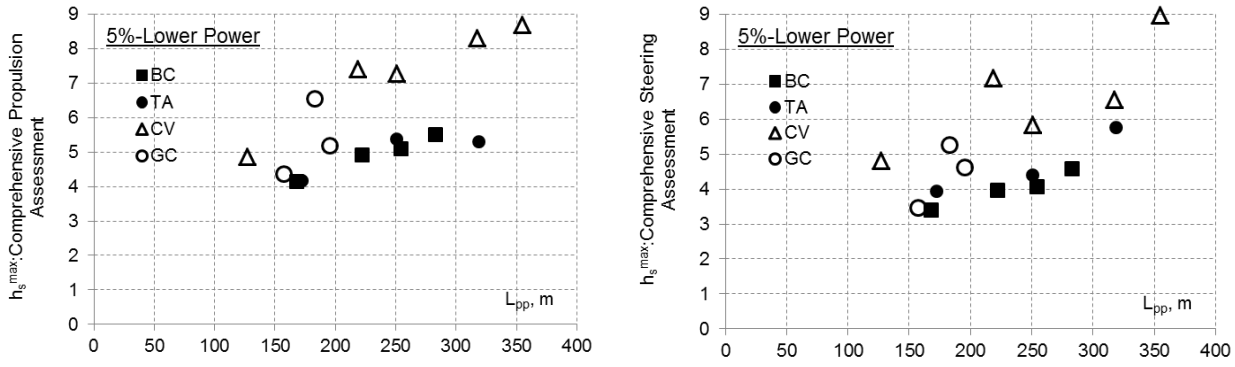


Figure 79. Marginal significant wave heights for bulk carriers (BC) and tankers (TA) with installed power corresponding to the 5% of low power vessels of HIS FairPlay database according to Comprehensive Propulsion (left) and Comprehensive Steering (right) assessments; results for low-power container vessels (CV) and general cargo (GC) vessels are shown for comparison

Figure 80 shows marginal significant wave heights for bulk carriers and tankers with an installed power corresponding to 20% of low power vessels of *FairPlay* database. The results indicate that, if only the propulsion ability is taken into account, bulk carriers and tankers with a power at about the 20% MCR line of the FairPlay database are slightly above the current standard ($h_s$=5.5 m at Lpp=250 m); Steering Ability appears to be more critical, i.e. it corresponds to lower marginal wave heights than Propulsion Ability.

Figure 81, Figure 82 and Figure 83 show marginal significant wave heights for bulk carriers and tankers marginally satisfying the requirements of EEDI implementation Phase 3, 2 and 1, respectively. The results show that if only propulsion ability is taken into account, the current standard $h_s$=5.5 m at Lpp=250 m is fulfilled by Phase 1-compliant tankers and bulk carriers and, marginally, by Phase 2 compliant tankers and bulk carriers.

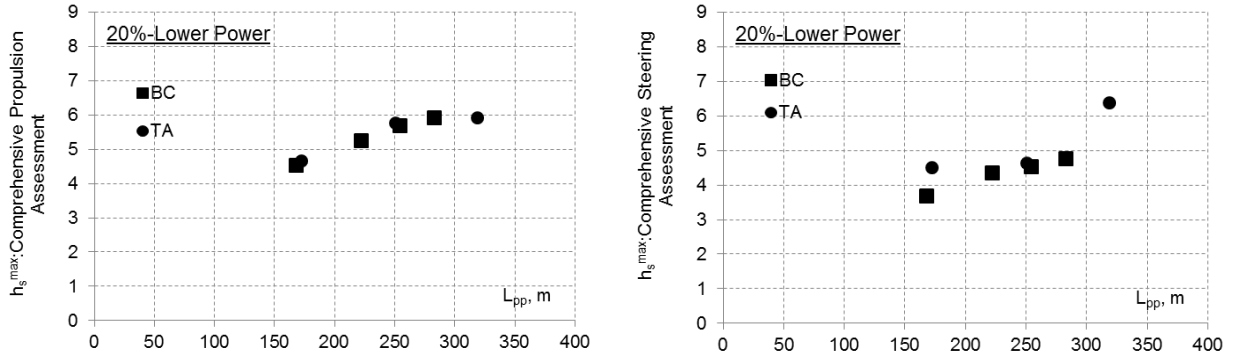


Figure 80. Marginal significant wave heights for bulk carriers (BC) and tankers (TA) with installed power corresponding to 20% of low power vessels of FairPlay database according to Comprehensive Propulsion (left) and Comprehensive Steering (right) assessments

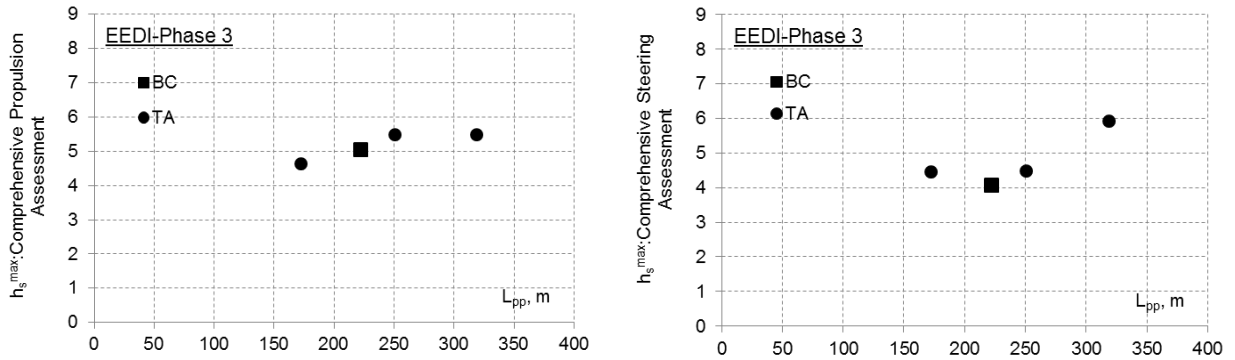


Figure 81. Marginal wave heights for EEDI-Phase 3 compliant bulk carriers (BC) and tankers (TA) according to Comprehensive Propulsion (left) and Comprehensive Steering (right) assessments

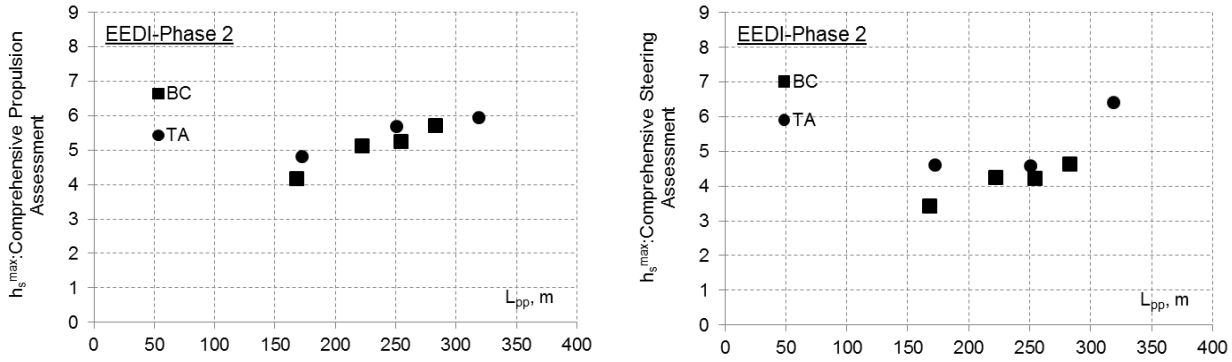


Figure 82. Marginal wave heights for EEDI-Phase 2 compliant bulk carriers (BC) and tankers (TA) according to Comprehensive Propulsion (left) and Comprehensive Steering (right) assessments

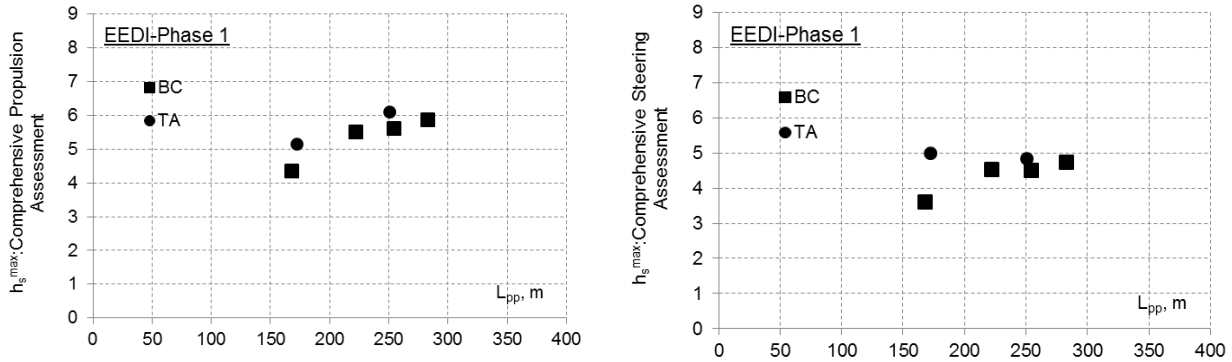


Figure 83. Marginal wave heights for EEDI-Phase 1 compliant bulk carriers (BC) and tankers (TA) according to Comprehensive Propulsion (left) and Comprehensive Steering (right) assessments

Figure 84 shows the marginal significant wave heights according to comprehensive propulsion and steering abilities assessments for bulk carriers and tankers, which marginally satisfy the Minimum Power Lines of 2013 Interim Guidelines.

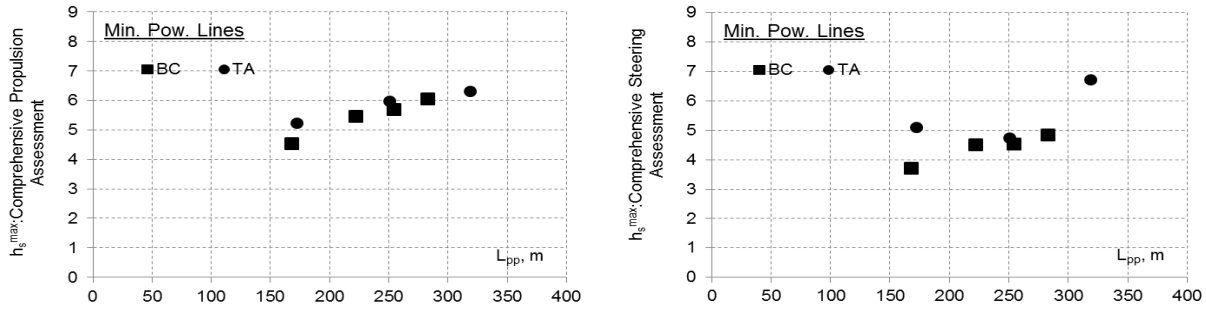


Figure 84. Marginal wave heights according to Comprehensive Propulsion (left) and Steering (right) Abilities assessment for bulk carriers (BC) and tankers (TA) marginally compliant with Minimum Power Lines of 2013 Interim Guidelines

Based on the obtained marginal wave heights for bulk carriers and tankers, and requiring that the standard wave height for the propulsion ability assessment is equal to the standard wave height according to the 2013 Interim Guidelines of 5.5 m for vessels with $L_{pp}$=250 m, the following can be proposed:

$$h_s = \min\left(2.2 + L_{pp}/75, 5.5\right),$$

or the standard wave heights can be set equal to those (slightly less conservative for vessels of Lpp < 250 m) in the 2013 Interim Guidelines. To define standard wave heights for the steering ability assessment, it was assumed that, on the average, the same percentage of vessels from the total number of vessels used should fail the steering ability assessment as the propulsion ability assessment (for the individual vessels, one or the other requirement can be dominating). This led to the following function:

$$h_s = 2.0 + L_{pp}/100 .$$

One observation from these results is that the marginal wave heights are ship size-dependent: larger vessels are able to fulfil both propulsion end steering requirements at greater significant wave heights than smaller vessels. This is understandable physically; in principle, ship size dependent standard wave heights may be acceptable from the pragmatic point of view: because consequences of accidents are greater for larger vessels, acceptable probability of accidents should be lower for larger vessels. Besides, ship size-dependent standard wave height would reflect existing design and operational practices: smaller vessels, obviously, do not operate in storms of the same severity as larger vessels. Note that standard wave heights in the 2013 Interim Guidelines are also ship-size dependent, however, this is a subject of on-going discussion.

Another observation from Figure 79 is that the marginal wave heights differ, partly substantially, between different ship types; this will be discussed in the next section, including results also for other ship types besides bulk carriers, tankers, container ships and general cargo vessels.

A final note concerns the possibility of contradiction between fulfilling the proposed requirements to manoeuvrability in adverse weather conditions and the possibility to fulfil EEDI requirements, which are progressively strengthening from Phase 1 to Phase 3. It is interesting to note that whereas the selected low-power general cargo vessels and container carriers satisfy the standard wave heights corresponding to the 2013 Interim Guidelines and, at the same time, easily fulfil the requirements to Phase 3 of EEDI implementation (as presently formulated), the selected bulk carriers and tankers, marginally satisfying standard wave heights of the 2013 Interim Guidelines, are able to marginally fulfil requirements of Phase 2 of EEDI implementation, but not the requirements of Phase 3.

Note, however, that standard wave heights can be adjusted to the marginal wave heights of Phase 3-compliant bulk carriers and tankers, i.e. effectively, slow-steaming designs; whether such vessels can be considered as representative vessels of fleet in service requires a prolonged discussion with all interested stakeholders.

### 2.6.4. Comparison between Ship Types using Simplified Assessment

The simplified assessment of propulsion and steering ability is more conservative than the comprehensive assessment, therefore, it was not applied to define the standard wave heights. On the other hand, it can be used to compare performance of vessels of different types with respect to EEDI requirements, when selected vessels of different types have comparable performance with respect to manoeuvrability in adverse conditions.

In this study, vessels of different types were selected, which have the same marginal wave heights (computed using simplified assessment procedure) as bulk carriers and tankers, marginally compliant with the requirements of either Phase 1, 2 or 3 of EEDI implementation, and it was analysed, requirements of which EEDI phase can these selected vessels satisfy. The analysis shows that the general cargo vessels satisfy either the same EEDI phase as the bulk carriers and tankers with the same marginal wave heights (this concerns old designs of general cargo vessels), to “higher” Phases; all other vessel types (Cruise Vessels, LNG and Gas Carriers, RoRo Cargo and RoPax) achieve significantly “higher” phases of EEDI implementation than bulk carriers and tankers if they have comparable marginal wave heights with respect to manoeuvrability in heavy weather.

Figure 85 illustrates these conclusions by showing marginal significant wave heights according to simplified propulsion (left) and simplified steering (right) abilities assessment for bulk carriers, tankers, container vessels, general cargo vessels, LNG and gas carriers, RoRo cargo vessels, reefers and RoPax vessels. In each plot, only vessels satisfying requirements of a certain EEDI implementation phase are shown: Phase 3 denotes vessels, satisfying requirements of Phase 3, Phase 2, vessels satisfying requirements of Phase 2, but not showing vessels satisfying Phase 3 requirements etc.

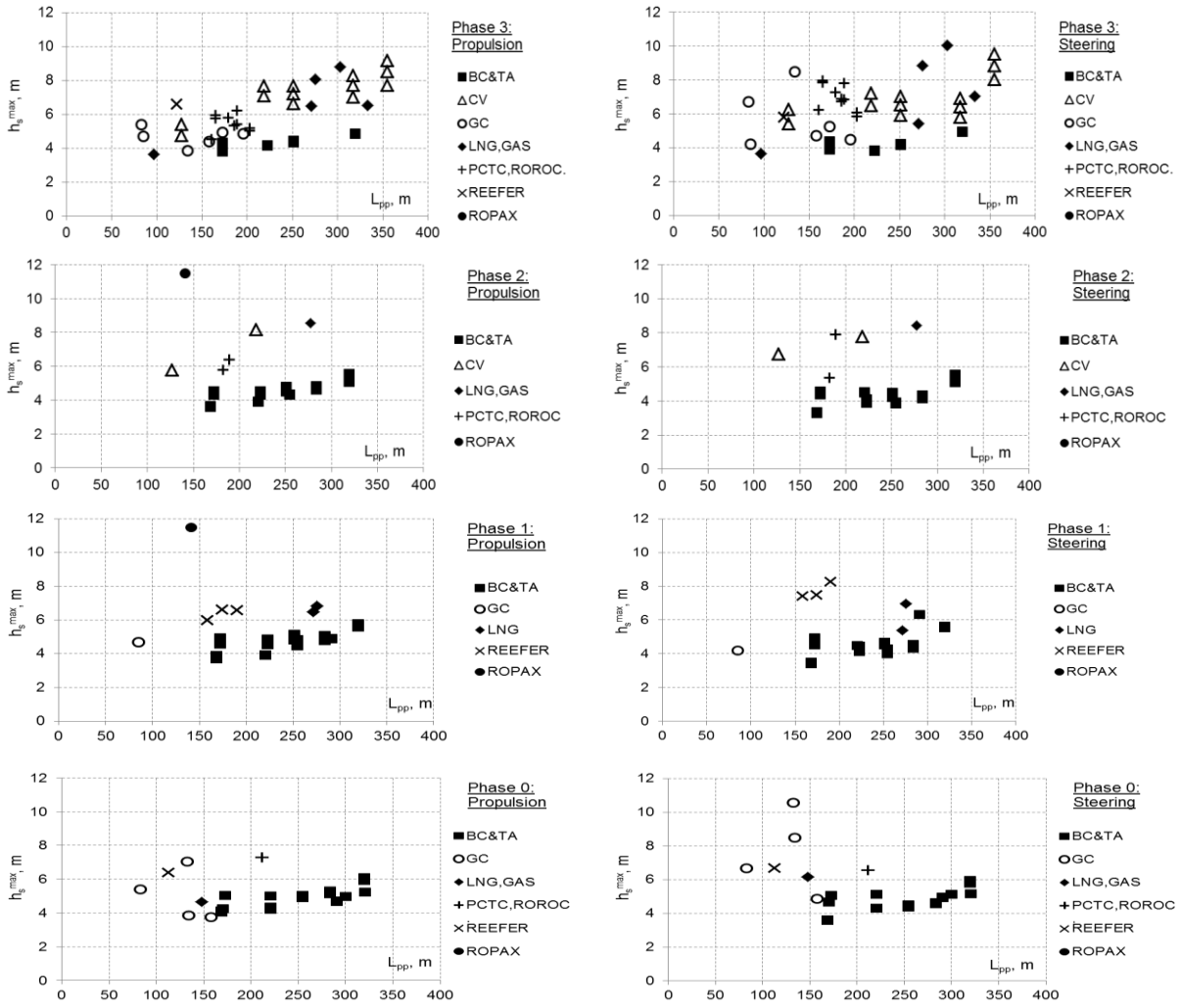


Figure 85. Marginal significant wave heights according to simplified propulsion (left) and simplified steering (right) abilities assessment for bulk carriers (BC), tankers (TA), container vessels (CV), general cargo vessels (GC), LNG and gas carriers (GAS), pure car and truck carriers (PCTC), RoRo cargo (ROROC), reefers and RoPax vessels, satisfying requirements of EEDI Phase 3 (denoted Phase 3), Phase 2 (denoted Phase 2; not showing vessels satisfying Phase 3 requirements), Phase 1 (denoted Phase 1; not showing vessels satisfying Phase 2 and 3 requirements) and Phase 0 (denoted Phase 0; not showing vessels satisfying Phase 1, 2 and 3 requirements).

Note that absolute values of the marginal wave heights in Figure 85 are not relevant, because they correspond to a more conservative, simplified assessment procedures, than the comprehensive assessment used in the previous section. However, relative differences between different ship types are correctly reproduced; they show that for each phase, bulk carriers and tankers show remarkably similar marginal significant wave heights, which are lowest over all ship types. Container vessels demonstrate high marginal wave heights due to high installed power; passenger vessels (RoPax and cruise vessels) show significantly higher marginal wave heights than other vessel types due to advanced propulsion and steering systems (twin screw, diesel-electric main propulsion, controlled pitch propeller, pods).

An important consideration is the possibility of contradiction between fulfilling the proposed requirements to manoeuvrability in adverse weather conditions and the need to fulfil EEDI requirements, which are progressively strengthening from Phase 0 to Phase 3. Note that all vessel types, with exception of bulk carriers and tankers can fulfil the requirements to Phase 3 of EEDI implementation, as presently formulated, and at the same time satisfy the requirements of the proposed criteria for manoeuvrability in adverse weather conditions with the proposed standards. On the other hand, bulk carriers and tankers, if they satisfy the proposed standards, are able to fulfil marginally requirements of Phase 2, of EEDI implementation. Note, however, that standard wave heights can be lowered to include also Phase 3-

compliant bulk carriers and tankers (which are, effectively, slow-steaming vessels); whether such vessels can be considered as representative vessels of fleet in service should be a subject of discussion with all interested stakeholders.

A final note concerns the question whether the standard wave heights should depend on ship type. On the one hand consequences of accidents, as well as operational practices, differ between different ship types, especially between passenger and cargo vessels. Besides, the revealed differences in the marginal wave heights between different ship types reflect established design and operational practices, which should not be drastically changed by new regulations, assuming that the present level of safety is satisfactory. Both these arguments are in favour of correspondingly different standard wave heights per ship type. On the other hand, the revealed difference in the manoeuvring characteristics in heavy weather reflects, obviously, different requirements to the operational performance of the propulsion and steering systems of ships of different types, not related to safety. Obviously, reaching a conclusion regarding ship type-dependency of standard wave heights requires a prolonged discussion with all interested stakeholders.

## 2.7. Dissemination, Exploitation, Submission to IMO, Other Activities

### 2.7.1. Dissemination Activities

Dissemination of the research output has been facilitated mainly through technical publications in international scientific journals, conferences and workshops. The consortium also facilitated the dissemination of the research output to a wider audience through a series of articles and presentations in public mass media. A project-specific web site has been created and is constantly updated and maintained by the coordinator during the elaboration of the project and for at least 3 years after the project's end. A public area is maintained on the project's web site, allowing free access to selected deliverables, reports and publications resulting from the elaboration of the project. To exchange views with external experts in ship design, hydrodynamics, safety and operation, shipowners, regulators and other stakeholders on hydrodynamic, design and regulatory aspects of norming manoeuvrability in adverse conditions, fine-tune the objectives of the project and the way ahead and, at the same time, facilitate acceptance of the project outcomes by the key stakeholders, four public workshops have been organised within the project.

- **Peer Reviewed Journal Papers:** *20 Papers, full list in D.7.6*
- **Peer Reviewed Conference Papers:** *58 Papers, full list in D.7.6*
- **SHOPERA Presentations:** 5 submissions, full list in D.7.6
- **Submissions to IMO:** 5 submissions to IMO
- **Mass media**

The SHOPERA project was selected among EU funded projects for presentation at the EURONEWS channel. The video was produced by EURONEWS Science with films/interviews at ULJANIK shipyards, Croatia and CEHIPAR, Spain. The video was first transmitted by EURONEWS on Monday 26/09/2016 and broadcasted the whole week after. The program is now available in all the 13 languages on EURONEWS' website: http://www.euronews.com/programs/futuris/ and, on the EURONEWS' YouTube channels (http://eurone.ws/MMZbq and https://www.youtube.com/user/euronewsknowledge/videos).

- **First Public SHOPERA Workshop**

The first workshop "Introduction of the Project to Key Stakeholders" was organised by GL with the assistance of NTUA on October 30, 2014, in Hamburg, to communicate the objectives of the project to the wider scientific and technical community and to the various stakeholders.

- **Second Public SHOPERA Workshop**

The second public SHOPERA workshop was organized by IST with the assistance of NTUA on October 15, 2015 in Lisbon. The aim of this workshop was to communicate the findings of the first two years of the elaboration of the project to the wider scientific and technical community as well as to the various stakeholders and to obtain valuable feedback from the external participants regarding the set objectives and the procedures adopted in order to meet these objectives.

- **Third Public SHOPERA Workshop**

The third public SHOPERA workshop was hosted by LR and jointly organised by LR, NTUA and ITTC Manoeuvring Committee on April 14, 2016 in London with representatives from the ITTC Seakeeping, Stability and Performance Committees. The aim of this workshop was to communicate the findings from the elaboration of the project to the wider scientific and technical community, to enhance collaboration of the SHOPERA partners with other research teams working on the same or similar research topics in Japan, Korea, The Netherlands as well as with the ITTC Manoeuvring Committee and Seakeeping Committee and to obtain valuable feedback from the external participants regarding the set objectives and the procedures adopted in order to meet these objectives.

- **Fourth Public SHOPERA Workshop**

The fourth public SHOPERA workshop was hosted and organised by NTUA on September 28, 2016 in Athens. The aim of this workshop was to provide the overall presentation of the elaboration of the project, with emphasis on the set objectives, adopted procedures towards the objectives, major achievements, key results, collaboration with similar studies in Japan and the Netherlands, conclusions and recommendations. In particular, the developed new guidelines for the required minimum propulsion power and steering performance of various types of ships to maintain manoeuvrability under adverse conditions were presented and discussed with the scientific community and key stakeholders.

### 2.7.2. Submission to IMO

The ultimate aim of the project is to develop revised guidelines for various types of ships to evaluate the ability of ships to maintain manoeuvrability under adverse conditions. The proposal for the guidelines has been prepared and submitted to IMO-MEPC 70 with the aim of their finalisation and adoption at MEPC 71. The key results and conclusions of the project have been submitted as an accompanying information paper. The submission was done through the flag state delegation of Norway and supported by the member states Denmark, Germany and Spain.

The full list of submissions from SHOPERA to IMO is given in the following:

1. IMO MEPC (2014) EU Project "Energy Efficient Safe SHip OPERAtion" (SHOPERA), Paper MEPC 67/INF.14 submitted by Germany, Norway and United Kingdom
2. IMO (2016) Progress report of SHOPERA and JASNAOE projects for development of the revised minimum propulsion power Guidelines, Paper MEPC 69/INF.23 submitted by Denmark, Germany, Japan and Norway 12 February 2016
3. IMO (2016) Progress report of SHOPERA and Japan's projects and outline of draft revised Guidelines for determining minimum propulsion power to maintain the maneuverability of ships in adverse conditions, Paper MEPC 70/5/20 submitted by Denmark, Germany and Japan
4. IMO (2016) Supplementary information on the draft revised Guidelines for determining minimum propulsion power to maintain the maneuverability of ships in adverse conditions, Paper MEPC 70/INF.30 submitted by Denmark, Germany and Japan
5. IMO (2016) Results of research project "Energy Efficient Safe Ship Operation" (SHOPERA), Paper MEPC 70/INF.33 submitted by Denmark, Germany, Norway and Spain 19 August 2016

### 2.7.3. List of project meetings, dates and venues

Table 11: List of arranged meetings

| a/a | Project Meeting | Date | Place | Participants |
|---|---|---|---|---|
| 1. | 1st Plenary Meeting (Kick-off Meeting) | 10-11/10/13 | Berlin | All + AC |
| 2. | Joint WP3 and WP4 meeting | 22/11/2013 | Berlin | GL MRTK, UDE, TUB |
| 3. | PMC and Invited Partners Meeting | 16-17/01/2014 | Athens | PMC & Invited Partners |
| 4. | PMC Meeting | 3-4/04/2014 | OSLO | PMC members, WP meetings |
| 5. | WP6 Meeting | 30/07/2014 | London | WP6 members |
| 6. | 2nd Plenary Meeting | 29-31/10/2014 | Hamburg | All + AC |
| 7. | 1st Project Workshop | 30/10/2014 | Hamburg | Open |

| | | | | |
|---|---|---|---|---|
| 8. | MTA Meeting | 23/04/2015 | Brussels | NTUA & P.O. |
| 9. | PMC Meeting | 15/09/2015 | Hamburg | PMC members |
| 10. | 3rd Plenary Meeting | 14-16/10/2015 | Lisbon | All + AC |
| 11. | 2nd Project Workshop | 15/10/2015 | Lisbon | Open |
| 12. | PMC Meeting | 13-15/04/2016 | London | PMC members |
| 13. | 3rd Project Workshop | 13-15/04/2016 | London | Open |
| 14. | WP6 Meeting | 01/06/2016 | Athens | WP6 members |
| 15. | 4th Project Workshop | 28/9/2016 | Athens | All + AC |
| 16. | 4th Plenary & WP Meetings | 28-30/9/2016 | Athens | All + AC |

### 2.7.4. Project website

A project-specific web site has been created and will be updated and maintained by the coordinator during the elaboration of the project and for at least 3 years after the project's end. A public area is maintained on the project's web site (http://shopera.org/), allowing free access to selected public domain deliverables, reports and publications resulting from the elaboration of the project.

### 2.7.5. Advisory Committee

An Advisory Committee (AC) has been formed consisting of representatives of major public regulatory bodies, European marine industry associations and other major stake holders. The AC is meant to act as a sounding board group for the consortium as well as a platform for early discussion of project results related to the preparation and consolidation of regulatory proposals to IMO, to ensure a broad acceptance by IMO member states. The AC members will participate in the yearly held workshops upon invitation of the Coordinator, acting on behalf of the General Assembly and have access to project deliverables, as decided by the PMC and after signing a Confidentiality Agreement. They shall not have any voting rights. The latest status of the members of the Advisory Committee (AC) is shown in Table 12.

Table 12: Members of the AC

| | Contact name | Participant organisation | Type | Country |
|---|---|---|---|---|
| 1 | W. Guntermann | HAPAG Lloyd (HLAG) | OPER | Germany |
| 2 | P. Guglia, A. Maccari | FINCANTIERI (FC) | YARD | Italy |
| 3 | Wim Hoebée | Port of Rotterdam (POR) | PORT | Netherlands |
| 4 | Tessy Vanhoenacker | Port of Antwerp (POA) | PORT | Belgium |
| 5 | Per Winther Christensen | Danish Shipowner Association (DSA) | OPER-ASSOC | Denmark |
| 6 | George Gratsos | Hellenic Chamber of Shipping (HCS) | OPER-ASSOC | Greece |
| 7 | Masaru Tsujimoto | National Maritime Research Institute (NMRI) | RES | Japan |
| 8 | Jonathan Simpson, Joanna Dormon | Maritime & Coastguard Agency (MCA) | ADM | United Kingdom |
| 9 | Apurba Ranjan Kar | Indian Register of Shipping (IRS) | CLASS | India |
| 10 | Ivan Sammut | Malta Transport Centre (TM) | ADM | Malta |
| 11 | Stavros Hatzigrigoris | MARAN Tankers Management Inc. | OPER | Greece |

| | | | | |
|---|---|---|---|---|
| 12 | Sander den Heijer | SEA Europe | ASSOC | EU |
| 13 | Niels van de Minkelis | Royal Association of Netherlands Ship-owners | ASSOC | Netherlands |

### 2.7.6. Co-operation with other projects/programmes

The project's co-operation with other projects, research programs and international scientific committees was significant and refers to the following list of systemic collaborations:

1. Co-operation with a parallel to SHOPERA RTD project of Japan, which was performed by the Japanese Society of Naval Architects and Ocean Engineers (JASNAOE) and was funded by the Ministry of Land, Infrastructure, Transport and Tourism of Japan, Class NK and the Research Assoc. of the Shipbuilding Industry of Japan. The scope of work of the parallel RTD project of Japan was similar to that of SHOPERA (as well its duration) and its ultimate goal was to prepare a submission to IMO regarding the "minimum powering of ships in adverse sea conditions". Through this collaboration, two additional joint workshops were co-organised by the two parties and held in Yokohama (4th March, 2015) and Athens (28th April 2015) preparing for relevant discussions at IMO-MEPC. Numerous meetings and additional, comparative studies of the two parties were planned and realised until the end of the SHOPERA project and they continue until today. The last meeting of the SHOPERA and JASNOAE projects was held in Hamburg on November 23-24, 2016 (DNV-GL premises). The meeting dealt with the joint submission to IMO-MEPC 70 and the elaboration of the joint proposal on the revised guidelines on the minimum powering of ships in adverse conditions until their adoption by IMO likely at MEPC 71 (June 2017). More meetings between representatives of the two projects are planned in the course of 2017.

2. Co-operation with the parallel project McRaw of the Netherlands Shipbuilder Association and the Netherlands delegation to IMO. Several meetings and joint comparative studies of SHOPERA and McRaw projects were planned and realised with the aim to consider possible common submissions of results to IMO.

3. Co-operation with the EU funded, FP7 project Extreme Seas, which was coordinated by DNV-GL and refers to part of the work conducted in WP1 (led herein also by DNV-GL).

3. Co-operation with the Manoeuvring, Performance, Stability and Seakeeping Committees of the International Towing Tank Conference (ITTC); invitation to all SHOPERA's dissemination activities; invitation to joint benchmark studies and dissemination events; jointly organised workshop discussing the results of the SHOPERA benchmark study (April 2016, London, LR premises).

## 2.8. References

1. EE-WG 1/4 (2010) Minimum required speed to ensure safe navigation in adverse conditions, submitted by IACS
2. IMO (2002) Standards for ship manoeuvrability, Res. MSC.137(76)
3. IMO (2012) Interim Guidelines for Determining Minimum Propulsion Power to Maintain the Manoeuvrability of Ships in Adverse Conditions, MSC-MEPC.2/Circ.11
4. IMO (2013) Interim guidelines for determining minimum propulsion power to maintain the Manoeuvrability in adverse conditions, IMO Res. MEPC.232(65)
5. IMO, 2008, International Code on Intact Stability, 2008 (2008 IS Code). IMO Resolution MSC.267(85),
6. MEPC 62/5/19 (2011) Reduction of GHG emissions from ships - Consideration of the Energy Efficiency Design Index for New Ships. Minimum propulsion power to ensure safe manoeuvring in adverse conditions, Submitted by IACS, BIMCO, CESA, INTERCARGO, INTERTANKO, WSC
7. MEPC 62/INF.21 (2011) Reduction of GHG emissions from ships - Consideration of the Energy Efficiency Design Index for New Ships. Minimum propulsion power to ensure safe manoeuvring in adverse conditions, Submitted by IACS, BIMCO, CESA, INTERCARGO, INTERTANKO, WSC
8. MEPC 64/4/13 (2012) Consideration of the Energy Efficiency Design Index for new ships – Minimum propulsion power to maintain the manoeuvrability in adverse conditions, Submitted by IACS, BIMCO, INTERCARGO, INTERTANKO and OCIMF
9. MEPC 64/INF.7 (2012) Background information to document MEPC 64/4/13, Submitted by IACS
10. MEPC (2014) EU Project “Energy Efficient Safe SHip OPERAtion” (SHOPERA), Paper MEPC 67/INF.14 submitted by Germany, Norway and United Kingdom
11. IACS, 2001, Standard Wave Data, International Association of Classification Societies, Recommendation No.34.
12. ITTC Manoeuvring Committee (2008) Final report and recommendations to 25th ITTC, Proc. 25th ITTC, Vol. I
13. MAIB (1996) Report on the investigation into the grounding of the passenger roro ferry Stena Challenger on 19 September 1995, Blériot-Plage, Calais, Marine Accidents Investigation Branch
14. MAIB (2002) Report on the investigation of the grounding of mv Willy, Marine Accidents Investigation Branch
15. MAIB (2009) Report on the investigation into the grounding, and subsequent loss, of the roro cargo vessel Reverdance, Shell Flats – Cleveleys Beach, Lancashire, 31. January 2008, Marine Accidents Investigation Branch
16. MAIB (2009a) Report on the investigation of the grounding of Astral on Princessa Shoal, East Isle of Wight, 10 March 2008, Marine Accidents Investigation Branch
17. MAIB (2012) Report on the investigation of the grounding of the cargo ship Carrier at Raynes Jetty in Llanddulas, North Wales on 3 April 2012, Marine Accidents Investigation Branch
18. MAIB (2012a) Report on the investigation of windlass damage, grounding and accident to person on the ro-ro ferry Norcape, Firth of Clyde and Troon, Scotland, on 26-27 November 2011, Marine Accidents Investigation Branch
19. ATSB (2008) Independent investigation into the grounding of the Panamian registered bulk carrier Pasha Bulker on Nobbys Beach, Newcastle, New South Wales, 8 June 2007, Australian Transport Safety Bureau (ATSB) Rep. Marine Occurrence Investigation No. 243
20. Papanikolaou, A., Zaraphonitis, G., Bitner-Gregersen, E., Shigunov, V., El Moctar, O., Guedes Soares, C., Reddy, D.N., Sprenger, F. (2015), “Energy Efficient Safe Ship Operation (SHOPERA)”, 2015 World Maritime Technology Conference (WMTC150), 3-7 Nov. 2015, Rhode Island (USA).
21. Papanikolaou, A., Zaraphonitis, G., Bitner-Gregersen, E., Shigunov, V., El Moctar, O., Guedes Soares, C., Reddy, D.N., Sprenger, F., “Energy Efficient Safe Ship Operation (SHOPERA)”, Proc. 12th Int. Marine Design Conference (IMDC2015 ), 11-14 May 2015, Tokyo (Japan)
22. Papanikolaou, A., Zaraphonitis, G., Bitner-Gregersen, E., Shigunov, V., El Moctar, O., Guedes Soares, C., Reddy, D. N., Sprenger, F., “Minimum Propulsion and Steering Requirements for Efficient and

Safe Operation (SHOPERA)", Invited paper, 37th Motorship Propulsion and Emissions Conference, 4-5 March 2015, Hamburg (Germany).

23. Ventikos, N., Koimtzoglou, A., Louzis, K. and Eliopoulou, E. (2014) "Database of ships and accidents" and "Risk analysis of accidents related to manoeuvring in adverse weather conditions", SHOPERA D1.3, D.1.4, NTUA
24. Fujiwara, T., Ueno, M. and Ikeda, Y. (2006) Cruising performance of a large passenger ship in heavy sea, Proc. 16-th Int. Offshore and Polar Engineering Conf., Vol. III, pp. 304-311
25. Söding, H. and Shigunov, V. (2015) Added resistance of ships in waves, Ship Technology Research - Schiffstechnik 62(1) 2-13
26. Söding, H., "Limits of Potential Theory in Rudder Flow Predictions", Proc. Symp. Naval Hydrod., Washington, 1998.
27. Söding, H., A. von Graefe, O. el Moctar and V. Shigunov. "A Rankine Source Method for Seakeeping Predictions", Proc. 31st Int. Conf. on Ocean, Offshore and Arctic Engineering OMAE2012, June 10-15, 2012, Rio de Janeiro, Brazil. - Paper Nr. OMAE2012-83450.
28. Söding, H., V. Shigunov, T.E. Schellin and O. El Moctar. "A Rankine Panel Method for Added Resistance of Ships in Waves", Proc. 31st Int. Conf. on Ocean, Offshore and Arctic Engineering OMAE2012, June 10-15, Rio de Janeiro, Brazil. - Paper Nr. OMAE2012-83457, 2012.
29. Söding, H., V. Shigunov, T.E. Schellin, T. E. and O. el Moctar. "A Rankine Panel Method for Added Resistance of Ships in Waves", *Journal of Offshore Mechanics and Arctic Engineering*, 2014, Vol. 136, Nr. 3, pp. 031601·1-031601·7.
30. Shigunov, V. and Papanikolaou, A. (2014) Criteria for minimum powering and maneuverability in adverse weather conditions, 14th Int. Ship Stability Workshop (ISSW 2014), Kuala Lumpur, Malaysia
31. Shigunov, V. (2015) Manoeuvrability in adverse conditions, Proc. 34th Int. Conf. on Ocean, Offshore and Arctic Engineering OMAE2015, St. John's, Newfoundland, Canada; Paper Nr. OMAE2015-41628
32. Shigunov, V., Papanikolaou, A. and Chroni, D. (2016) Maneuverability in adverse conditions: Assessment framework and examples, Proc. 15th Int. Ship Stability Workshop, 13-15 June, Stockholm, Sweden
33. Liu, S.K. and A. Papanikolaou. "Added Resistance of Ships in Quartering Seas", V International Conference on Computational Methods for Coupled Problems in Science and Engineering, COUPLED PROBLEMS, 2013.
34. Liu, S.K., A. Papanikolaou and G. Zaraphonitis. "Prediction of Added Resistance of Ships in Waves", Ocean Engineering, 2011.
35. Liu, S.K., A. Papanikolaou and G. Zaraphonitis. "Time domain simulation of nonlinear ship motions using an impulse response function method", ICMT conference, July 2014, Glasgow, UK, 2014.
36. Liu, S.K., A. Papanikolaou and G. Zaraphonitis. "Practical approach to the added resistance of a ship in short waves", 25th International Ocean and Polar.
37. Amini Afshar, M. *Towards Predicting the Added Resistance of Slow Ships in Waves*, PhD thesis, Lyngby: Technical University of Denmark, 2014.
38. el Moctar, O., V. Shigunov and T. Zorn. "Duisburg Test Case: Post-Panamax Container Ship for Benchmarking", *Journal of Ship Technology Research*, Vol.59, No.3, pp. 50-65, 2012.
39. Ley, J., S. Sigmund and O. el Moctar. "Numerical Prediction of the Added Resistance of Ships in Waves", Proc. 33rd ASME Int. Conf. on Ocean, Offshore and Arctic Engineering , San Francisco, USA. - Paper Nr. OMAE2014-24216, 2014.
40. Cura Hochbaum, A. and M. Voigt. "Towards the Simulation of Seakeeping and Manoeuvring based on the Computation of the Free Surface Viscous Ship Flow", Fukuoka, Japan, 24th ONR Symposium on Naval Hydrodynamics, 2002.
41. Sánchez-Caja, A., J. Martio, I. Saisto and T. Siikonen. "On the Enhancement of Coupling Potential Flow Models to RANS Solvers for the Prediction of Propeller Effective Wakes", Journal of Marine Science and Technology, February 2014, pp. DOI 10.1007/s00773-014-0255-4, 2014.

42. Havelock, T.H. The Pressure of Water Waves upon a Fixed Obstacle. Proceedings of the Royal Society of London, Series A, Mathematical and Physical Sciences, Vol. 175, No. 963 pp. 409-421, 1940.
43. Fujii, H. and T. Takahashi. "Experimental Study on the Resistance Increase of a Ship in Regular Oblique Waves," Proceeding of the 14th ITTC, pp. 351–360, 1975.
44. Sakamoto, T. and E. Baba. "Minimization of Resistance of Slowing Moving Full Hull Forms in Short Waves," Proc. 16th Symposium on Naval Hydrodynamics.
45. Abott, I. H. and A. E. von Doenhoff. Theory of Wing Sections, Dover Publications Inc., 1959.
46. Brix, J. E. (1993) Manoeuvring Technical Manual. – Seehafen Verlag, Hamburg
47. Blendermann, W. (1993) Schiffsform und Windlast- Korrelations- und Regressionsanalyse von Windkanalmessungen am Modell, Rep. 533, Institut für Schiffbau, Harburg
48. Andrews, D., Papanikolaou, A., Erichse, S. and Vasudevan, S., IMDC2009 state of the art report on design methodology. Proc. 10th International Marine Design Conference, May 2009.
49. Hochkirch, K. and Bertram, V., "Hull Optimization for Fuel Efficiency – Past, Present and Future", COMPIT 2012, Liege, Belgium, Apr. 16-18 2012.
50. Nowacki, H., "Developments in marine design methodology: routes, results and future trends", keynote presentation, Proc. 10th International Marine Design Conference, IMDC'09- 2009.
51. Nowacki, H., "Five decades of Computer-Aided Ship Design", Journal of Computer-Aided Design, vol. 42 (2010) pp 956-969.
52. Papanikolaou, A., "Holistic ship design optimization", Journal of Computer-Aided Design, vol. 42 (2010) pp1028-1044.
53. Papanikolaou, A., Zaraphonitis, G., Skoupas, S. and Boulougouris, E.,"An integrated methodology for the design of Ro-Ro Passenger ships", Journ. Ship Technology Research, vol. 57, No. 1 (2010).
54. Sames, P., Papanikolaou, A., Harries, S., Coyne, K., Zaraphonitis, G. and Tillig, F., "BEST Plus – Better Economics with Safer Tankers", Proc. Of the 2011 Annual Conference of the Society of the Naval Architects and Marine Engineers (SNAME), Nov. 2011.
55. Zaraphonitis, G., "Set-up of integrated optimization platform and definition of optimization problem", SHOPERA Deliverable D5.1.
56. Happonen K., Martio, J., Zaraphonitis, G., Zagkas, V., Papanikolaou, A., "Development and Implementation of Parametric Models", SHOPERA Deliverable D5.2.
57. NAPA Software, NAPA Oy, https://www.napa.fi/
58. CAESES Software, FRIENDSHIP SYSTEMS, https://www.caeses.com/
59. Hogben, N., Da Cunha, L. F., and Oliver, H. N., 1986, British Maritime Technology. Global Wave Statistics. – Unwin Brothers Limited, London, England.
60. Flemish Banks Monitoring Network, 2016, http://www.meetnetvlaamsebanken.be/
61. Michel, W. H., 1999, "Sea Spectra Revisited", J. Marine Technology, **36**(4), 211-227.
62. NATO, 1983, "Standardized Wave and Wind Environments and Shipboard Reporting of Sea Conditions", STANAG No. 4194.